Geological Society, London, Special Publications Online First

Stratigraphic continuity and fragmentary sedimentation: the success of cyclostratigraphy as part of integrated stratigraphy

Frederik J. Hilgen, Linda A. Hinnov, Hayfaa Abdul Aziz, Hemmo A. Abels, Sietske Batenburg, Joyce H. C. Bosmans, Bas de Boer, Silja K. Hüsing, Klaudia F. Kuiper, Lucas J. Lourens, Tiffany Rivera, Erik Tuenter, Roderik S. W. Van de Wal, Jörn-Frederik Wotzlaw and Christian Zeeden

Geological Society, London, Special Publications, first published October 3, 2014; doi 10.1144/SP404.12

Stratigraphic continuity and fragmentary sedimentation: the success of cyclostratigraphy as part of integrated stratigraphy

FREDERIK J. HILGEN[1]*, LINDA A. HINNOV[2], HAYFAA ABDUL AZIZ[3], HEMMO A. ABELS[1], SIETSKE BATENBURG[4], JOYCE H. C. BOSMANS[1,12], BAS DE BOER[1,9], SILJA K. HÜSING[5], KLAUDIA F. KUIPER[6], LUCAS J. LOURENS[1], TIFFANY RIVERA[7], ERIK TUENTER[8], RODERIK S. W. VAN DE WAL[9], JÖRN-FREDERIK WOTZLAW[10] & CHRISTIAN ZEEDEN[11]

[1]*Department of Earth Sciences, Utrecht University, Budapestlaan 4, 3584 CD Utrecht, The Netherlands*

[2]*Department of Earth and Planetary Sciences, Johns Hopkins University, Baltimore, Maryland, 21218, USA*

[3]*ENRES International, Euclideslaan 201, 3584 BS Utrecht, The Netherlands*

[4]*Institute of Geosciences, Goethe-University Frankfurt, D-60438 Frankfurt, Germany*

[5]*Paleomagnetic Laboratory 'Fort Hoofddijk', Utrecht University, Budapestlaan 17, 3584 CD Utrecht, The Netherlands*

[6]*Institute of Earth Sciences, Vrije Universiteit Amsterdam, De Boelelaan 1085, 1081 HV Amsterdam, The Netherlands*

[7]*Department of Geosciences, Isotope Geology Lab, Boise State University, 1910 University Drive, Boise, ID 83725, USA*

[8]*Royal Netherlands Meteorological Institute (KNMI), P.O. Box 201, 3730 AE De Bilt, The Netherlands*

[9]*Institute for Marine and Atmospheric Research Utrecht, Utrecht University, Princetonplein 5, 3584 CC Utrecht, The Netherlands*

[10]*Section of Earth and Environmental Sciences, University of Geneva, Rue des Maraìchers 13, CH-1205 Geneva, Switzerland*

[11]*Department of Geography, Wüllnerstr. 5b, RWTH Aachen University, D-52056 Aachen, Germany*

[12]*Present address: Department of Physical Geography, Utrecht University, Heidelberglaan 2, 3584 CS Utrecht, The Netherlands*

**Corresponding author (e-mail: F.J.Hilgen@uu.nl)*

Abstract: The Milankovitch theory of climate change is widely accepted, but the registration of the climate changes in the stratigraphic record and their use in building high-resolution astronomically tuned timescales has been disputed due to the complex and fragmentary nature of the stratigraphic record. However, results of time series analysis and consistency with independent magnetobiostratigraphic and/or radio-isotopic age models show that Milankovitch cycles are recorded not only in deep marine and lacustrine successions, but also in ice cores and speleothems, and in eolian and fluvial successions. Integrated stratigraphic studies further provide evidence for continuous sedimentation at Milankovitch time scales (10^4 years up to 10^6 years). This combined approach also shows that strict application of statistical confidence limits in spectral analysis to verify astronomical forcing in climate proxy records is not fully justified and may lead to false negatives. This is in contrast to recent claims that failure to apply strict statistical standards can lead to false positives in the search for periodic signals. Finally, and contrary to the argument that changes in insolation are too small to effect significant climate change, seasonal insolation

From: SMITH, D. G., BAILEY, R. J., BURGESS, P. M. & FRASER, A. J. (eds) *Strata and Time: Probing the Gaps in Our Understanding*. Geological Society, London, Special Publications, **404**, http://dx.doi.org/10.1144/SP404.12

variations resulting from orbital extremes can be significant (20% and more) and, as shown by climate modelling, generate large climate changes that can be expected to leave a marked imprint in the stratigraphic record. The tuning of long and continuous cyclic successions now underlies the standard geological time scale for much of the Cenozoic and also for extended intervals of the Mesozoic. Such successions have to be taken into account to fully comprehend the (cyclic) nature of the stratigraphic record.

Astronomically induced climate forcing and its expression as cycles in the stratigraphic record play an important role in the construction of high-resolution time scales and in understanding past sedimentation and climate change on Milankovitch (10^4 years up to 10^6 years) time scales. The tuning of stratigraphic cycles to astronomical target curves calculated with the help of astronomical solutions for the Solar System now underlies the age calibration of the Geological Time Scale (GTS) for most of the Cenozoic Era (Hilgen *et al.* 2012; Vandenberghe *et al.* 2012). A significant part of the Mesozoic Era has been astronomically scaled for the GTS as well (Ogg & Hinnov 2012*a*, *b*; Ogg 2012). Moreover, all $^{40}Ar/^{39}Ar$ ages in the new GTS are calculated relative to an astronomically calibrated age for the Fish Canyon sanidine (FCs) dating standard (Kuiper *et al.* 2008; Schmitz 2012). Despite this progress, critical papers on cyclostratigraphy have been published (e.g. Miall & Miall 2004; Bailey 2009; Vaughan *et al.* 2011) focusing on the following points:

(1) Stratigraphic successions are punctuated by hiatuses and changes in sedimentation rate and are thus by definition discontinuous and unsuitable for astronomical calibration (Miall & Miall 2004; Bailey 2009; Miall 2014). The fragmentary character of the stratigraphic record will not allow the study of Milankovitch cycles in detail and, in particular, the use of these cycles to build high-resolution time scales. It has been asserted that the stratigraphic record is 'more gap than record' (Ager 1973), but this statement depends on the time scale of reference, as sedimentation rate v. duration follows an inverse power law with an increasing percentage of time missing in hiatuses at longer time scales (Sadler 1981). Hence, it is concluded that stratigraphic continuity and constant sedimentation rates are myths that require balance between subsidence and sedimentation that in practice does not exist.

(2) The statistical basis for Milankovitch cyclicity is weak as low significance levels are often employed in combination with improper statistical treatment, which may lead to a situation in which false positives might become the norm (Vaughan *et al.* 2011). This point is also related to the question of whether the discrimination of a stratal (i.e. cycle) hierarchy in the stratigraphic record is real or merely an arbitrary subdivision of an uninterrupted continuum (Bailey & Smith 2008).

(3) Other critical points concern the weakness of the astronomical forcing, uncertainty in the periods of the astronomical cycles in the geological past, and insufficient precision of independent time calibration of cyclostratigraphic data to establish models based on tuning, filtering and other kinds of statistical treatment.

Here, we address these critical points first by reviewing a number of cases in which Milankovitch cycles occur in long sedimentary successions that are shown to be continuous on Milankovitch time scales. We present these cases for various time intervals, focussing in particular on the youngest, Cenozoic, part of the record because it includes sediments deposited under widely varying environmental conditions for which good time control is available. This approach is key for demonstrating that sedimentary cycles were controlled by astronomical climate forcing, that cyclic successions can be stratigraphically continuous up to million year time scales, and that these successions can be used to build high-resolution tuned time scales. We then address critical issues concerning the nature and continuity of the stratigraphic record, and the statistical analysis of cyclostratigraphy, and discuss additional concerns regarding the inferred weakness of the forcing, independent age constraints for testing the astronomical theory of climate change, the stability of astronomical frequencies in the past and the primary character of limestone-marl alternations used for tuning.

Milankovitch cyclicity in the stratigraphic record

Pleistocene

The study of the influence of Earth's orbital–rotational cycles on climate, including the construction of astronomically tuned time scales, goes back

to the nineteenth century (e.g. Imbrie & Imbrie 1979; Hilgen 2010 and references therein). Research focused initially on the astronomical theory of the Ice Ages, as first formulated by Adhémar (1842) and Croll (1864). Progress, however, was slow as only discontinuous records of river terraces and moraine deposits were available for study, while independent age control was essentially lacking (Imbrie & Imbrie 1979).

With the recovery of the first piston cores of deep marine sediments from the ocean floor during the first Swedish Deep-Sea Expedition in 1947 (Kullenberg 1947; Pettersson *et al.* 1951), continuous records of Ice Age history became available for the first time (Emiliani 1955). This recovery heralded the beginning of the revival – and the general acceptance – of the astronomical theory of the Ice Ages and the construction of astronomical time scales (Hays *et al.* 1976; Imbrie *et al.* 1984). The development of new climate proxies, statistical techniques and dating methods also played a crucial role in the acceptance of the theory (see Imbrie & Imbrie 1979).

The detailed marine records of the Ice Ages of the last 800 kyr (kiloyears) are dominated by a *c*. 100 kyr cycle and were tuned to boreal summer insolation or, alternatively, an ice volume model that used the astronomical parameters as input (Imbrie *et al.* 1984). Extension beyond 800 ka (kiloyears ago) using normal piston cores proved problematic as low sedimentation rate areas had to be targeted, which lacked adequate temporal resolution. This difficulty was solved by the adoption of a multiple hole drilling strategy in deep-sea drilling, which was developed to overcome problems of stratigraphic completeness at core breaks (e.g. Ruddiman *et al.* 1987). This strategy was used to extend the tuned marine oxygen isotope record back to 2.6 Ma (million years ago) (Raymo *et al.* 1989; Ruddiman *et al.* 1989), the time that marks the onset of major Northern Hemisphere glaciations. In contrast to the late Pleistocene, these older records are dominated by the 41 kyr axial obliquity cycle predicted by Milankovitch (1941) for all glacials.

The Marine Isotope Stages (MIS), based on the standardization of the characteristic pattern of benthic oxygen isotope variations as stages, provided a critical tool for the study of the Ice Ages in the marine realm. The MIS that were introduced with the publication of Emiliani (1955) allow deep-sea records to be synchronized along a common high-resolution astronomically tuned age model, with the latest version being the LR04 stack of Lisiecki & Raymo (2005) based on a stack of 57 globally distributed isotope records.

The expression of the Quaternary ice ages is not limited to the deep marine realm but is also found in shallow marine and continental successions, as well as in climate archives of ice cores and speleothems. High-resolution records of sea-level change were identified in stratigraphic sequences of shallow-marine successions in the Wanganui Basin, New Zealand (Naish *et al.* 1998), linking sequence stratigraphy to cyclostratigraphy, and confirmed by magnetobiostratigraphic and radio-isotopic dating. Integrated stratigraphic correlations were further used to identify ice ages in continental successions, most notably in the lacustrine succession of Lake Baikal (e.g. Prokopenko *et al.* 2006) and Lake El'Gygytgyn (Melles *et al.* 2012), and the eolian record of the Chinese loess plateau. Astrochronologies have long been built for these loess deposits, which have been based on independent tuning (Ding *et al.* 1994) and correlation of the loess-soil alternations to the MIS (e.g. Hovan *et al.* 1989). This approach has led to a detailed understanding of the evolution of the East Asian monsoon (An 2000).

Fluvial successions have been considered least suitable for cyclostratigraphic studies because it is assumed that tectonics and autocyclic processes dominate in the dynamic fluvial system (e.g. Beerbower 1964). Nevertheless, fluvial successions of Quaternary age have revealed the imprint of cyclic climate change (e.g. Blum *et al.* 1994; Törnqvist 1998), and a further example of astronomical control on a fluvial system comes from Pleistocene sequences in the Pannonian Basin (Nador *et al.* 2003).

Other archives of climate change in ice cores and speleothems are of great importance as well. The Antarctic ice core record extends back to 0.8 Ma, covering the last eight full glacial–interglacial cycles (e.g. Epica community members 2004). In particular, deuterium (δD), as a proxy for mid- to high-latitude temperature, reveals an excellent fit with the MIS (EPICA community members 2004; Loulergue *et al.* 2008). The ice cores also provide records of atmospheric CO_2 and CH_4 (Siegenthaler *et al.* 2005; Loulergue *et al.* 2008; Lüthi *et al.* 2008) that match the patterns observed in the marine record. The precession signal is amplified in the CH_4 record, as it probably picks up additional low latitude sources that operate independently from the ice ages (Ruddiman & Raymo 2003). A low latitude monsoon-related and precession-dominated signal is well documented in the speleothem $\delta^{18}O$ record of the Sanbao/Hulu caves (Wang *et al.* 2008).

Neogene

The Astronomical Time Scale (ATS) for the last 800 kyr was extended to the base of the Pliocene (5.33 Ma) following the introduction of the multiple hole drilling strategy in deep-sea drilling and the incorporation of land-based marine sections

(Shackleton *et al.* 1990; Hilgen 1991*a*, *b*; Fig. 1). The ATS was extended into the Miocene with deep marine sections now exposed on land in the Mediterranean (e.g. Hilgen *et al.* 1995, 2003; Krijgsman *et al.* 1999; Hüsing *et al.* 2007, 2009; Figs 1 & 2). As in the Pliocene, integrated stratigraphic correlations to parallel sections, using magnetostratigraphy combined with planktonic foraminiferal biostratigraphy, were used to verify the inferred continuity of the successions at the Milankovitch scale (Fig. 2).

Astronomical tuning of the Mediterranean sections underlies the age calibration of the standard GTS for the Neogene Period (Lourens *et al.* 2004; Hilgen *et al.* 2012). Hilgen *et al.* (2006) proposed that some of the sections be formally designated as unit stratotypes for stages, with the Rossello Composite section as unit stratotype for the Zanclean and Piacenzian stages of the Pliocene, and Monte dei Corvi as unit stratotype for the Tortonian stage of the Miocene; the Global Stratotype Section and Points (GSSPs) of these stages had already been defined in these sections (Castradori *et al.* 1998; Van Couvering *et al.* 2000; Hilgen *et al.* 2005). Moreover, units defined by the astronomically controlled cyclicity can be designated as chronozones, that is, formal chronostratigraphic units of minor rank (Hilgen *et al.* 2006).

Cyclic terrestrial successions were also incorporated in the high-resolution astrochronologic framework of the Mediterranean Neogene. Independently from one another, magnetostratigraphic and $^{40}Ar/^{39}Ar$ dating revealed a precession origin for lignite–marl alternations of Pliocene age in the Ptolemais Basin of Greece (Steenbrink *et al.* 1999); these alternations have been correlated in detail to the marine Capo Rossello section (van Vugt *et al.* 1998). Miocene lacustrine successions in Spain also proved suitable for the study of astronomically forced climate change (Abdul Aziz *et al.* 2003, 2004; Abels *et al.* 2009*a*, *b*). Cycles in these lacustrine successions are dominated by precession and their number fits that of the deep marine Monte dei Corvi section for each magnetic polarity interval (Abels *et al.* 2009*a*, *b*; Fig. 3). The study of these continental successions contributes to a better understanding of astronomical climate forcing in the circum-Mediterranean area and may shed light on the climate system responsible for sapropel formation.

In addition to the Mediterranean, Neogene marine cyclic successions are encountered in numerous deep-sea cores. Sediments from Ceara Rise in the eastern Equatorial Atlantic are a prime example, as they reveal the expression of all astronomical parameters in sediment colour and magnetic susceptibility variations, and have been used for tuning (Shackleton & Crowhurst 1997; Zeeden *et al.* 2012; Fig. 4). High-resolution stable isotope records have also been generated that reveal the clear imprint of astronomical climate forcing (e.g. Holbourn *et al.* 2007, 2013; Liebrand *et al.* 2011).

Palaeogene

The tuning of climate proxy records of Ocean Drilling Program (ODP) Site 1218 in the Pacific with its detailed magneto- and biostratigraphy resulted in an ATS for the entire Oligocene, providing insight into the astronomical climate forcing and the functioning of the global carbon cycle, as expressed in the carbon isotope record (Pälike *et al.* 2006*a*). Deep marine cyclic sections in the northern Apennines, including the Massignano section that houses the formally defined Eocene–Oligocene boundary, have been analysed cyclostratigraphically as well, resulting in a further extension of the ATS (Jovane *et al.* 2006; Brown *et al.* 2009; Hyland *et al.* 2009).

Following an Eocene gap, resulting from a relatively shallow position of the Carbonate Compensation Depth (CCD) in the ocean (Pälike & Hilgen 2008), attempts have also been made to tune the older part of the Palaeogene down to the Cretaceous–Palaeogene (K/Pg) boundary (e.g. Kuiper *et al.* 2008; Westerhold *et al.* 2008). The Paleocene ATS currently has uncertainties in both the exact number and tuning of 405 kyr orbital eccentricity cycles (Hilgen *et al.* 2010; Westerhold *et al.* 2012; Renne *et al.* 2013). Nevertheless, sedimentary cycle patterns in the Zumaia section in Spain and Atlantic ODP Leg 208 sites exhibit the well known *c.* 1:5:20 ratio characteristic of *c.* 20 precession cycles proportionate to *c.* 4 short eccentricity (*c.* 100 kyr) and one long eccentricity (405 kyr) cycle; this interpretation fits with results of integrated stratigraphy (Fig. 3 in Kuiper *et al.* 2008; Westerhold *et al.* 2007). Detailed cyclostratigraphies down to the precession scale have been established in particular for the interval between the Paleocene–Eocene Thermal Maximum (PETM) and Eocene Thermal Maximum (ETM) 2 in Leg 208 sites (Lourens *et al.* 2005; Westerhold *et al.* 2007) and in the classical succession of northern Italy (Galeotti *et al.* 2010).

Cycles in the Zumaia section have been correlated at the precession scale to the Bjala section in Bulgaria for the interval of the Danian–Selandian transition; this interval covers magnetochronozone C27n and includes the so-called top C27n carbon isotope excursion (Dinarès-Turell *et al.* 2010, 2012). Paleocene and early Eocene hyperthermals are further recorded as distinct carbon isotope excursions in the fluvial succession in the Bighorn Basin of the USA (Bowen *et al.* 2001; Abels *et al.* 2012). This floodplain succession also exhibits distinct cyclicity, which on the basis of magneto- and

Fig. 1. (**a**) Deep marine sections of Punta di Maiata (Pliocene) and (**b**) Monte Gibliscemi (Miocene) on Sicily (Italy), and (**c**) shallow lacustrine-floodplain successions exposed in the Orera and (**d**) Cascante sections (Miocene, Spain). Punta di Maiata is a partial section of the Rossello Composite proposed as unit stratotype for the Zanclean and Piacenzian Stages. Sapropels at Monte Gibliscemi show characteristic cycle hierarchy with sapropels grouped into bundles, reflecting the amplitude modulation of precession by eccentricity.

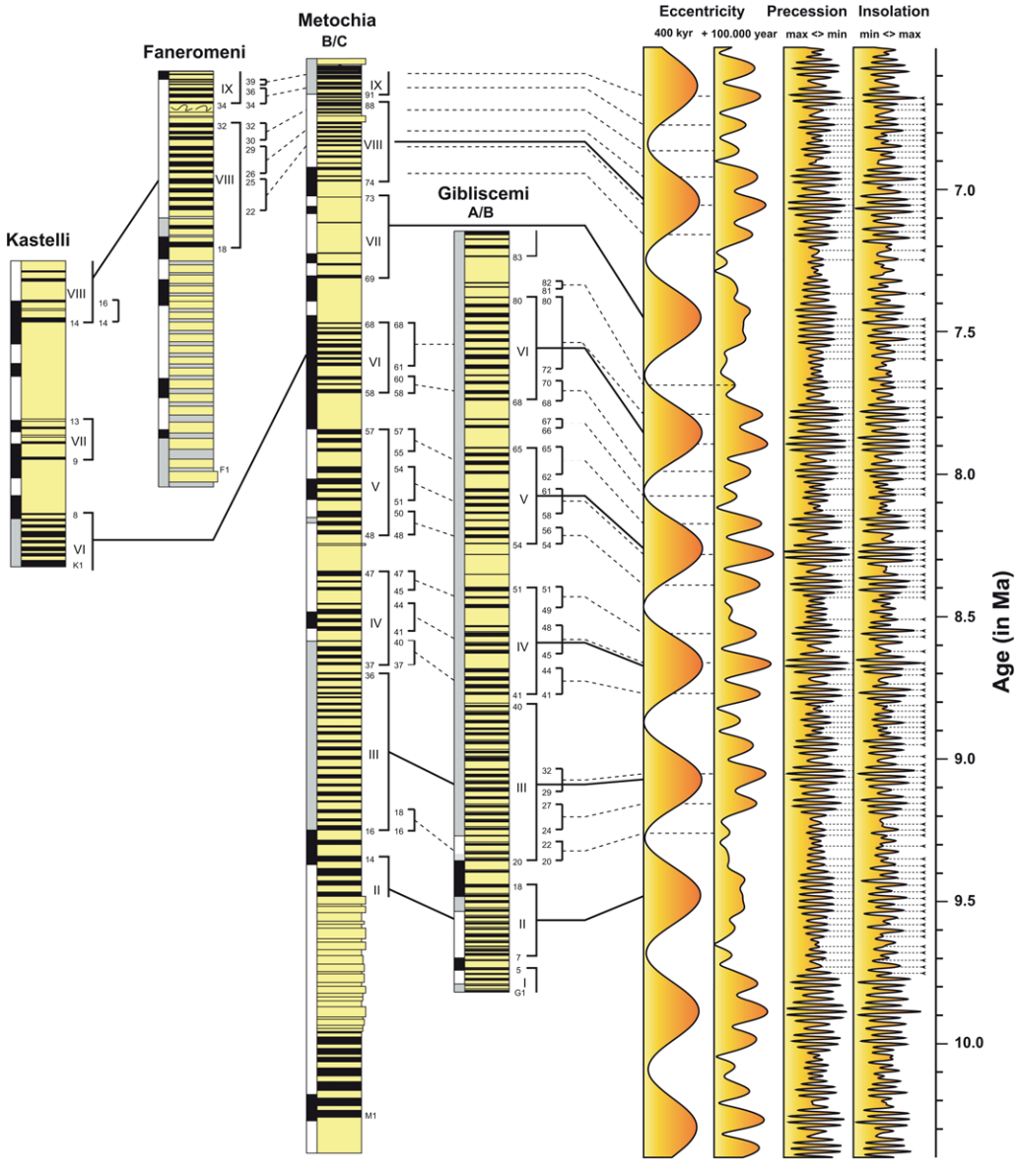

Fig. 2. Astronomical tuning of sapropels and associated grey marls in land-based deep marine sections in the Mediterranean for the interval between 10 Ma and 7 Ma. Colours in the lithological columns indicate sapropels (black), associated grey marls (grey) and homogeneous marls (yellow). Colours in the magnetostratigraphic columns indicate normal polarities (black), reversed polarities (white) and uncertain polarities (grey). Sapropels and associated grey marls have been numbered per section and lumped into large-scale groups (roman numerals) and small scale groups (after Krijgsman *et al.* 1995; Hilgen *et al.* 1995). The initial age model is based on magnetobiostratigraphy. Phase relations between sapropel cycles and the orbital parameters/insolation used for the tuning are based on the comparison of the sapropel chronology for the last 0.5 myr with astronomical target curves. Tuning was carried out in successive steps starting with matching the large scale sapropel bundles to long period eccentricity and ending with matching the individual sapropels to precession minima and insolation maxima. The astronomical solution used is La93 (Laskar *et al.* 1993).

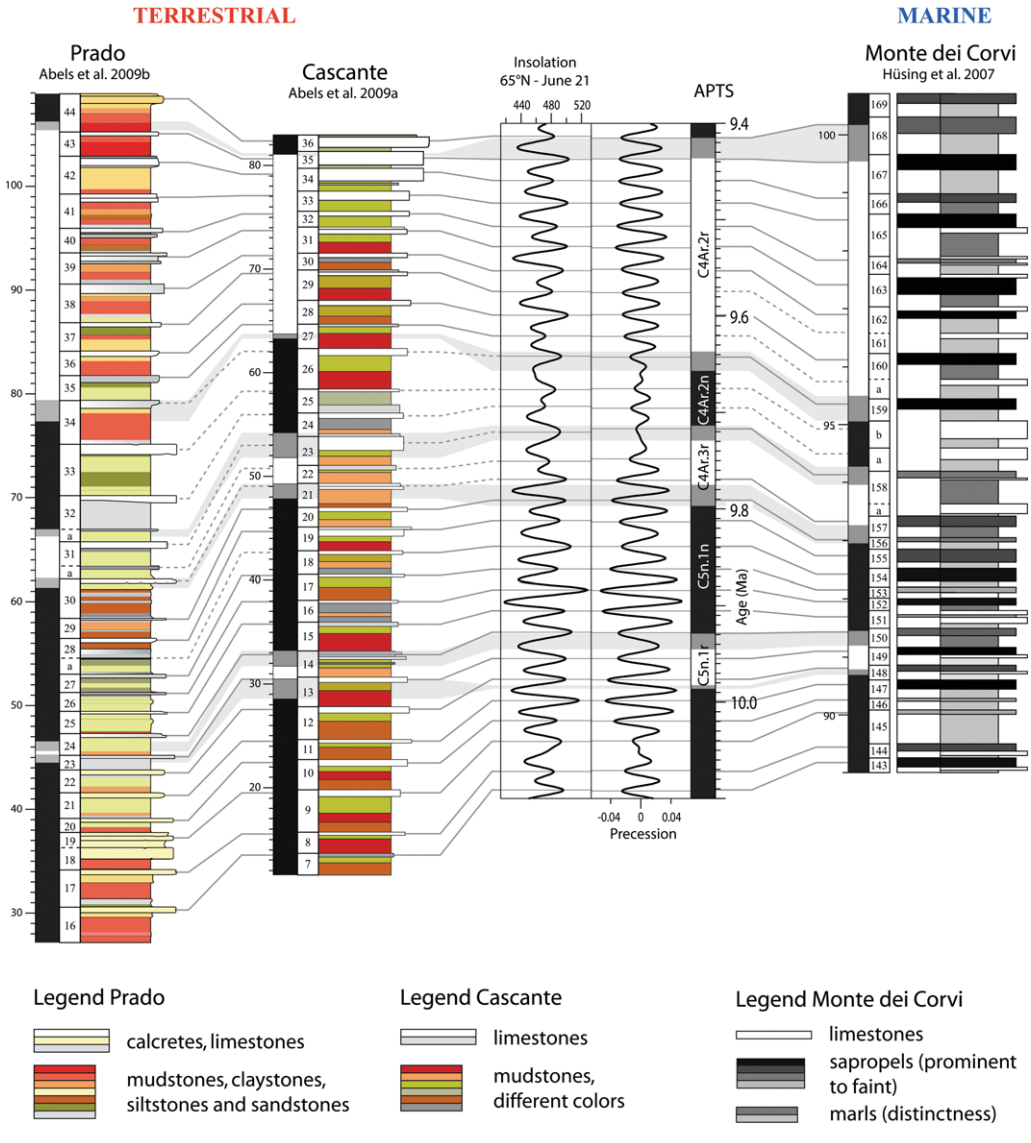

Fig. 3. High-resolution precession-scale cyclostratigraphic correlations between and tuning of the continental sections of Prado and Cascante in Spain (Abels *et al.* 2009*a*, *b*) and the marine reference section of Monte dei Corvi in Spain (Hilgen *et al.* 2003; Hüsing *et al.* 2009). The correlations and tuning are tightly constrained by the excellent magnetostratigraphy in all sections. Note the similar number of cycles per magnetochronozone/subchron, despite differences in lock-in depth and – potentially – delayed acquisition of magnetization. Cycles are numbered per section.

biostratigraphic constraints has been related to precession (Abdul Aziz *et al.* 2008*a*; Abels *et al.* 2013). This interpretation is further validated by the consistency between astrochronologic age models developed independently for the ETM2 and H2 hyperthermals in the continental and marine realm (Stap *et al.* 2009; Abels *et al.* 2012). An important outcome of these studies is that floodplain sedimentation and avulsion frequency is regionally controlled by astronomically induced climate change rather than by autogenic processes alone (Abels *et al.* 2013). The sections studied thus far form part of a fluvial succession that seems essentially continuous over at least ~one million years. In this respect, Blum & Törnqvist (2000) have stated that 'the response of pre-Quaternary fluvial

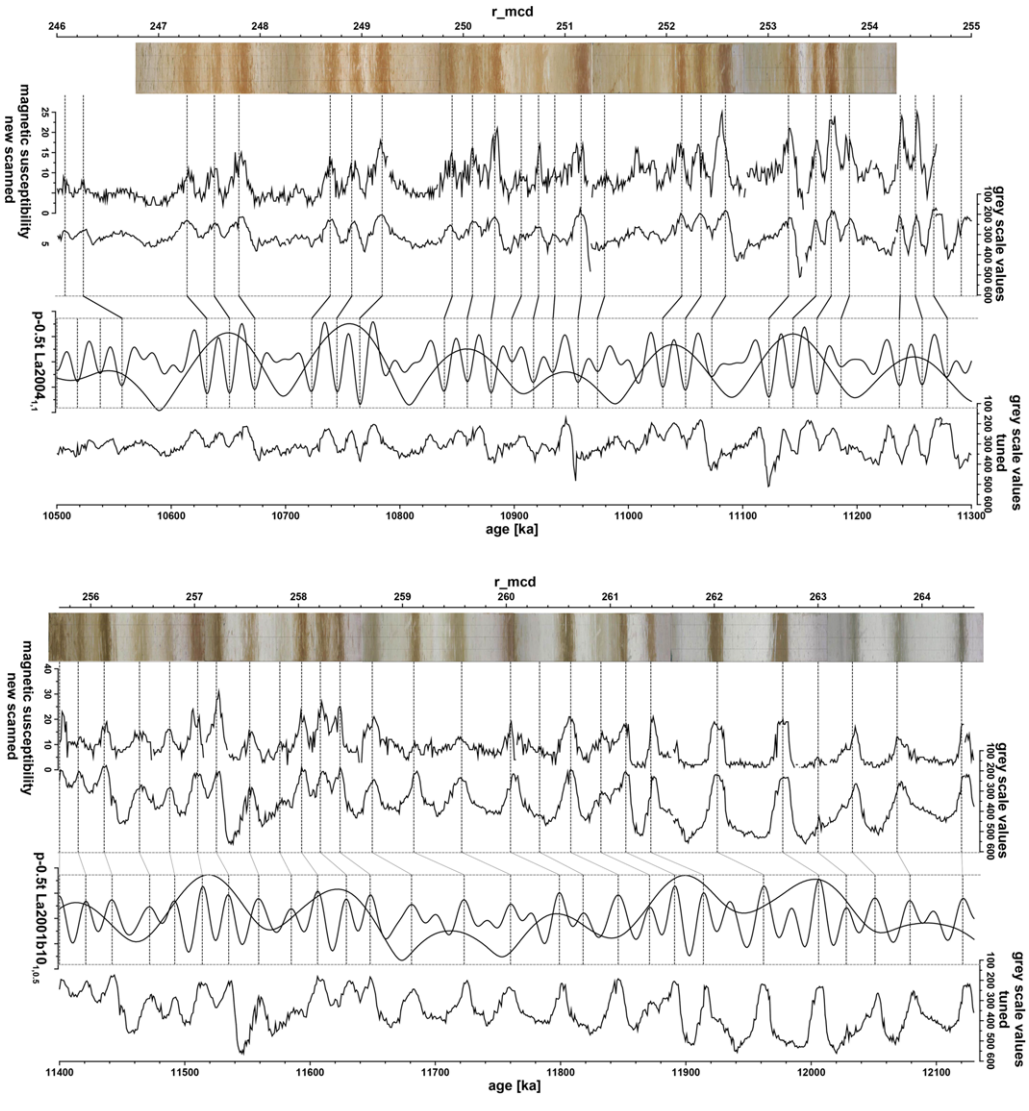

Fig. 4. Tuning of colour cycles in cores 25 (left) and 26 (right) of ODP Leg 154 Site 926A (after Zeeden *et al.* 2012). The initial age model for constraining the tuning is based on calcareous plankton biostratigraphy. Tuning was established from the top downwards after establishing a spliced record. Cycle patterns in core 25 are dominantly controlled by precession/eccentricity while the lower part of core 26 is dominated by obliquity. The excellent fit between the complex cycle patterns in the cores and the insolation target partly depends on values for tidal dissipation and dynamical ellipticity introduced into the astronomical solution. The abrupt switch to obliquity in core 26 is also seen in the insolation target and is related to a minimum in the very long 2.4 myr period eccentricity cycle.

systems to climate change is one of the most challenging and potentially rewarding research topics in fluvial sedimentology for the new millennium'.

The interpretation of lacustrine cycles in terms of precession forcing goes back to Bradley (1929) with his classic study of the Eocene Green River Formation in North America. Later work revealed the additional influence of the *c*. 100 kyr and 405 kyr eccentricity cycles through bundling of the precession-related cycles (Fischer & Roberts 1991; Machlus *et al.* 2008). Recently, cycles in the Wilkins Peak Member have been placed in a basin-scale cyclostratigraphic framework (Aswasereelert *et al.* 2012). The detailed stratigraphic framework

reveals that hiatuses are present in marginal settings, as expected, while basinal successions are continuous at Milankovitch time scales.

Mesozoic

Recently, the Maastrichtian part of the Zumaia section has been investigated in detail, using an integrated stratigraphic approach (Batenburg *et al.* 2012; Dinarès-Turell *et al.* 2013). The study was directed at establishing a carbon isotope stratigraphy and an astronomically tuned age model based on the 405 kyr cycle (this cycle is stable in the astronomical solution beyond 50 Ma) (see Laskar *et al.* 2011*a*; Westerhold *et al.* 2012). Combined with the nearby Sopelana section, the record covers almost the entire Maastrichtian in an essentially continuous succession (Batenburg *et al.* 2012, 2013). The continuity is confirmed by the excellent agreement with the tuned age model developed independently for the Maastrichtian in Deap Sea Drilling Project (DSDP)/ODP cores (DSDP Sites 525A and 762C, and ODP Site 1267B: Husson *et al.* 2011; Thibault *et al.* 2012; see Figs 7 & 8 in Batenburg *et al.* 2012). The ATS can thus be extended to the Campanian–Maastrichtian boundary once the Palaeogene time scale controversy is solved.

Upper Cretaceous cyclostratigraphy from the Western Interior Basin (WIB), USA, was assessed by Gilbert (1895) for an early astronomically based estimate of a 20 myr duration (with an uncertainty of 'either twice or only one-half') for Late Cenomanian–Coniacian time (Fischer 1980; Hilgen 2010). Recently, a detailed cyclostratigraphy and floating astrochronology was developed for the entire Niobrara Formation by Locklair & Sageman (2008) based on the 405 kyr cycle, using geophysical well logs and covering the entire Coniacian and Santonian stages with astrochronologic durations of 3.40 ± 0.13 myr and 2.39 ± 0.15 myr, respectively. Further cyclostratigraphic studies of the WIB focused on the Cenomanian–Turonian boundary interval (Meyers *et al.* 2012); this interval was extended both upwards and downwards by Ma *et al.* (2014) (see also the section on *Radio-isotopic ages consistent with Milankovitch forcing*). Evidence of Milankovitch forcing in the terrestrial record of the Late Cretaceous (Turonian–Santonian) has also been reported in lacustrine sediments of the Songliao Basin in China (Wu *et al.* 2009, 2013*a*).

The Lower Cretaceous rhythmic pelagic succession exposed in the northern Apennines, Italy provides another classic example of Milankovitch cyclicity. The succession is well exposed in the Contessa and Bottaccione river valleys near Gubbio (e.g. Lowrie *et al.* 1982). Following integrated stratigraphic studies, including cyclostratigraphy, the succession may well be continuous over tens of millions of years (Sprovieri *et al.* 2013). Classic studies further come from the 77-m-long Piobbico core (Herbert *et al.* 1995; Grippo *et al.* 2004). A recent detailed cyclostratigraphic study of this core produced a floating astrochronology of 405 kyr cycles indicating a duration of 25.85 myr for the combined Albian–Aptian stages in an apparently continuous succession (Huang *et al.* 2010*a*).

Magneto- and biostratigraphic boundary ages provide the main independent time controls for Jurassic cyclostratigraphy. The exception is the basal Jurassic, which is highly precisely radioisotope dated and intercalibrated with cyclostratigraphy (Blackburn *et al.* 2013). Multi-million year long cyclic marine sequences from the Kimmeridgian–Tithonian (Weedon *et al.* 2004; Boulila *et al.* 2008; Huang *et al.* 2010*b*), Oxfordian (Boulila *et al.* 2010), Toarcian (Boulila *et al.* 2014), and Sinemurian–Hettangian (Ruhl *et al.* 2010; Hüsing *et al.* 2014) with high-resolution records of total organic carbon, carbon isotopes, carbonate content and magnetic susceptibility show evidence for distinct 405 kyr orbital eccentricity cycles. Most of these sequences have been tuned to interpreted 405 kyr cycles, resulting in a sharpening of higher-frequency power preferentially in the obliquity and precession bands.

The Triassic provides excellent examples of Milankovitch forcing in the continental successions of the Newark Basin (Olsen & Kent 1996, 1999; Olsen *et al.* 1996). The Newark series consists of cyclic lacustrine deposits that are supposedly continuous over *c.* 25 myr. The identification of 405 kyr, *c.* 100 kyr and *c.* 20 kyr cyclicity resulted in a floating astrochronology that has been anchored to an age of 201.464 Ma for the Triassic–Jurassic boundary based on radio-isotopic age constraints from basalts overlying the main Triassic portion of the lacustrine sediments (Kent & Olsen 2008; Olsen *et al.* 2011; Blackburn *et al.* 2013). Evidence for Milankovitch forcing also comes from Triassic fluvio-lacustrine and playa deposits in the North German Basin in Germany (Reinhardt & Ricken 2000; Szurlies 2007; Vollmer *et al.* 2008). Finally, the Triassic hemi-pelagic rhythmically bedded chert succession of Japan, covering some 30 myr, reveals a full hierarchy of precession and eccentricity cycles, including very low frequency components (Ikeda *et al.* 2010; Ikeda & Tada 2013).

Palaeozoic

Investigations are underway to seek evidence for Milankovitch forcing in the Palaeozoic. A prime example comes from the upper Permian marine sections of Meishan, the stratotype for the Changhsingian Stage, and Shangsi in China (Wu *et al.* 2013*b*). These sections were used to estimate an

astronomical duration of 7.793 myr for the Lopingian Epoch. Combined with multiple radioisotopic ages, this signifies an important first step towards extending the ATS into the Palaeozoic.

Anderson (1982, 2011) used annual laminae thickness counts to interpret Milankovitch forcing of more than 260 000 marine evaporite varves in the Late Permian (Ochoan) Castile Formation. Classical shallow marine cyclothems of the Carboniferous have been related to the *c*. 100 kyr and especially 405 kyr eccentricity cycles (Heckel 1986, 1994). They have been correlated from the Donets Basin in the Ukraine to their North American counterparts, suggesting a global forcing mechanism of sea level at Milankovitch timescales (Davydov *et al.* 2010; Martin *et al.* 2012). Further back in the Palaeozoic, the Devonian has produced examples of astronomical climate forcing in marine successions by mainly the precession and eccentricity. The evidence indicates an astrochronologic duration of 6.5 $\pm$ 0.4 myr for the Frasnian stage (House 1985; de Vleeschouwer *et al.* 2012*a*, *b*, 2013). The Early Palaeozoic has an extensive Milankovitch-band cyclostratigraphy (e.g. Read 1995) that is in need of high-quality geochronologic control and re-analysis (Hinnov 2013*a*).

Discussion

Milankovitch and the nature of the stratigraphic record

Integrated stratigraphy and completeness. The examples given in the first part of this paper provide evidence that astronomical climate forcing is recorded, that both marine and continental cyclic successions can be continuous over multi-million-year-long time scales, and that these successions can be used to build high-resolution time scales. The evidence mainly comes from applying an integrated stratigraphy approach. Integrated stratigraphy is the combined application of multiple stratigraphic subdisciplines, including biostratigraphy, magnetostratigraphy, chemostratigraphy, cyclostratigraphy and geochronology, to solve stratigraphic issues often related to geological time (e.g. Montanari *et al.* 1997; Abdul Aziz *et al.* 2008*b*). In the study of Milankovitch cycles, integrated stratigraphy is used to independently test whether sedimentary cycles are related to astronomical climate forcing by precession, obliquity and eccentricity, and whether successions are continuous at the Milankovitch time scale (Hilgen *et al.* 2003; Hüsing *et al.* 2009). It remains difficult to demonstrate such continuity by showing that all cycles with the shortest orbital period are recorded. In fact, this is at present only possible for the Neogene where initial magnetobiostratigraphic and radio-isotopic age models were used as the starting point for a stepwise tuning; large(r)-scale cycles were first tuned to eccentricity followed by the tuning of small-scale cycles to precession and insolation. The astronomical target curves show that all precession- and/or obliquity-related cycles are recorded (e.g. Lourens *et al.* 1996; Hüsing *et al.* 2009). The development and application of the marine isotope stratigraphy (Lisiecki & Raymo 2005), fully integrated with magnetobiostratigraphy, tells the same story for the Plio-Pleistocene. Such a continuity does not only hold for cyclic deep marine successions but also for continental successions of Neogene age (Abdul Aziz *et al.* 2003) (see also Fig. 3). For older time intervals, the integrated stratigraphic approach combined with an exact match in number of cycles between cyclic successions and target curves on the shortest Milankovitch time scales is not yet possible. Here, integrated stratigraphy is used to show that Milankovitch cycles are present. This approach further reveals that no major gaps are present, and there is no reason to assume that these successions might not be continuous, as we consider it unlikely that continuous successions are restricted to the Neogene. In an increasing number of cases, high-resolution precise radio-isotopic age determinations are fully consistent with, and thus confirm, the initial Milankovitch interpretation of the cyclicity. Issues related to the Milankovitch interpretation of cyclic successions, such as nature and continuity, independent testing and strength of forcing, are discussed in more detail below.

Chaos, continuity and sedimentation rate. Sadler (1981) used large compilations of accumulation rates and their dependence upon the measured time span to show that sedimentation rates follow an inverse linear relationship when plotted against time on a log-log scale, with proportionally more time missing at longer time scales. Such a negative power law is considered to be characteristic of fractal behaviour. Plotnick (1986) used the fractal 'Cantor bar' model of Mandelbrot (1983) to explain the log-linear relationship between sedimentation rates and the time span of Sadler (1981). Plotnick's hypothetical section showed an ever-increasing number of hiatuses at shorter time scales and that more time is missing at longer time scales. However, it is difficult to distinguish such a model in the real world from one where hiatuses are controlled by Milankovitch forcing (Kemp 2012). This is especially the case because shallow marine successions are notoriously difficult to date accurately, a problem that has troubled sequence stratigraphy from the beginning (e.g. Miall 1992). In that sense, shallow marine successions are more likely to follow the inverse power law of Sadler (1981) between

sedimentation rates and time than deep marine archives and to a lesser extent (deep) lacustrine successions.

Alleged fractal attributes of the stratigraphic record, such as the increase in cumulative length of hiatuses or its self-similarity and non-scale dependent nature, suggest that sedimentary processes are governed by non-linear dynamics and chaotic behaviour (Bailey 1998). Chaos theory predicts complex non-random responses from systems in which feedback mechanisms and thresholds are important, potentially competing with the Milankovitch hypothesis as an explanation for sedimentary cyclicity (Smith 1994). Complex dynamic systems may involve pseudo-periodic repetition, but lack predictability. Smith (1994) does not envisage chaos theory as an alternative explanation for Milankovitch cyclicity, but rather that external forcing controlled by the astronomical parameters may interact with a complex dynamical system (i.e. the climate and depositional system), for example through phase locking with the external oscillator and reinforcing or dampening the original forcing. In that case, the initial astronomical forcing will still be preserved as cyclic variations in the stratigraphic record. Indeed, the response of the climate and depositional system to astronomical forcing is expected to include non-linearity and thresholds (see section on *Rectification and distortion*), but this does not preclude that the initial forcing is recorded as cycles in the stratigraphic record.

Bailey (1998) argues that the dynamic systems that govern the stratigraphic record are so complex and chaotic, and their output so repetitive, that it is tenuous to assume that any recorded cyclicity may reflect the initial cyclic forcing by a deterministic periodic system. Algeo & Wilkinson (1988) argue that the recurrence of regular alternations in the Milankovitch frequency band is coincidental and related to sedimentary processes constrained by subsidence. They cite fluvial channel migration and deltaic lobe switching as examples of sedimentary processes governed by internal autogenic processes and thus by a non-linear dynamic system. However, there is evidence that river avulsion may in some cases be dictated by astronomically forced climate change rather than by autogenic control (see sections on *Pleistocene* and *Palaeogene*); this evidence is supported by independent time control (Abels *et al.* 2012). Thus, an integrated stratigraphic approach and, in particular, independent radioisotopic age control is critically important to distinguish among different working hypotheses for stratigraphic cyclicity, as the Milankovitch theory has well-defined expectations in terms of cycle thickness and scale. It is this approach that is advocated in the present paper.

Kemp (2012) modelled the behaviour of the shallow marine depositional system, starting from a cyclic model of sedimentation in combination with stochastic variability. Accordingly, hiatuses pervade successions at shorter time scales potentially associated with Milankovitch control, but these successions may be continuous on time scales equal to and longer than the forcing period. Kemp further observed a step in the Milankovitch frequency band in the data of Sadler (1981) from shallow marine settings, and linked that step to the prevalence of hiatuses related to the *c*. 100 kyr cycle (Kemp 2012, his Fig. 4). Sadler (1999) arrived at the same Milankovitch interpretation of hiatuses to explain the observed slope steepening in a sedimentation rate v. time plot for shallow marine successions (see also Kemp & Sadler 2014).

Deep-sea data were included in the analysis of the continuity of the stratigraphic record in a similar way (Anders *et al.* 1987; Sadler & Strauss 1990). Anders *et al.* (1987) examined pelagic sediments from the DSDP database and concluded that sediment is preserved in at least 65% of 100 kyr scale intervals. Thus they supported the conclusion that pelagic environments produce sequences of calcareous oozes with only rare hiatuses and generally higher completeness. The deep marine archive is most suitable for demonstrating the registration and preservation of astronomical climate forcing in the form of Milankovitch cycles in the stratigraphic record and for using the cycles to build astronomically tuned time scales with unprecedented accuracy, precision and resolution. Before the recovery of the first deep-sea piston cores, it was generally assumed that deep marine records would be continuous. However, the deep marine record proved more fragmentary than anticipated, from disturbances caused by, for example, deep-sea currents, basin starvation and slumping as a consequence of earthquakes and slope oversteepening (e.g. Keller & Barron 1983; Aubry 1991). Nevertheless, various areas remained relatively undisturbed during prolonged time intervals. These areas are often targeted for palaeoclimate-oriented legs in deep-sea drilling as they are located away from the continental margins on submarine highs and suitable for recovering the pelagic signal above the CCD. This approach makes carbonate-rich successions with higher sedimentation rates available that are excellent archives for palaeoclimatic studies and astronomical tuning. Today, much is known about the seafloor from previous drilling and seismic surveys, and sites can be carefully selected to ensure stratigraphic continuity for particular intervals. For instance, temporal reconstruction of the CCD played an important role in the selection of IODP (International Ocean Discovery Program) Leg 320/321 drilling sites (Pälike *et al.* 2009,

2012). As a consequence, numerous long records are now available from the ocean that are continuous often for several millions to tens of millions of years, as proven by integrated stratigraphic studies. Hiatuses are detected using integrated stratigraphy (e.g. Gale *et al.* 2011) or spectral analysis (Meyers & Sageman 2004).

The analysis of Anders *et al.* (1987) does not take into account the deep-sea sections and cores that were subsequently drilled and used to construct the Cenozoic ATS. The age control of these sections and cores, which is based on astronomical tuning and independently confirmed by magnetobiostratigraphic and radio-isotopic dating, is excellent. At the Milankovitch time scale, these successions are continuous over millions of years and have sedimentation rates that are near constant or only slightly varying. The variations may also be related to the cyclicity itself (Herbert 1994; Van der Laan *et al.* 2005) or represent longer-term tectonic or climatic trends. The sediment accumulation rates of these successions will likely have fluctuated on short time scales below 10^4 years. Sedimentation in the pelagic realm, for example, is partly dictated by seasonal changes in carbonate–biogenic opal production and terrigenous input (e.g. Turner 2002). As a consequence, El Niño and, on longer-time scales, centennial- and millennial-scale cycles will have had their impact. Nevertheless, it has been shown that sedimentation rate can be near constant at 10^4-yr to occasionally 10^6-yr time scales. Consequently, these successions will plot as a horizontal line in sedimentation rate v. time on a log-log scale (see Fig. 3 of Anders *et al.* 1987), with sedimentation rate being essentially the same over five to seven temporal orders of magnitude. Prime examples of such successions are the Capo Rossello composite and Monte dei Corvi-La Vedova sections of the Mediterranean Neogene (Hilgen 1991*a*, *b*; Lourens *et al.* 1996; Hüsing *et al.* 2009), Ceara Rise and Walvis Ridge sites in the Atlantic (e.g. Lourens *et al.* 2005; Westerhold *et al.* 2007; Liebrand *et al.* 2011; Zeeden *et al.* 2012) and ODP Site 1218 for the Oligocene in the Pacific (Pälike *et al.* 2006*a*). As a consequence, these sections/cores do not follow the inverse power law between sedimentation rate and time of Sadler (1981) below 10^6-yr time scales. However, the treatment of, for example, Sadler (1981), is a statistical one and does not exclude that successions are continuous on the Milankovitch time scale over 10^5–10^6 years. Another example of a continuous marine record comes from the evaporite cycles of the Permian Castile Formation where Anderson (1982) demonstrated Milankovitch control of sedimentary cycles on annual lamina thickness counts, comprising in total more than 260 000 years. Annual laminae were shown to be continuous for distances up to 113 km in the basin (Anderson *et al.* 1972). These laminae further revealed the presence of sub-Milankovitch periodicities in addition to the annual cycle and precession and eccentricity control (Anderson 2011). It suggests an essentially continuous and only slightly variable sedimentation rate over five temporal orders of magnitude.

Such examples are not restricted to the marine record but include the continental record as well. Bradley (1929) used laminae thicknesses in the oil shales of the Eocene Green River Basin to underpin his precessional interpretation of sedimentary cycles, which are now known to be part of *c*. 100 kyr and 405 kyr eccentricity related bundles (Roehler 1993; Machlus *et al.* 2008; Meyers 2008). As with the Permian evaporites, this implies near constant and continuous sedimentation rates over at least six temporal orders. Other examples come from lacustrine successions of the Miocene in Spain and the Triassic Newark Basin succession in North America, while in these cases continuity and near constant sedimentation rates are not shown to start at the annual scale.

Fluvial successions may also be continuous over millions of years at Milankovitch time scales. An important example is the Eocene Bighorn Basin in North America (see section on *Palaeogene*). In this case, the formation of long and continuous fluvial successions occurs in settings favoured by relatively high subsidence rates. Despite continuity in the fluvial succession in the Bighorn Basin at the Milankovitch scale, sedimentation within the shortest precession-related cycles is likely discontinuous and sporadic (Abels *et al.* 2013). As a consequence, sediment accumulation rates remain constant from the precession cycle upwards over two to three temporal orders of magnitude, again not following the inverse relation between sediment accumulation rate and time. At the same time, successions deposited in a more marginal setting of the same basin might be less continuous and follow the inverse rule. This is likely also the case for the lacustrine successions of the Eocene Green River Basin where marginal successions do not record all the forcing cycles and are therefore less complete than the basinal successions (e.g. Aswasereelert *et al.* 2012).

Shallow marine and continental successions are vulnerable to erosion and are thus particularly susceptible to hiatuses. This opens the possibility that the inverse relation observed by Sadler (1981) is partly biased towards stratigraphic successions affected by (global) sea level located in marginal marine settings. Such a bias may also be related to the vast literature and interest in eustasy and sequence stratigraphy, while the cyclostratigraphic community has focused mainly on deep marine archives in the search for continuous records of

climate change. The deep marine archives represent a significant portion of the total archive and should not be overlooked when exploring the nature of the stratigraphic record. Ideally, these complementary, and not opposing, views of the stratigraphic record should be reconciled before a true understanding of the nature of the stratigraphic record can be achieved. Steps in this direction have been made by Schlager (2010) and Kemp (2012).

The significance of cyclostratigraphic spectra

Hypothesis testing. A fundamental problem in cyclostratigraphy is whether or not the hypothesis of astronomical forcing (H1) is supported by representative data. H1 is presented as a time series with astronomical frequencies – for example, insolation – presumed to be consistent with the data. The null hypothesis (H0) is taken as the case for no Milankovitch forcing, for which a noise time series (null model) is assumed that is also consistent with the data. The goal is to attempt to reject H0 by comparing the data with the null model within the statistical constraints of the data, and to accept H1. Two errors accompany this procedure: Type 1 errors, or 'false positives' or 'false alarms,' that is, rejecting H0 when H0 is true, and Type 2 errors, or 'false negatives,' that is, accepting H0 when H1 is true.

In the basic hypothesis test, the data spectrum ('spectrum' short for 'power spectrum') is compared to a noise (the 'null') spectrum. Spectrum estimators have statistical properties that allow the construction of confidence intervals defined by a (χ^2-distributed) probability level α. The lower confidence limit (CL) of the data spectrum is compared with the noise spectrum; if data power at the lower CL exceeds noise power at a given frequency (or frequencies), H0 may be rejected. The practice has developed to graph the noise spectrum, using the data spectrum CL factor to reposition the noise spectrum at an equivalent 'significance level' relative to the data spectrum. This allows convenient assessment of multiple CLs in terms of noise spectrum significance levels plotted together with the data spectrum.

Recently, Vaughan *et al.* (2011) identified shortcomings in this approach. First, there is usually no accounting for multiple tests in the case of many independent frequencies. This means that the probability level α used to set the threshold confidence interval should be adjusted downwards: this is known as the Bonferroni correction. A discussion of multiple tests in climate spectral analysis is given in Mudelsee (2010). Second, the first-order autoregressive (AR(1)) model commonly adopted as the null model for hypothesis testing often does not describe the data well. Alternative approaches include a simple or bending power law null spectrum (Vaughan *et al.* 2011; Kodama & Hinnov 2014).

The sedimentation rate problem. Sedimentary cyclicity implies changes in sedimentation rate and is inherent to cyclostratigraphy (Herbert 1994). The result is an uncertain, distorted time scale and frequency dispersal of spectral power (Meyers *et al.* 2001; Westphal *et al.* 2004). The problem leads to elevated false negatives if α is too small. Therefore, a balance must be found between the issues of false positives v. statistical power (or false negatives). The overriding challenge is to estimate the sedimentation rate variations.

Geologists have long recognized the role of the insolation 'canon' as a built-in time scale for cyclostratigraphy. Thus arose the practice of 'astronomical tuning' to estimate and reduce the distorting effects of variable sedimentation rates. Astronomical tuning can be as all-encompassing as matching a cyclic data sequence to an assumed insolation-based model – a long-used technique (e.g. Hays *et al.* 1976; Imbrie *et al.* 1984; Lourens *et al.* 1996, 2004; Lisiecki & Raymo 2005; and countless others, including results presented in this paper, Figs 2–5 & 7) – or as simple as tuning to a single frequency, for example, the 405 kyr eccentricity cycle (e.g. Kent & Olsen 1999; Grippo *et al.* 2004; Huang *et al.* 2010*a*, *b*; Wu *et al.* 2013*b*; and many others). An independent time scale is needed for initial calibration to an astronomical target, for example, radio-isotope dating of ashes in the section that is to be tuned, or dated ashes from elsewhere and projected into the section by bio-chemo-magnetostratigraphic correlation. Astronomical tuning also has disadvantages and must be applied with caution (see section on *Tuning-induced Milankovitch spectra*).

Rectification and distortion. Stratigraphic distortion leads to dispersal of spectral power with the emergence of side bands and harmonics as spectral artefacts (Herbert 1994; Meyers *et al.* 2001; Westphal *et al.* 2004). The cycle with the highest frequency (usually related to precession) undergoes the most intense distortion and peak broadening. In case of multiple distortions from eccentricity-modulated changes in sedimentation rates, it will become hard to recognize the higher frequency periodicities with conventional spectral methods even in the case of a purely deterministic sedimentary series (see Fig. 8 in Herbert 1994). Importantly for our discussion, this distortion is accompanied by an apparent lowering of the significance level of spectral power.

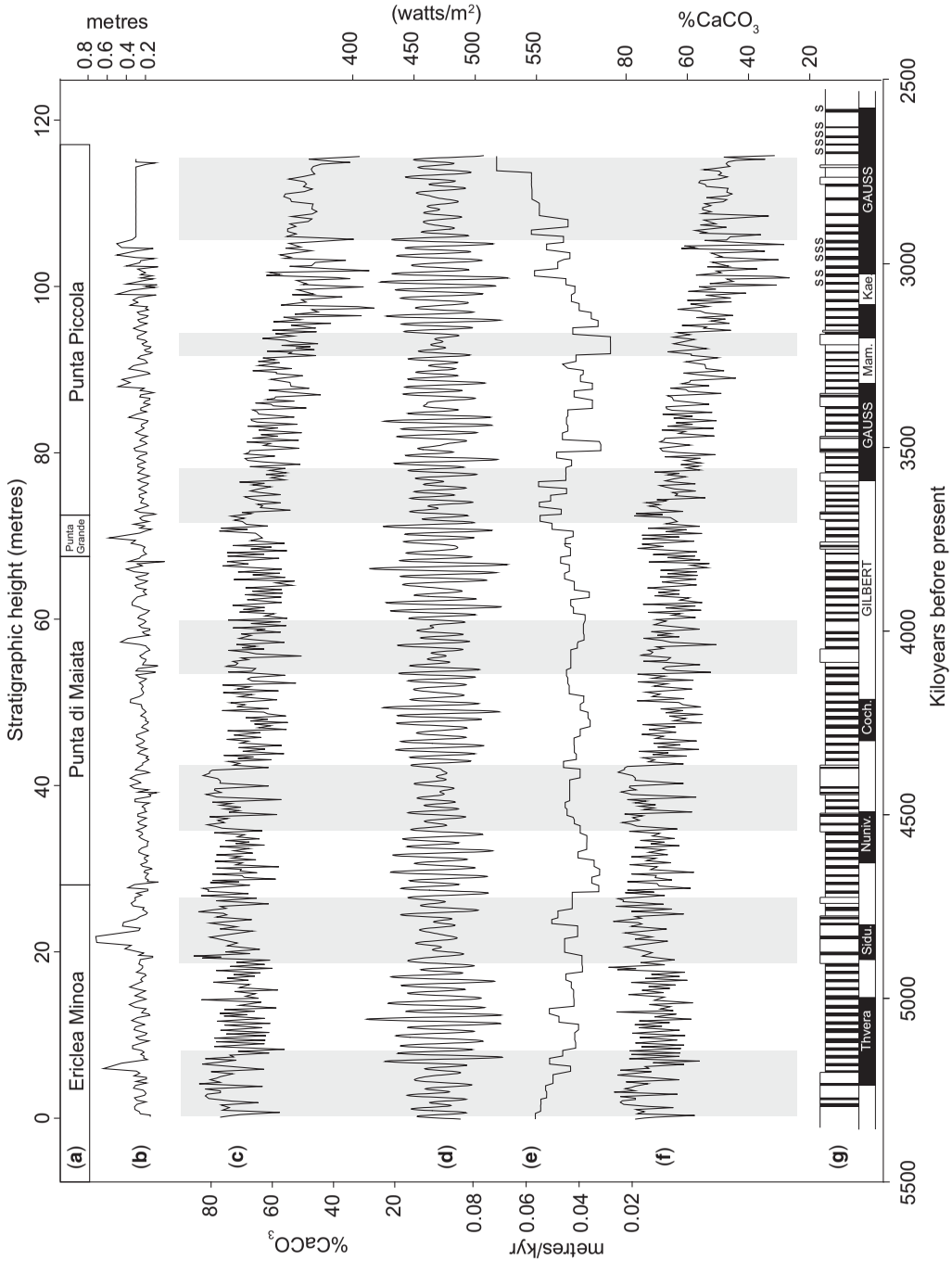

Ripepe & Fischer (1991) (see also Fischer *et al.* 1991) modelled a sinusoidal precession index forcing function, which is subsequently distorted by a non-linear response of the climate system, followed by non-linear recording in the stratigraphic domain, and lastly, subjected to effects of bioturbation. With each step, more power is transferred from the precession into the eccentricity band: the final spectrum is dominated by eccentricity, while precession-related peaks are almost eliminated. This modelled spectrum compares favourably with the carbonate spectrum of the Albian Fucoid Marls in the Piobbico core (Italy). The dominance of eccentricity in the spectrum cannot be explained by the direct effect of *c*. 0.25% of eccentricity on annual global insolation, but results from the eccentricity modulation of the precessional amplitude (e.g. Fig. 7 in Grippo *et al.* 2004). This implies that the precession cycle is present but masked by the disturbing effects of non-linear responses, thresholds and mixing. As a consequence of these complications, the power in the precession band is significantly reduced. Nevertheless, precession-related cycles can still be visually detected as thin black shale layers bundled in clusters that reflect the eccentricity modulation of the precession amplitude (see Fig. 11 in Hinnov 2013*b*). It is important to emphasize that eccentricity does not register in the spectrum of the precession index (or insolation forcing), as it only modulates precession amplitude. Thus, the presence of eccentricity in palaeoclimatic spectra is explained by non-linear or rectifying responses of the climate and/or depositional system to astronomical forcing (Weedon 2003; Huybers & Wunsch 2003). The eccentricity modulation of the precession signal can be investigated in these records (e.g. Hinnov 2000) although with caution (Huybers & Aharonson 2010; Zeeden *et al.* 2013). Such distortions also point to the problem of false negatives rather than that of false positives in the spectral analysis of palaeoclimatic records. The precession-related spectral peaks in Ripepe & Fischer (1991) hardly rise above background, despite the fact that precession completely dominated the original forcing.

Examples. We demonstrate spectral analysis and hypothesis testing of two sedimentary records in which the presence of Milankovitch cycles is generally accepted: (1) the marine carbonate record of the Pliocene Capo Rossello composite section (RCS), Sicily (5.3–2.7 Ma) (Hilgen & Langereis 1989; Langereis & Hilgen 1991), and (2) the marine benthic oxygen isotope and weight percent aluminium records of the Late Miocene Ain el Beida (AEB) section, Morocco (6.5–5.5 Ma) (Krijgsman *et al.* 2004; Van der Laan *et al.* 2005, 2012). The astrochronology of both records is supported by independent magnetobiostratigraphic age models, which are based on magnetostratigraphic calibration to the geomagnetic polarity time scale (GPTS). The purpose of the analysis is to assess the (in-) adequacy of the AR(1) null model and to evaluate false negatives at the 99% CL. To highlight typical issues arising in these analyses, we present two approaches: (1) Lomb–Scargle (L–S) spectral analysis for unevenly spaced time series using REDFIT (Schulz & Mudelsee 2002); and (2) prolate multi-taper spectral analysis for evenly spaced time series using the Matlab procedure of RedNoise_ConfidenceLevels (Husson 2013). The confidence levels in the examples were estimated without considering a multiple test correction as advocated by Vaughan *et al.* (2011), although REDFIT provides information for such a correction ('Critical false-alarm level'; see Figs 6 & 8). While we acknowledge the strict statistical view taken by Vaughan *et al.* (2011), we also have to take account of competing problems such as 'false negative' assessments resulting from stratigraphic distortions, coupled with the low spectral power for the short eccentricity (*c*. 100 kyr) terms.

Pliocene Capo Rossello, Sicily. The RCS covers the entire Pliocene in a rhythmic deep marine succession (Hilgen & Langereis 1989). The tuning of the RSC underlies the standard GTS for this time interval. The origin of the carbonate cycles is complicated as carbonate dilution, dissolution and productivity all play a role (Van Os *et al.* 1994). A special characteristic of the basic precession-related carbonate cycles in the RCS is their quadripartite build-up with two carbonate maxima and minima per cycle (Fig. 5). The minima occur in the grey and beige marl beds of the basic grey-white-beige-white colour cycles. The grey marl beds have been tuned to summer insolation maxima

Fig. 5. Carbonate record of the Capo Rossello composite section (RCS) (Hilgen & Langereis 1989). (**a**) The four localities on Sicily contributing to the composite section. (**b**) Stratigraphic spacing for the collection of samples for carbonate content analysis; the average spacing is $\Delta d = 0.25$ m. (**c**) Carbonate content as a function of composite stratigraphic height. (**d**) Mean June plus July insolation at 65° North according to the La2004 nominal solution (calculated with AnalySeries 2.0.4.2), with increasing insolation downward. (**e**) Sedimentation rates estimated from tuning the succession of insolation maxima in (d) to the grey marl beds of the RCS (depicted as black layers in (g)). (**f**) Carbonate content as a function of time based on tuned age model. (**g**) Above: RCS bedding with white and beige marls (white layers) and grey marls (black layers); below: geomagnetic polarity chrons in the RCS.

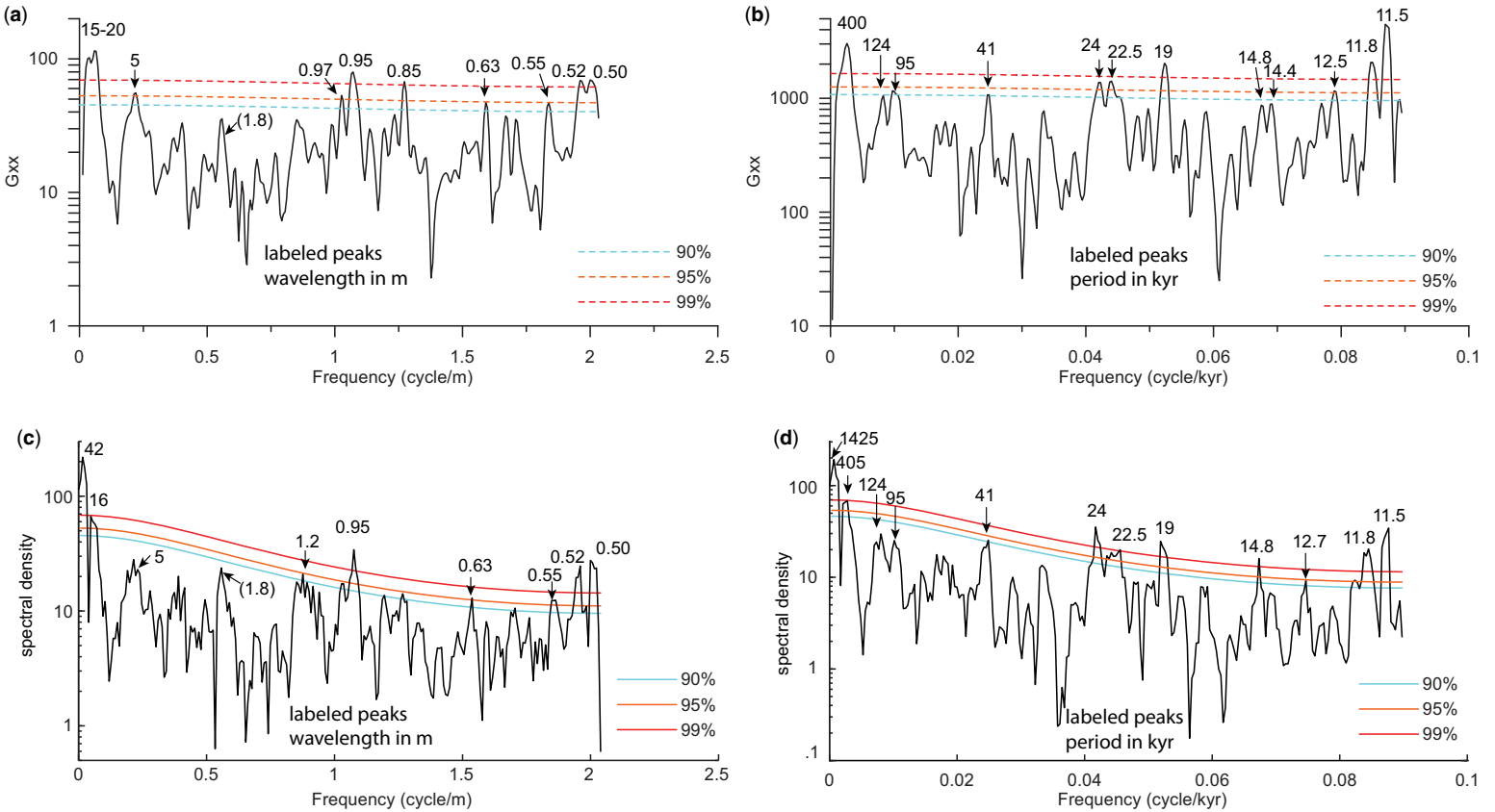

(Fig. 5), as they are equivalent to sapropels, which are known to correspond to insolation maxima (Lourens *et al.* 1996, 2004). The RCS carbonate record was originally analysed using the Blackman–Tukey correlogram method, applying an 80% CL (Hilgen & Langereis 1989). Here we analyse the RCS carbonate record, untuned in the stratigraphic domain and tuned in time to the La2004 astronomical solution (Lourens *et al.* 2004; Fig. 5). The astronomical tuning assigns grey marl and sapropel midpoints to maxima of the 65°N summer insolation curve. The sedimentation rate curve that results from this tuning is shown in Figure 5.

The untuned carbonate L–S spectrum (Fig. 6a) reveals peaks of 15–20 m and of 0.95 m and 0.85 m that are significant at 99% CL: these correspond roughly to long eccentricity (405 kyr) and to 23 kyr and 19 kyr precession. Another peak above 99% CL occurs at 0.5 m, which is close to the Nyquist frequency of the original sample set. This results from the quadripartite structure of the precession-related cycles. The *c*. 5 m peak associated with the short eccentricity cycle is significant at 95% CL, while an obliquity-related peak at *c*. 2 m falls far below these CLs. This obliquity influence is weak compared to the precession–eccentricity combination, but it is consistently found in the Mediterranean Neogene, and precession–obliquity interference patterns in the RCS reveal a close fit with the astronomical target curve (Lourens *et al.* 1996; Hilgen *et al.* 2003).

The tuned carbonate L–S spectrum (Fig. 6b) reveals 405 kyr, 19 kyr and 11.5 kyr peaks significant at 99% CL, 24 kyr and 22.5 kyr peaks significant at 95%, and 124 kyr, 95 kyr and 41 kyr peaks significant at 90%. Enhancement and sharpening of spectral peaks at the obliquity and precession frequencies is expected, due to tuning, to a mix of obliquity and precession in the insolation target curve. However, the low (90%) CL of the obliquity peak is unexpected, because it is a tuned frequency. The appearance of eccentricity terms is also not expected and can be interpreted as independent evidence for astronomical forcing. The eccentricity is present due to signal rectification of the precession forcing by deposition (see discussion above) (Ripepe & Fischer 1991). Moreover, the observed CLs of the long (405 kyr) and short (124 kyr and 95 kyr) eccentricity terms follow expectation: over multi-million year-long time intervals, the long eccentricity cycle advances as a single 405 kyr term and therefore registers at a high spectral CL, but short eccentricity continually fluctuates in periodicity between 132 kyr and 95 kyr and cannot achieve a high spectral CL (e.g. Table 3 in Meyers 2012). This is reflected in the >99% CL of the 405 kyr peak and the *c*. 90% CL of the 124 kyr and 95 kyr peaks in the tuned spectrum. The presence of two carbonate minima per precession-related cycle is reflected by the dominant 11.8 kyr and 11.5 kyr peaks.

The multi-tapered spectra (Fig. 6c & d) bear out similar results as the L–S spectra, but there are also significant differences. The resolution of the spectra is similar: the multi-tapered spectra have eight degrees of freedom (dofs) compared with seven dofs in the L–S spectra. The estimated AR(1) null spectra for the L–S spectra are very 'white', that is, there is little decline to lower power toward the Nyquist frequency. In the multi-tapered spectra, the AR(1) null spectra, which are computed with the data linearly interpolated to the average sample spacing, have a classic 'red' structure, tapering to low power toward the Nyquist frequency. In the multi-tapered spectra, not one but two high-power spectral peaks are measured in the lowest frequencies, at 42 m and 16 m in the untuned spectrum, corresponding to 1425 kyr and 405 kyr periods in the tuned spectrum. Possibly the original non-uniform sampling has a systematic bias that enhances low frequencies when the data are linearly interpolated. In the untuned precession band, one peak at 0.95 m exceeds the 99% CL, although in the tuned multi-tapered spectrum all three precession terms (24 kyr, 22.5 kyr and 19 kyr) are present at the 99% CL.

Fig. 6. Spectral analysis of the Pliocene RCS carbonate record using REDFIT (Schulz & Mudelsee 2002) and RedNoise_ConfidenceLevels (Husson, 2013). (**a**) Untuned L–S spectrum: OFAC = 4.0, HIFAC = 1.0 (compute Nyquist range), n50 = 5, Iwin = 0 (no tapering), Nsim = 2000; variance = 50.92, Avg. Δd = 0.24 m, Avg. Nyquist = 2.04 cycles/m, Avg. autocorr. coeff. $\rho = 0.03$, Avg. $\tau = 0.07$ m, degrees of freedom = 7.14, 6-dB Bandwidth = 0.03 cycles/m, critical false-alarm level = 99.36%, corresponding scaling factor for red noise = 2.78. (**b**) Tuned L–S spectrum: OFAC = 4.0, HIFAC = 1.0 (compute Nyquist range), n50 = 5, Iwin = 0 (no tapering), Nsim = 2000; variance = 53.27, Avg. Δt = 5.57 kyr, Avg. autocorr. coeff. $\rho = 0.03$, Avg. $\tau = 1.59$ kyr, degrees of freedom = 7.14, 6-dB bandwidth = 0.001 cycles/kyr, critical false-alarm level = 99.36%, corresponding scaling factor for red noise = 2.78. (**c**) Untuned 2π multi-tapered spectrum: the 115.48 m-long stratigraphic carbonate record was linearly interpolated to the mean sample spacing of 0.24 m; four 2π prolate tapers provide spectral estimates with 8 degrees of freedom (dofs) and an averaging bandwidth of 4/(115.48 m) = 0.03 cycles/m; estimated $\rho = 0.37$. (**d**) Tuned 2π multi-tapered spectrum: The 2623.2 kyr-long tuned carbonate time series was linearly interpolated to the mean sample spacing of 5.57 kyr; four 2π prolate tapers provide spectral estimates with 8 dofs and an averaging bandwidth of 4/(2623.2 kyr) = 0.001 cycles/kyr; estimated $\rho = 0.42$.

As with the tuned L–S spectrum, two short eccentricity terms are well separated and visible at 124 kyr and 95 kyr in the tuned multi-tapered spectrum but do not even attain 90% CL. As with the tuned L–S spectrum, there are dominant peaks at 11.8 kyr and 11.5 kyr, related to the double carbonate minima between sapropels. Other significant terms possibly related to the precession index are present at 14.8 kyr and 12.7 kyr (small theoretical terms in the La2004 solution occur at 14.9 kyr, 14.4 kyr and 13.0 kyr, see also *Stability of astronomical frequencies in the past*).

Miocene Ain el Beida (AEB), Morocco. An example of distortion in the stratigraphic domain is provided by the Miocene marine AEB section, where sedimentary cyclicity is dominantly related to carbonate dilution by clastic input (Van der Laan *et al.* 2005). The AEB section has a reliable magnetobiostratigraphy and records the onset of the Messinian Salinity Crisis (MSC) with strong cyclic sedimentation (Krijgsman *et al.* 2004). Changes in sedimentation rate with increases up to five times background values occur in the thickest and most prominent reddish marl layers. These have been interpreted as controlled by eccentricity-related changes in precession amplitude at times of precession minima (strong *c.* 100 kyr cycles in Fig. 7f). This causes frequency displacements of the precession-related spectral peaks and broadening of the obliquity-related peak. These distortions disappear from the spectrum after applying astronomical tuning to the section, as will be demonstrated below. For the astronomical tuning, midpoints of the reddish and beige layers (Fig. 7i) were used as calibration points: reddish layers are correlated to $La2004_{(1,1)}$ 65°N summer insolation maxima, and beige layers to insolation minima (Van der Laan *et al.* 2012). Here we analyse the benthic marine oxygen isotope ($\delta^{18}O$) and weight percent aluminium (%Al) records of the AEB section.

The untuned $\delta^{18}O$ L–S spectrum (Fig. 8A a) reveals 1.20 m, 1.82 m, 2.43 m and 3.46 m spectral peaks at the 99% CL. Following tuning (Fig. 8A b), 12.4 kyr, 19 kyr, 23 kyr and 41 kyr spectral peaks appear, all significant at the 99% CL, as well as sub-Milankovitch peaks at 6.6 kyr and 6.0 kyr (these latter, however, are at power levels that are an order of magnitude lower than the Milankovitch terms). The tuned and untuned $\delta^{18}O$ multi-tapered spectra have the same four spectral peaks that calibrate to precession and obliquity, but no significant sub-Milankovitch power.

The untuned %Al L–S spectrum (Fig. 8B a) reveals many significant peaks in the spectrum, except for $f < 0.3$ cycles/m (wavelengths greater than 3 m). It has a high-power 1.85 m peak at the 99% CL in common with the untuned $\delta^{18}O$ spectrum, as well as a 2.43 m peak at the 95% CL, but no *c.* 3.4 m peak: and there is an 8.8 m peak at the 99% CL in the %Al spectrum that does not appear in the untuned $\delta^{18}O$ L–S spectrum. The tuned %Al L–S spectrum (Fig. 8B b) shows how the high-power untuned peaks have now shifted into the precession band (19 kyr and 23 kyr) at the 99% CL: there is no obliquity peak, but a weakly significant 100 kyr peak at the 90% CL. Additionally, there are multiple sub-Milankovitch peaks exceeding the 99% CL at very low power levels. The tuned and untuned %Al multi-tapered spectra each have five spectral peaks that correspond to precession, obliquity and short eccentricity, but register no significant sub-Milankovitch power.

Implications. Astronomical tuning produces palaeoclimatic time series that are vulnerable to circular reasoning (see section on *Tuning-induced Milankovitch spectra*). The RCS and AEB records were tuned to insolation dominated by the obliquity and precession; consequently, the obliquity and precession bands of the tuned records are expected to acquire spectral peaks with high significance. The eccentricity, however, is not present in the insolation at a measurable level, and so tuned spectral terms that are sharpened in the eccentricity band provide impartial evidence for astronomical forcing.

The following conclusions can be drawn for RCS:

(1) Significant sedimentation rate variations distort the time scale and hence the spectrum of the carbonate record.
(2) Correcting the RCS time scale by astronomical tuning sharpens precession and obliquity frequencies, and importantly, aligns low-frequency variations to the three main eccentricity terms: 405 kyr, 124 kyr and 95 kyr.
(3) The short eccentricity terms at 124 kyr and 95 kyr do not achieve a high CL, but this is an expected outcome (Meyers 2012) and an example of false negatives.
(4) The low CL of the tuned obliquity term is evidence of another false negative.
(5) The non-uniform sampling of the RCS carbonate record significantly affects the spectrum estimation and AR(1) null modelling, although in this case the applied L–S and multi-taper algorithms resulted in consistent outcomes (see Appendix for discussion on *Differences in the L–S and multi-taper spectra*).

To summarize the AEB example:

(1) The section shows evidence for significant changes in sedimentation rate related to precession amplitude that distort the spectrum (see also Van der Laan *et al.* 2005).
(2) The $\delta^{18}O$ spectrum shows significant obliquity and precession spectral peaks, whereas

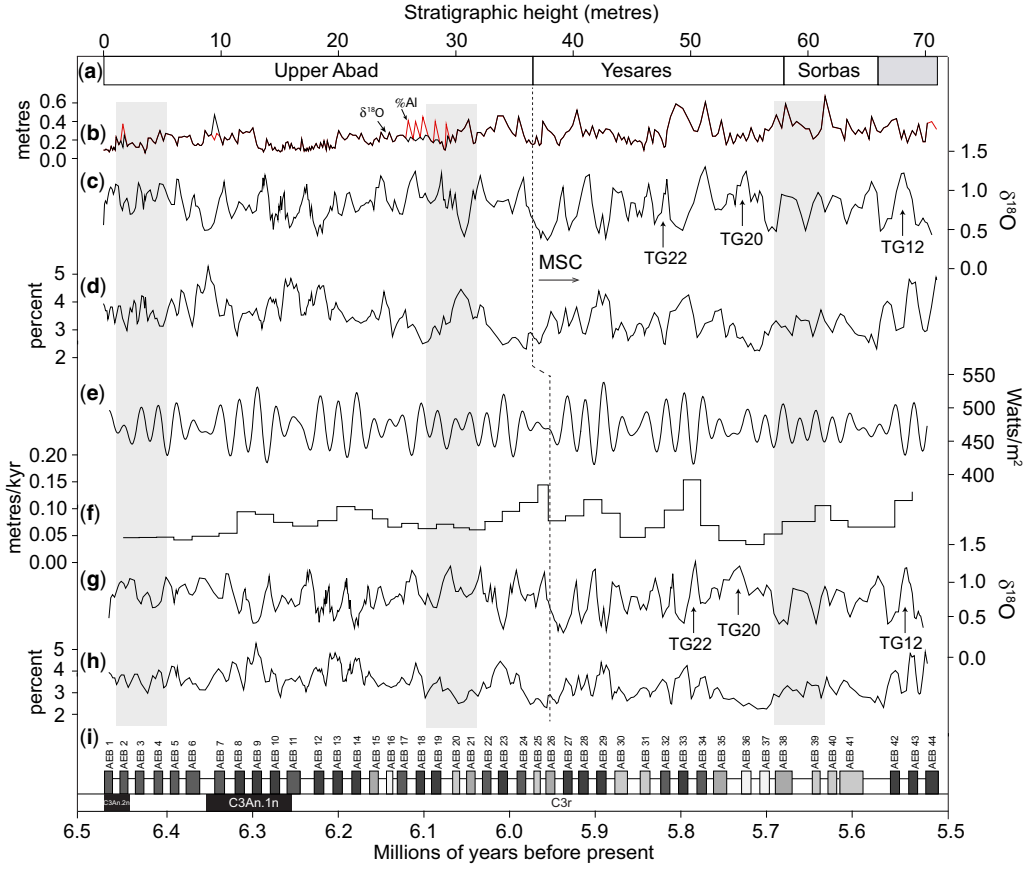

Fig. 7. Benthic $\delta^{18}O$ and weight percent aluminium records of the Upper Miocene Ain El Beida (AEB) section, northwestern Morocco (Van der Laan *et al.* 2005). MSC = Messinian Salinity Crisis. (**a**) Formations: the Upper Abad is part of the pre-evaporitic Messinian, and the Yesares and Sorbas comprise the Lower Evaporites of the MSC; TG12, TG20 and TG22 are peak glacials. (**b**) Stratigraphic spacing for the collection of samples for carbonate content analysis; the average spacing is $\Delta d = 0.22$ m. (**c**) Benthic $\delta^{18}O$ as a function of stratigraphic height. (**d**) Weight percent aluminium as a function of stratigraphic height. (**e**) Mean June + July insolation at 65° North according to the La2004 nominal solution (calculated with AnalySeries 2.0.4.2). (**f**) Sedimentation rates estimated from tuning the succession of insolation maxima in (e) to the midpoints of the reddish marls (shaded units in the AEB beds depicted in (i)). (**g**) Benthic $\delta^{18}O$ as a function of the insolation-tuned time. (**h**) Weight percent aluminium as a function of the insolation-tuned time. (**i**) Above: AEB bedding units with indurated beige marls (white) and softer, reddish marls (shaded); below: geomagnetic polarity chrons. Vertical shaded areas indicate times of theoretical 405 kyr eccentricity minima.

the %Al spectrum has significant precession and eccentricity spectral peaks and no obliquity power.

(3) Eccentricity related components do not always reach a high CL and provide another example of false negatives.

(4) Finally, the $\delta^{18}O$ data were not tuned directly, but the %Al data track the sedimentary cycles that were used for the tuning, that is, %Al is higher in the reddish marls and is lower in the beige layers, and so %Al is directly connected with the tuning. Thus, despite the tuning to insolation, which has substantial obliquity power, the tuned %Al spectrum does not have a statistically significant obliquity peak.

In both cases (RCS and AEB), statistically significant spectral peaks exceeding the 99% CL with respect to the AR(1) null model occur in the Milankovitch band. The 1.8 m and 5 m cycles in the untuned RCS carbonate record are most likely false negatives: these calibrate, respectively, to the obliquity and short eccentricity in the tuned RCS spectra (Fig. 6b & d). In the case of AEB, other proxies collected from this section have been

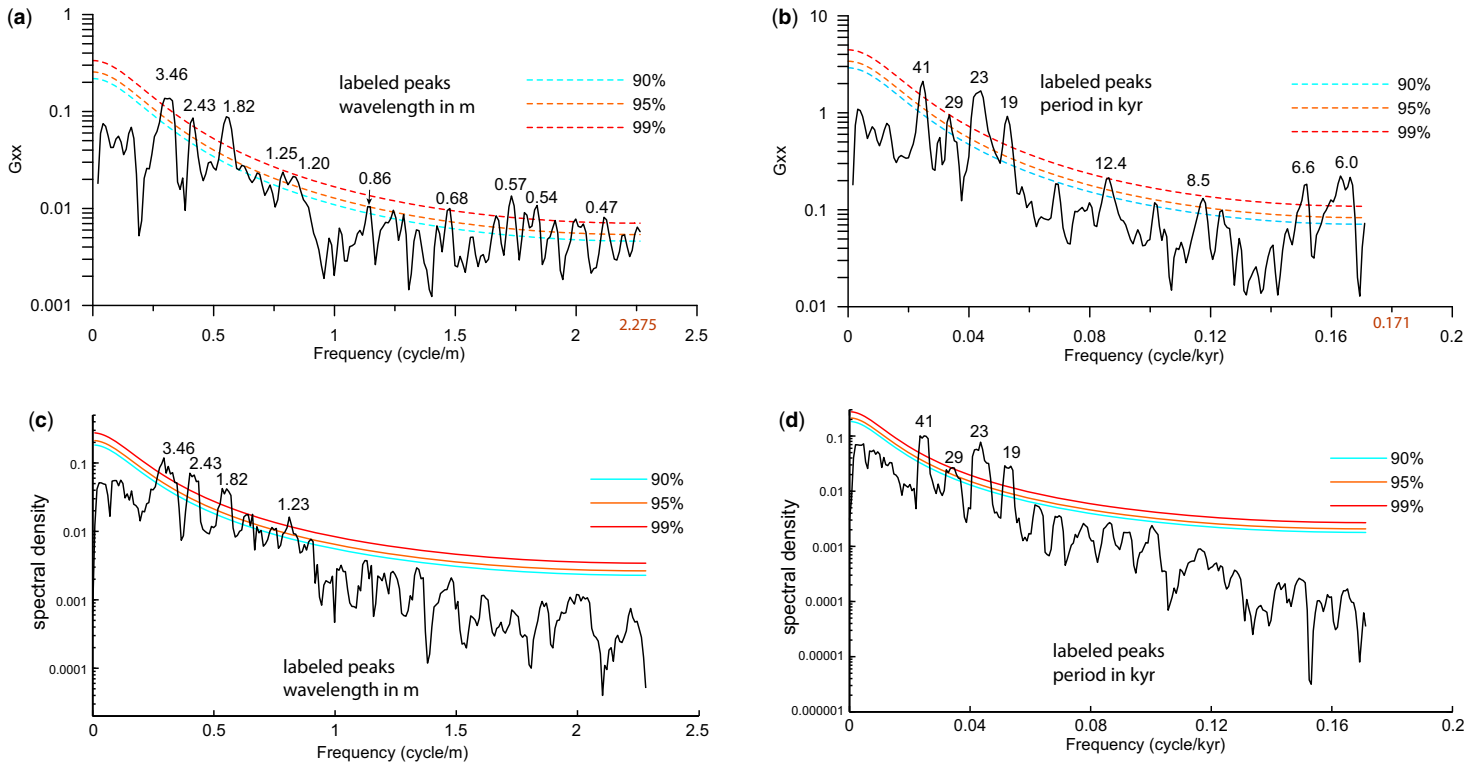

Fig. 8A. Spectral analysis of the Ain el Beida benthic $\delta^{18}O$ record using REDFIT (Schulz & Mudelsee 2002) and RedNoise_ConfidenceLevels (Husson 2013). (**a**) Untuned L–S spectrum: OFAC = 4.0, HIFAC = 1.0 (compute Nyquist range), n50 = 5, Iwin = 0 (no tapering), Nsim = 2000; Data variance = 0.04, Avg. Δd = 0.22 m, Avg. autocorr. coeff., $\rho = 0.75$, Avg. $\tau = 0.75$ m, Degrees of freedom = 7.14 6-dB Bandwidth = 0.05 cycles/m, Critical false-alarm level = 99.07%, corresponding scaling factor for red noise = 2.64. (**b**) Tuned L–S spectrum: OFAC = 4.0, HIFAC = 1.0 (compute Nyquist range), n50 = 5, Iwin = 0 (no tapering), Nsim = 2000; Data variance = 4.61E-02, Avg. Δt = 2.92 kyr, Avg. autocorr. coeff., $\rho = 0.73$, Avg. $\tau = 9.28$ kyr, Degrees of freedom = 7.14 6-dB Bandwidth = 0.004 cycles/kyr, Critical false-alarm level = 99.36%, corresponding scaling factor for red noise = 2.64. (**c**) Untuned 2π multi-tapered spectrum: the 70.56 m-long stratigraphic $\delta^{18}O$ record was linearly interpolated to the mean sample spacing of 0.22 m; four 2π prolate tapers provide spectral estimates with 8 degrees of freedom and an averaging bandwidth of $4/(70.56\text{ m}) = 0.05$ cycles/m; estimated $\rho = 0.80$. (**d**) Tuned 2π multi-tapered spectrum: the 938.59 kyr-long tuned time series was linearly interpolated to the mean sample spacing of 2.92 kyr; four 2π prolate tapers provide spectral estimates with 8 dofs and an averaging bandwidth of $4/(938.59\text{ kyr}) = 0.004$ cycles/kyr; estimated $\rho = 0.82$.

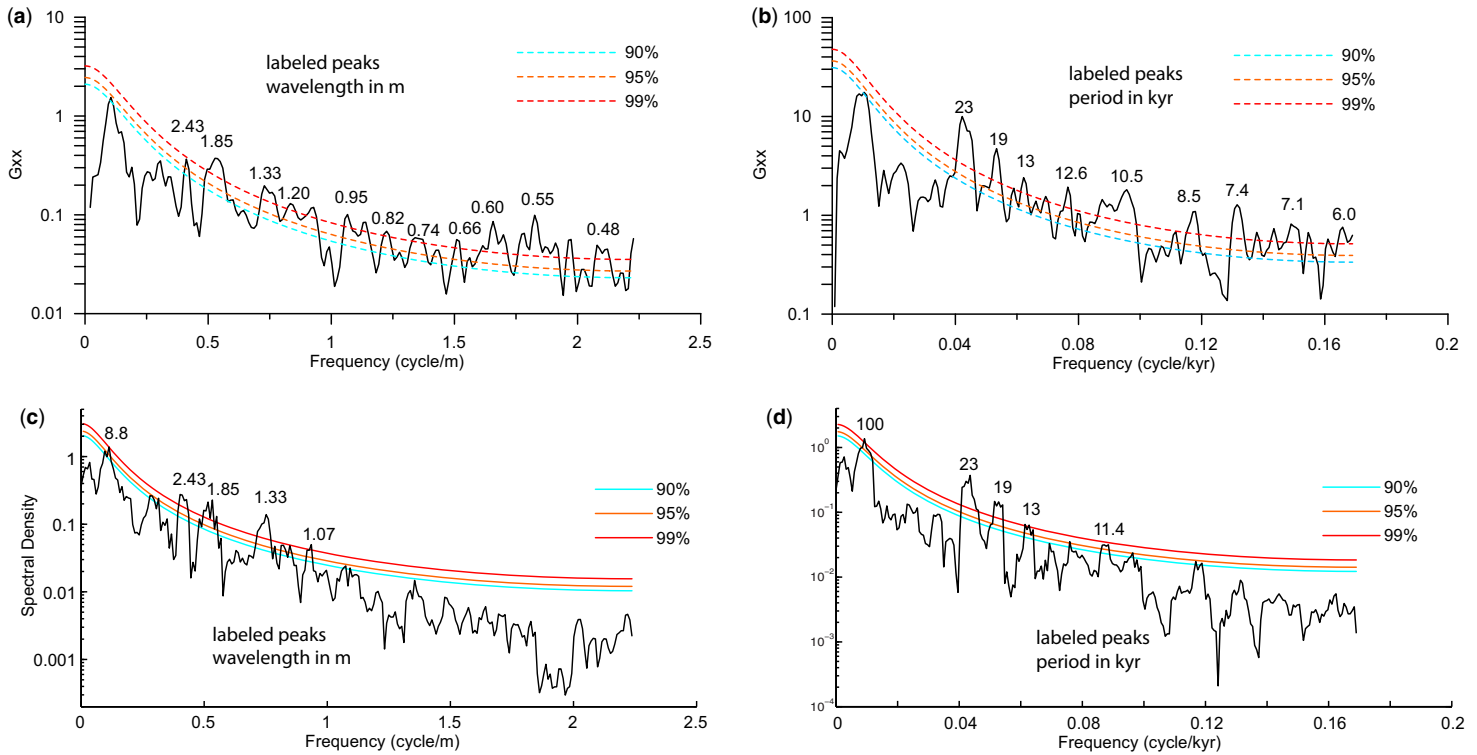

Fig. 8B. Spectral analysis of the Ain el Beida weight percent aluminium record using REDFIT (Schulz & Mudelsee 2002) and RedNoise_ConfidenceLevels (Husson 2013). (**a**) Untuned L–S spectrum: OFAC = 4.0, HIFAC = 1.0 (compute Nyquist range), n50 = 5, Iwin = 0 (no tapering), Nsim = 2000; Data variance = 0.29, Avg. Δd = 0.22, Avg. autocorr. coeff., $\rho = 0.81$, Avg. $\tau = 1.06$ m, Degrees of freedom = 7.14, 6-dB Bandwidth = 0.05 cycles/m, Critical false-alarm level = 99.06%, corresponding scaling factor for red noise = 2.64. (**b**) Tuned L–S spectrum: OFAC = 4.0, HIFAC = 1.0 (compute Nyquist range), n50 = 5, Iwin = 0 (no tapering), Nsim = 2000; Data variance = 0.33, Avg. Δt = 2.96 kyr, Avg. autocorr. coeff., $\rho = 0.81$, Avg. $\tau = 14.21$ kyr, Degrees of freedom = 7.14, 6-dB Bandwidth = 0.004 cycles/kyr, Critical false-alarm level = 99.06%, corresponding scaling factor for red noise = 2.64. (**c**) Untuned 2π multi-tapered spectrum: the 71.28 m-long stratigraphic weight percentage record was linearly interpolated to the mean sample spacing of 0.22 m; four 2π prolate tapers provide spectral estimates with 8 degrees of freedom and an averaging bandwidth of 4/(71.28 m) = 0.06 cycles/m; estimated $\rho = 0.87$. (**d**) Tuned 2π multi-tapered spectrum: the 943.84 kyr-long tuned time series was linearly interpolated to the mean sample spacing of 2.96 kyr; four 2π prolate tapers provide spectral estimates with 8 dofs and an averaging bandwidth of 4/(943.84 kyr) = 0.004 cycles/kyr; estimated $\rho = 0.842$.

shown to have statistically significant short eccentricity components: records of *Globigerinoides* total %, nannofossils SST (sea surface temperature), and counts of planktonic foraminifera per gram correlated with the $La2004_{(1,1)}$ astronomical solution all register a statistically significant spectral coherency peak in the short eccentricity band (Fig. 4 in Van der Laan *et al.* 2012). Thus, the short eccentricity peak in the tuned %Al spectrum (Fig. 8B b) is likely a false negative: it exceeds the 99% CL in the interpolation-based AR(1) model of the Multi-Taper method (MTM) spectrum (Fig. 8B d). The 29 kyr peak in the tuned $\delta^{18}O$ AEB spectrum that almost reaches the 99% CL may be evidence for a minor obliquity term.

The prospects for detecting false negatives in the RCS and AEB spectra stem from the detailed integrated stratigraphy that accompanies these two records, in particular, the independent magnetobiostratigraphic age models (Langereis & Hilgen 1991; Krijgsman *et al.* 2004). The age models provide clear predictions (before tuning) at which frequencies spectral peaks are to be expected that are related to astronomical climate forcing. If such peaks are found close to or at the expected frequencies, then a logical conclusion is that these are related to the astronomical parameters, even if they do not reach high CLs.

In closing, a '99% CL' can be unrealistically high when analysing cyclostratigraphic records. The relevant CL will vary depending on the assumed null model, and with the degree of distortion of the recorded signal and the accompanying reduction in spectral power, and the expectation of what the CL should be. For example, short eccentricity terms are not expected to achieve a high CL. Unless these countervailing problems are taken into account, estimated statistical confidence will not provide a realistic basis for judging whether spectral peaks reflect astronomically controlled cyclicity or not. Certainly none of these problems are anticipated by a strict statistical approach. Instead, an integrated stratigraphic approach must be applied to test whether cyclostratigraphic variations are related to astronomically forced climate change. This should ideally be combined with climate modelling of astronomical extremes for the time and location under consideration (example in section on *Weakness of forcing*). Such an integrated approach will help to reveal which spectral peaks should be considered false positives (Type 1 error) or false negatives (Type 2 error).

Tuning-induced Milankovitch spectra. The potential for Milankovitch frequencies to be introduced into records through astronomical tuning is well known and is a serious drawback (e.g. Shackleton *et al.* 1995; Hinnov & Park 1998; Rial 1999; Rial & Anaclerio 2000; Proistosescu *et al.* 2012). Random noise series tuned to astronomical target curves will entrain periods of the target curve; however, tuning a random noise series will also reveal erratic changes in sedimentation rates, while sedimentation rate changes resulting from tuning an astronomically controlled data set can be expected to be related to the amplitude of the forcing (Herbert 1994; Van der Laan *et al.* 2005).

Furthermore, proxy records often reveal clear amplitude variations, which may reflect the eccentricity modulation of the precession amplitude. These real amplitude variations are not introduced by the tuning process but are an attribute of the climate proxy data themselves. Such variations can thus be used to test whether a tuned time series is consistent with an astronomical target, as was performed by, for example, Pälike & Shackleton (2000), Pälike *et al.* (2004, 2006*b*), Shackleton & Crowhurst (1997), Shackleton *et al.* (1999), Westerhold *et al.* (2007) and Zeeden *et al.* (2013). Complex amplitude demodulation provides the statistical means to use amplitude for testing an astronomical tuning in the time domain (Shackleton & Crowhurst 1997). However, this method may also be affected by frequencies introduced by the tuning process, when no real amplitudes are present in the data (Huybers & Aharonson 2010). Nevertheless, given that real data amplitudes (and not frequencies introduced by the tuning process) are investigated, amplitudes of precession-related signals filtered from a geological record can be compared to orbital eccentricity, which modulates the precession amplitude. A reasonable fit between the amplitude of a precession-related component from a geological record and eccentricity is a very convincing argument for the orbital forcing of a geological time series (Zeeden *et al.* 2013). Datasets showing real amplitudes corresponding to amplitudes of Milankovitch parameters can be interpreted as astronomically forced. Much care should be taken when no clear amplitude variations are present, or when tuned time series are investigated.

Drawbacks resulting from tuning can be overcome by conducting time series analysis in the stratigraphic domain, or in the time domain with an independent (e.g. magnetobiostratigraphic) age model. For instance Hays *et al.* (1976) tested several age models using a very limited number of calibration points ultimately derived from radioisotopic dating. Huybers & Wunsch (2004) and Huybers (2007) developed a new chronology for the past two million years that is based on a depth-derived age estimate: weak non-linearities involving short eccentricity and obliquity are observed in the response, which disappear if a tuned age model is assumed for the time series. Independent (i.e. non-astronomical) age models have been

developed for non-sedimentary successions such as ice and speleothems, using for example, ice flow modelling and U/Th dating, respectively (Wang *et al.* 2008). These are not discussed here, but the results provide strong support for the presence of Milankovitch cyclicity.

A new class of 'objective' tuning techniques has recently appeared in the literature that approaches the problem of estimating sedimentation rates with statistical models. These harken back to the methods developed by Martinson *et al.* (1982), Schiffelbein & Dorman (1986) and Brüggemann (1992). Meyers & Sageman (2007) developed an 'average spectral misfit' (ASM) metric to evaluate the fit of a stratigraphic spectrum to an astronomical spectrum, given a range of likely sedimentation rates. The applied sedimentation rate resulting in the lowest number of misfits to a large number of realizations of randomized spectra with the same resolution constraints as the stratigraphic spectrum is taken as the most likely solution. A related method based on Bayesian inversion to evaluate the fit of test sedimentation rates to an astronomical model is described in Malinverno *et al.* (2010). These transformational methodologies provide statistics on the fitted sedimentation rates, and allow for failure, that is, lack of a unique solution for a data fit to an astronomical model.

Independent age constraints

Miall & Miall (2004) raise the issue of whether independent age constraints are precise enough to validate orbital tuning and the interpretation of recurrent variations in the stratigraphic record in terms of orbital climate forcing. Radio-isotopic dating is often used for this purpose, either by direct dating of sections or indirectly by employing the GPTS. Here we discuss uncertainties in radio-isotopic ages, radio-isotopic ages that are consistent with Milankovitch cyclicity, radio-isotopic age constraints for astronomical tuning and the intercalibration of independent numerical dating methods ($^{40}Ar/^{39}Ar$, U/Pb, astronomical).

Uncertainties in radio-isotopic ages. Radio-isotopic dating is often used as an independent test for the presence of Milankovitch cycles. Radio-isotopic dates can provide absolute numerical tie points while pairs or sets of radio-isotopic dates can also be used to calculate durations. When calculating durations from a set of dates derived from the same decay scheme (e.g. $^{40}K/^{40}Ar$ or $^{238}U/^{206}Pb$), employing the same reference material (natural standard or tracer solution) and the same decay constant(s), systematic uncertainties associated with the calibration of the reference material and the decay constant(s) can be ignored. In the case of the $^{40}Ar/^{39}Ar$ system, precise and accurate knowledge of the neutron fluence monitor age and the ^{40}K branching decay constants is not required to precisely determine durations, given that all experiments employ the same values for these constants. Similarly, for any of the U–Pb systems, tracer solution calibration and the decay constant uncertainties can be ignored when calculating the duration between two U–Pb dates, provided that the dates are calculated using the same tracer solution. In contrast, systematic uncertainties must be taken into account when calculating durations based on dates derived from different decay schemes (e.g. between a U–Pb and a $^{40}Ar/^{39}Ar$ date) or when dates based on a single decay scheme are calculated relative to different reference materials (e.g. different U–Pb tracer solutions or $^{40}Ar/^{39}Ar$ neutron fluence monitors). These systematic uncertainties also have to be considered when absolute radio-isotopic dates are compared with ages derived from orbital tuning. This implies that for any radio-isotopic system, durations can be constrained more accurately and more precisely than absolute ages. However, in both $^{40}Ar/^{39}Ar$ and U–Pb dating, geological uncertainties may play a critical role in estimating both the duration and age (e.g. residence time, or loss of radiogenic parent or daughter).

Schoene *et al.* (2013) provide a detailed description of uncertainties in radio-isotopic dating. The $^{40}Ar/^{39}Ar$ dating of sanidine and U–Pb dating of zircon are presently the 'gold standards' of geochronology. Researchers now report full (analytical and systematic) 2σ level age uncertainties that are on the order of 0.1% for $^{40}Ar/^{39}Ar$ and U–Pb dating in inter-comparison studies (Blackburn *et al.* 2013; Renne *et al.* 2013). This is at the scale of the orbital eccentricity cycle for Mesozoic rocks.

Radio-isotopic ages consistent with Milankovitch forcing. While systematic and geological uncertainties limit the accuracy of radio-isotopic dates, testing the hypothesis that astronomical climate forcing is recorded in the stratigraphic record requires accurate and precise quantification of durations rather than absolute numerical ages. As outlined before, systematic uncertainties (e.g. the uncertainty associated with the age of the FCs dating standard) can be ignored when calculating the age difference between two dates that were measured with the same method relative to the same reference material. This allows durations to be measured accurately and precisely enough to test the potential Milankovitch origin of cyclicities in the sedimentary record.

Precession induced monsoonal variations recorded in speleothem $\delta^{18}O$ records of the Sanbao/Hulu caves (China) are consistent with precise

^{230}Th dating (Wang *et al.* 2008). Single crystal ^{40}Ar/^{39}Ar sanidine ages for a number of ash beds in a Pliocene lignite-bearing lacustrine succession (Ptolemaïs, northern Greece) are in excellent agreement with the magnetostratigraphic age model for the same succession and with a precession origin of the lignite–marl alternations (Van Vugt *et al.* 1998; Steenbrink *et al.* 1999). The astrochronology for the Mediterranean Neogene was independently confirmed using ^{40}Ar/^{39}Ar and U/Pb dating (e.g. Kuiper 2004; Wotzlaw *et al.* 2014).

The Milankovitch origin of lacustrine cyclicity in the Eocene Green River Formation of North America is also validated through consistency between cyclostratigraphy and radio-isotopic ages (Machlus *et al.* 2008; Smith *et al.* 2010). Application of the astronomically calibrated FCs age of 28.201 Ma of Kuiper *et al.* (2008) to the sanidine ages of the volcanic ash beds allows a direct comparison of the Green River cycles to the astronomical solution for the Early Eocene for the first time (Smith *et al.* 2010).

Meyers *et al.* (2012) intercalibrated astronomical and radio-isotopic time for the Bridge Creek Limestone of the WIB, resulting in an age of 93.90 $\pm$ 0.15 Ma for the Cenomanian–Turonian boundary. Sageman *et al.* (2014) integrated ^{40}Ar/^{39}Ar, U/Pb and astronomical clocks by combining the floating astrochronology of Locklair & Sageman (2008) for the Coniacian and Santonian in the WIB with new ^{40}Ar/^{39}Ar and U/Pb ages for eight ash layers. This resulted in ages of 89.75 $\pm$ 0.38 Ma, 86.49 $\pm$ 0.44 Ma and 84.19 $\pm$ 0.38 Ma for the Turonian–Coniacian, Coniacian–Santonian and Santonian–Campanian boundaries, respectively. Both studies revealed consistency between cyclostratigraphic interpretations going back more than one century (Gilbert 1895) and state-of-the-art radio-isotopic ages. The ^{40}Ar/^{39}Ar and U/Pb age pairs further support the astronomically calibrated FCs age of 28.201 Ma of Kuiper *et al.* (2008) (see under *Age of Fish Canyon sanidine (FCs) standard*). The cyclostratigraphic interpretation and associated astrochronology of the lacustrine succession of Early Turonian–Early Campanian age in the Songliao Basin, northeastern China, is also consistent within error with published U–Pb dates of four bentonites (Wu *et al.* 2013*a*).

Furthermore, the late Triassic astrochronology of Olsen *et al.* (2011) developed on the basis of the sedimentary cyclicity in the Newark Basin has recently been corroborated in detail by high-resolution U–Pb zircon ages (Blackburn *et al.* 2013). Consistency is further established between high-precision U–Pb dating and Milankovitch interpretation of the upper Permian sections of Meishan, the stratotype for the Changhsingian Stage, and Shangsi in China (Wu *et al.* 2013*b*). These sections were used to obtain an astrochronologic duration of 7.793 myr for the Lopingian epoch. Similarly, new high precision U–Pb zircon ages of numerous ash layers in the Donets basin (Davydov *et al.* 2010) are consistent with the classic interpretation of shallow marine to continental sequences of Carboniferous age in terms of astronomical forcing and glacio-eustatic sea-level change (e.g. Heckel 1986; Heckel *et al.* 2007).

Intercalibration of radio-isotopic and astronomical time, and age of the Fish Canyon sanidine (FCs) standard. Intercalibration of radio-isotopic and astronomical dating methods has been instrumental to developments in both fields and has revealed some fundamental limitations in the accuracy and precision of the different methods. The extension of the ATS from the late Pleistocene to the Miocene–Pliocene boundary resulted in chron boundary ages that were 3–12% older than in the existing GPTS (Shackleton *et al.* 1990; Hilgen 1991*a*, *b*). These discrepancies were explained by incomplete degassing of (bulk) basalt samples dated with the K/Ar method when new ^{40}Ar/^{39}Ar ages became available (e.g. Baksi *et al.* 1992; Spell & McDougall 1992; Renne *et al.* 1993). A decade later, the ^{40}Ar/^{39}Ar community realized that the full uncertainty of *c.* 2.5% in ^{40}Ar/^{39}Ar seriously compromised numerical dating by this method (Renne *et al.* 1998; Min *et al.* 2000). Following early attempts of intercalibrating ^{40}Ar/^{39}Ar and astronomical dating methods (Renne *et al.* 1994; Hilgen *et al.* 1997), the most widely used FCs fluence monitor was determined to have an astronomically calibrated ^{40}Ar/^{39}Ar age of 28.201 $\pm$ 0.046 Ma (Kuiper *et al.* 2008). This age, adopted in GTS2012 (Schmitz 2012), has been confirmed by Rivera *et al.* (2011: 28.172 $\pm$ 0.028 Ma), using the same method as Kuiper *et al.* (2008), but a different astronomically dated standard, and by Wotzlaw *et al.* (2013: 28.196 $\pm$ 0.038 Ma), who applied U–Pb zircon dating on the Fish Canyon Tuff itself using state-of-the-art techniques. The consistency between U–Pb and astronomical dating has been substantiated by single crystal U–Pb zircon dating of several ash layers in the tuned Monte dei Corvi and La Vedova sections of northern Italy (Wotzlaw *et al.* 2014). Single crystal ^{40}Ar/^{39}Ar dating of Pleistocene silicic volcanics that incorporate an astronomically calibrated age of the FCs neutron fluence monitor yield eruption ages that achieve concordance or near concordance with CA-ID-TIMS ^{238}U/^{206}Pb zircon late-crystallization dates (Rivera *et al.* 2013, 2014; Singer 2014). The use of these (or similar) radio-isotopic dating methods also nears or achieves concordance with independently determined astronomical ages for the same units, extending from the

Pleistocene to the Cretaceous (Smith *et al.* 2010; Meyers *et al.* 2012; Wu *et al.* 2013*a*; Ma *et al.* 2014; Sageman *et al.* 2014). In particular, new $^{40}Ar/^{39}Ar$–U/Pb age pairs of ash beds from the cyclic succession of the Eocene Green River Formation (Smith *et al.* 2010) and the Upper Cretaceous of the WIB support the FCs age of 28.201 Ma (Meyers *et al.* 2012; Sageman *et al.* 2014) and cast doubt on other ages (see below).

An astronomically calibrated FCs age has been questioned by Renne *et al.* (2010, 2011), who used a statistical optimization model with input of both $^{40}Ar/^{39}Ar$ and U–Pb data to obtain an FCs age of 28.294 ± 0.036 Ma. Channell *et al.* (2010) arrived at an FCs age of 27.93 Ma based on intercalibration of $^{40}Ar/^{39}Ar$ ages with astronomical ages for the Brunhes–Matuyama boundary, and Westerhold *et al.* (2012) reached an age of 27.89 Ma based on intercalibration with tuned Eocene records. Singer (2014) reports $^{40}Ar/^{39}Ar$ ages for some transitional Pleistocene lavas that become too old compared to the astrochronologic age when the FCs age of Kuiper *et al.* (2008) is used for computation, although others are in good agreement.

Finally, Phillips & Matchan (2013), using ultra-high precision $^{40}Ar/^{39}Ar$ step-heating analyses of multi-crystal aliquots of FCs, calculated a revised eruption age of 28.008 ± 0.040 Ma for the Fish Canyon Tuff relative to the astronomically calibrated age of the A1 ashbed of Rivera *et al.* (2011). However, it is not clear whether the sanidine of the Fish Canyon tuff used by Kuiper *et al.* (2008) and Rivera *et al.* (2011) also contained extraneous argon, while other factors such as isotopic fractionation during step heating may play a critical role as well. Clearly, this interpretation of a young eruption age is inconsistent with the youngest U–Pb zircon age of 28.196 ± 0.038 Ma of Wotzlaw *et al.* (2013), although it cannot be excluded that even the youngest dated zircons crystallized some tens of thousands of years before eruption. Thus, the problem of the FCs age is still unresolved, although the numerical age seems to converge to approximately 28.2 Ma.

Radio-isotopic age constraints for astronomical tuning. The tuning of the Neogene has now been extended to the K–Pg boundary and beyond. In this older time interval, only the *c.* 405 kyr eccentricity cycle can be reliably used for tuning as the chaotic behaviour of the Solar System limits the accuracy of the most recent La2011 solution to *c.* 50–55 Ma as far as full eccentricity (i.e. including the *c.* 100 kyr and 2.4 myr cycles) is concerned (Westerhold *et al.* 2012). As a consequence of the Eocene gap in the ATS (Pälike & Hilgen 2008), independent age constraints are needed for the tuning of cyclic marine successions to the correct 405 kyr cycle in order to establish an ATS for the early Palaeogene (Kuiper *et al.* 2008). The absolute accuracy of such 'floating astrochronologies' thus depends on the accuracy of the radioisotopic dates that provide the numerical tie points for the cyclostratigraphic record. In such a case, systematic uncertainties associated with the different radioisotopic dating methods have to be taken into account. Renne *et al.* (2013) provide $^{40}Ar/^{39}Ar$ age constraints for the tuning of the K–Pg boundary interval to the beginning of the 405 kyr minimum around *c.* 66.0 Ma, using either the Kuiper *et al.* (2008) or Renne *et al.* (2011) ages for the FCs dating standard (see above). The tuning of the K–Pg boundary proposed by Kuiper *et al.* (2008) stood at the base of the astronomical age model that underlies the early Palaeogene time scale in GTS2012 (Vandenberghe *et al.* 2012). However, an alternative ATS gives much younger ages for the boundary (65.25 Ma) and the FCs (27.89 Ma) (Westerhold *et al.* 2012). This tuning differs by two 405 kyr cycles from the one proposed by Kuiper *et al.* (2008) and Hilgen *et al.* (2010), the latter being consistent with an age of 28.201 Ma for the FCs. The (early) Palaeogene time scale of Vandenberghe *et al.* (2012) is further consistent with single crystal U–Pb zircon ages of 55.785 ± 0.034 Ma for an ash layer in the Paleocene–Eocene Thermal Maximum (PETM) on Spitsbergen (Charles *et al.* 2011) and with U–Pb dates between 56.0 Ma and 55.8 Ma for intrusive rocks associated with the East Greenland flood basalts of the North Atlantic Magmatic Province, one of the proposed triggers for the PETM (Wotzlaw *et al.* 2012). Ideally, a combination of different radio-isotopic dating methods (U–Pb, $^{40}Ar/^{39}Ar$) should yield identical results to constrain the tuning.

Weakness of forcing

An argument that has been made against Milankovitch theory is a supposed weakness of the astronomical forcing. Bailey (2009) states that 'it seems implausible that minor, largely precession-induced, variations in terrestrial insolation, averaging ± 3.5% about the mean value during the last 20 Ma (Laskar *et al.* 2004), should routinely have elicited a linear (direct, proportionate and, thus, correspondingly cyclic) sedimentary response'. This view is echoed in an analysis of observed Quaternary climate change by Wunsch (2004) (although see Meyers *et al.* 2008) and in theoretical arguments made by Rubincam (1994, 2004) (although see comment by Berger 1996 and reply by Rubincam 1996). Indeed the insolation has a weak obliquity component in a spectrum that is dominated by annual and daily cycles (Huybers & Wunsch 2003; Huybers & Curry 2006). The evidence that the

palaeoclimate system has responded strongly and persistently to the astronomical parameter variations demands an explanation that is best provided by climate modelling.

One of the earliest palaeoclimate modelling studies (Kutzbach & Otto-Bliesner 1982) suggested that astronomically forced insolation changes are at least partly responsible for the different climate of the early Holocene. In particular, the monsoon system was found to respond strongly to insolation changes: the *c.* 7% higher July insolation 9000 years B.P. (compared to present-day values) results in a precipitation difference of 26% in the summer months over the North-African and Asian monsoon regions (Kutzbach & Otto-Bliesner 1982). Many more modelling studies have followed, showing that monsoonal precipitation can have a large response to insolation changes, likely due to the non-linear relationship between temperature and saturation vapour pressure (e.g. Kutzbach & Street-Perrott 1985; Kutzbach & Guetter 1986; Prell & Kutzbach 1987, 1992; Kutzbach *et al.* 2008). For the Mid-Holocene, the astronomically induced changes are rather consistent among the models used in the Paleoclimate Model Intercomparison Project (Joussaume *et al.* 1999; Braconnot *et al.* 2007).

A more recent study using a high-resolution ocean-atmosphere general circulation model shows that the increased Northern Hemisphere summer insolation during the Mid-Holocene (*c.* 5% higher than present) results in precipitation changes of up to 46% for the North African summer monsoon (Bosmans *et al.* 2012). These changes are stronger than in other models (e.g. Braconnot *et al.* 2007), likely due to higher resolution and a more sophisticated parameterization (Fig. 9a). In particular, a modelled shift in precipitation from ocean to land, induced by precession, may be sufficient to explain precession signals in sedimentary records such as the Mediterranean sapropels (e.g. Rossignol-Strick 1985). The annual mean temperature change is non-zero due to climatic feedbacks, showing that, despite a near-zero change in annual insolation, climate responds strongly to interannual changes caused by the astronomical parameters. Figure 9b shows that annual mean temperature differences between the Mid-Holocene and pre-industrial time are mostly negative. This is due to reduced insolation in boreal winter and to feedbacks that cool the monsoon-affected areas in response to strengthened monsoons induced by increased summer insolation (Bosmans *et al.* 2012). The cooler monsoon areas are in agreement with previous modelling (Braconnot *et al.* 2007).

Thus, climate and depositional systems appear to have been sensitive to small changes in insolation: various thresholds and (positive) feedbacks are at play, such as the temperature response described above and vegetation feedbacks (Kutzbach *et al.* 1996; Claussen 2009). For example, a closed lake system will be very sensitive to any change in net evaporation: the evidence for dominantly precession-related pluvial phases in the large lakes of North Africa and adjacent Asia is overwhelming (e.g. Crombie *et al.* 1997; Vaks *et al.* 2010).

During ice ages, the effect of changes in insolation can be strongly amplified by feedback mechanisms such as greenhouse gases and ice-albedo. This amplification was recently demonstrated in transient simulations using CLIMBER 2, a low-resolution

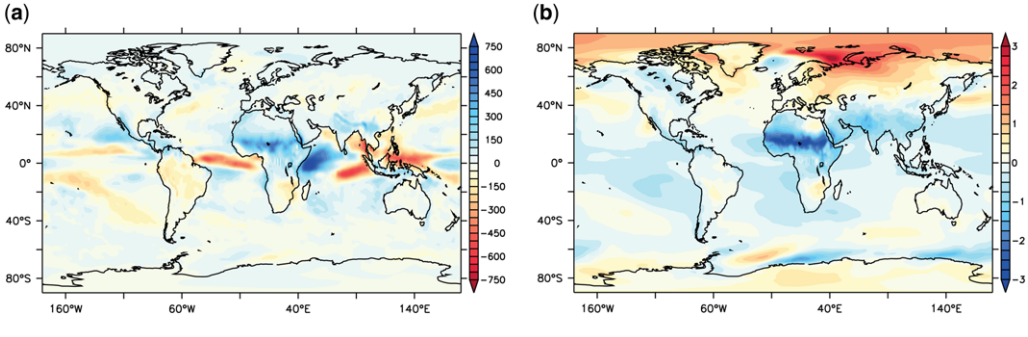

Fig. 9. (**a**) Differences in annual mean precipitation between the Mid-Holocene and the pre-industrial, from EC-Earth model experiments (Bosmans *et al.* 2012). Annual global mean precipitation over land is increased by 2.9% (21 mm a^{-1}) and by 4.5% (48 mm a^{-1}) over the tropical land areas (23°S–23°N). Precipitation over the ocean is decreased by 0.8% globally, and by 1.2% over the tropics. The precipitation changes over the tropics are dominated by changes in the summer monsoons (see Bosmans *et al.* 2012). (**b**) Differences in annual mean surface air temperature between the Mid-Holocene and the pre-industrial, from EC-Earth model experiments (Bosmans *et al.* 2012). Annual global mean temperature is decreased by 0.11°, and by 0.35° over the tropical land areas (23°S–23°N) despite a near-zero change in annual mean insolation.

coupled model of intermediate complexity (Petoukhov *et al.* 2000), which was used in transient simulations with adequate results (Claussen *et al.* 1999; Tuenter *et al.* 2005; Weber & Tuenter 2011). This version of CLIMBER-2 (i.e. version 2.3) includes a dynamic vegetation model and a thermodynamic sea-ice model, but it does not include a carbon-cycle model and a dynamical ice-sheet model. The reader is referred to the Appendix for a more detailed description of the model and input data.

Using CLIMBER-2, two transient simulations for the past five million years were performed. For the first simulation (Run O) only the astronomical parameters from the La2004 solution (Laskar *et al.* 2004) varied, while the ice sheets were kept fixed at their present day size, and the atmospheric CO_2 concentration was set to the pre-industrial value of 280 ppmv. For the second simulation (Run OIG) the same astronomical parameters as for Run O were used but the height and area of the ice sheets (Greenland, Eurasia, North America and Antarctica), as well as the CO_2 concentration were allowed to vary. The fraction of the surface area covered by ice in the spatial grid of CLIMBER-2 was obtained by summing the areas of all ice-covered grid points of the ice-sheet model located within one grid cell. The change in height due to ice thickness variations was obtained by averaging all height changes in the same grid points of the ice-sheet model.

For Run O the annual surface air temperature for the grid point in which Lake Baikal is located shows an astronomically forced amplitude of about 1 °C while the seasonal amplitude is much larger, reaching up to 12 °C in summer (Fig. 10). For the period 3–5 Ma, the amplitude for Run OIG is comparable to Run O, but for the last 3 million years, the CO_2 and the ice-sheet forcings strongly amplify the temperature change up to 10 °C (annual and winter) and locally a difference of about 20 °C between glacials and interglacials in summer (Fig. 10). Furthermore, in Run OIG a strong cooling trend beginning at 3 Ma is observed that is absent in Run O.

Spectral analyses of the modelled temperature series (not shown) reveal that the annual surface air temperatures respond to obliquity and precession with comparable amplitude in Run O. In the seasonal air temperature data, precession strongly dominates over obliquity. In Run OIG, the obliquity signal in the surface air temperatures is strongly amplified. This results in comparable strengths of precession and obliquity in the seasonal temperatures and a much larger obliquity signal compared to precession in the annual temperature response. Furthermore, atmospheric CO_2 and ice sheets introduce a *c.* 95 kyr signal in the temperature for Run OIG which is absent in Run O.

From these modelling results it can be concluded that astronomically forced insolation can cause large seasonal climate variations that can also lead to large annual variations. Furthermore, the direct astronomically forced insolation can be strongly amplified by feedback mechanisms such as greenhouse gases and ice sheets (Clark *et al.* 1999; Loutre *et al.* 2007; Yin & Berger 2012). Nevertheless, driving an Atmosphere-Ocean General Circulation Model (AOGCM) with only astronomical forcing and without additional constraints will not lead to ice ages, indicating that the feedbacks in the system are still not understood.

Stability of astronomical frequencies in the geological past

Miall & Miall (2004) touch on the issue of the long-term stability of the astronomical cycles. In the geologic past, frequencies were different for precession and obliquity due to Earth–Moon dynamics. Figure 11 summarizes the spectrum of the astronomical parameters over the past ten million years. The Earth's rotation rate has been decelerating through geologic time due to the phenomenon of tidal dissipation; consequently, the Earth-Moon distance was shorter in the past, and the Moon has been receding over time (recent review in Coughenour *et al.* 2012). The outcome is an ever-lengthening precession rate for the Earth, leading to a lengthening of the precession and obliquity cycle periodicities. This effect has been calculated for different time intervals in the past (e.g. Berger *et al.* 1989); a decreasing rotation rate based on empirical evidence is included in the La2004 astronomical solution (Laskar *et al.* 2004). The exact values of the dissipation effect are not known and depend on the geologic evidence. Independent evidence from corals, bivalves and tidalites appears to confirm a faster rotation rate in the past (e.g. Kvale *et al.* 1999; Williams 2000). Spectral peak ratios in a Permian red bed succession in France are also consistent with the inferred shortening (Kruiver *et al.* 2000).

Precession and obliquity are also affected by Earth's dynamical ellipticity. In principle, this effect can be determined through modelling mantle viscosity and convection (Forte & Mitrovica 1997): in practice, it can also be assessed through detailed comparison with cyclostratigraphy (Pälike & Shackleton 2000; Lourens *et al.* 2001; Zeeden *et al.* 2014). The latter studies reveal that present day values of tidal dissipation and dynamical ellipticity can be assumed over the last ten million years: slight adjustments may be necessary for older geologic intervals (Hilgen *et al.* 2003; Hüsing *et al.* 2007). The uncertainty associated with these

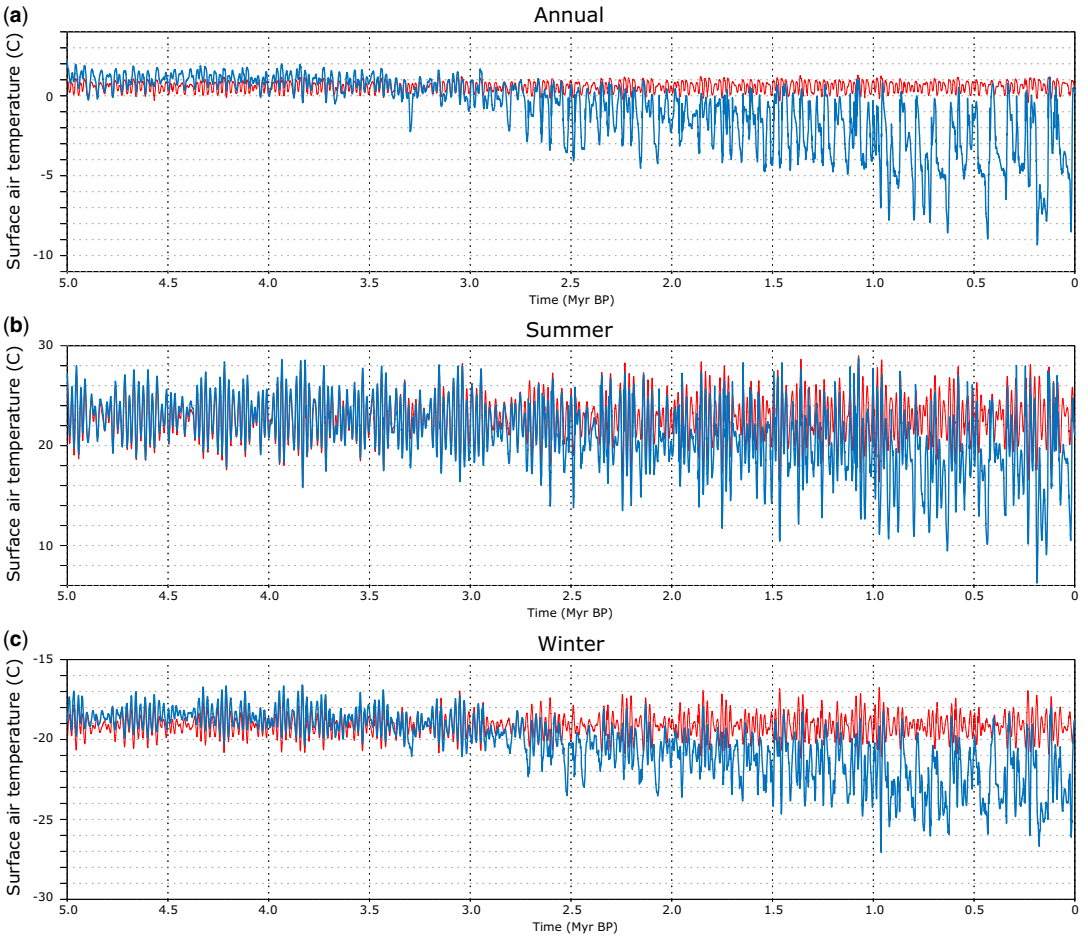

Fig. 10. Surface air temperature (in degrees Celsius) for Run O (red) and Run OIG (blue) for gridbox (50°N–60°N; *c.* 63°E–114°E). (**a**) Annual averaged, (**b**) averaged over June-July-August and (**c**) averaged over December-January-February. Horizontal axis: Time in million years Before Present. The temperatures are averages over 100 years. Note that the vertical axes differ.

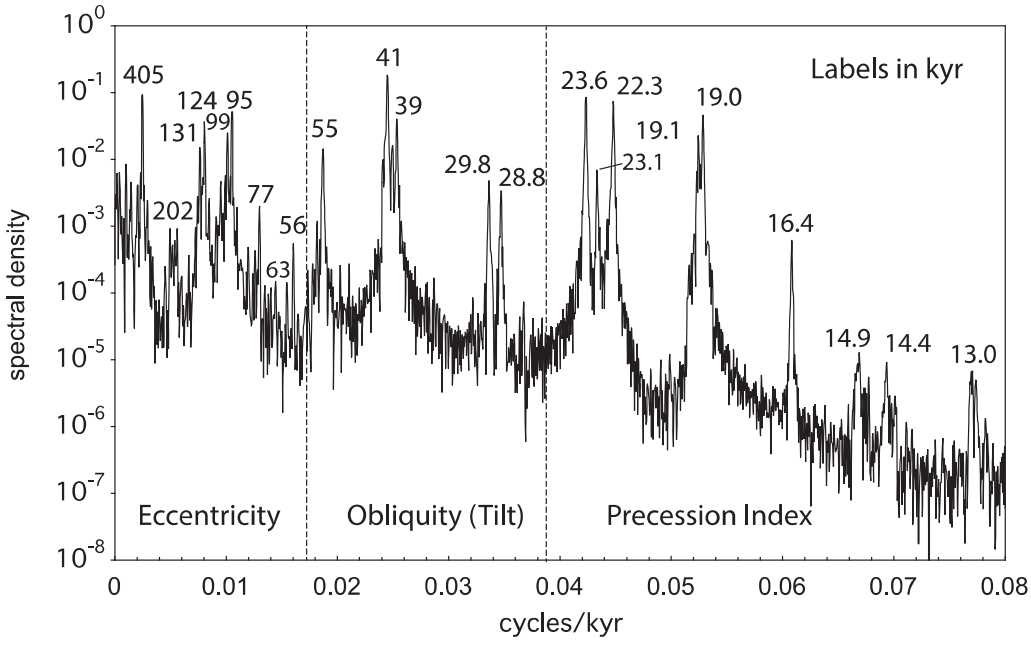

Fig. 11. Power spectrum of Earth's astronomical parameters, valid for the past ten million years. The nominal La2004 astronomical solution (Laskar *et al.* 2004) was processed at $\Delta t = 1$ kyr over 0–10 Ma as an ETP time series (Imbrie *et al.* 1984). Its spectrum is displayed above as the squared modulus of the Fast Fourier Transform, that is, spectral density v. frequency. The orbital eccentricity, obliquity (tilt) and precession index frequency bands are indicated.

effects increases back in time and implies a risk that precession- and obliquity-forced stratigraphic cycles may end up tuned to the wrong astronomical cycle (Lourens *et al.* 2004). However, the amplitude modulation of the precession by eccentricity provides a means to correct for such errors as far back as 50–55 Ma.

Eccentricity remains stable back to *c.* 50–55 Ma, according to the most recent astronomical solutions La2010 and La2011 (Laskar *et al.* 2011*a*; Westerhold *et al.* 2012). Various terms such as the 2.4 myr eccentricity modulation cannot be calculated reliably further back in time due to the chaotic behaviour of the Solar System (caused by the asteroids Vesta and Ceres: Laskar *et al.* 2011*b*). In fact, the 2.4 myr cycle could shift to a 1.2 myr period (and back) as a consequence of transient resonances in the Solar System (Laskar 1999). Such transitions should leave a marked imprint in the cyclostratigraphic record, but the timings cannot be precisely predicted from the astronomical models. Results thus far suggest that the period of this cycle was indeed shorter during part of the Mesozoic. For instance, a 1.7 myr period was found in the Triassic Newark Basin (Olsen & Kent 1999) and a period between 1.6 and 1.8 myr in a Triassic to Jurassic chert succession in Japan (Ikeda & Tada 2013).

However, the 405 kyr eccentricity cycle remains stable over much longer time intervals (at least back to 250 Ma), although the uncertainty in its computation increases with time. It is the 405 kyr cycle that is used for tuning early Cenozoic, Mesozoic and older cyclostratigraphies (Hinnov & Hilgen 2012; Hinnov 2013*a*, *b*).

Primary origin of limestone-marl alternations

A final issue to be discussed is the inferred primary climatic origin of the limestone–marl alternations used for tuning. This primary character has been questioned (e.g. Westphal *et al.* 2008) with diagenetic unmixing providing an alternative mechanism to explain such alternations (e.g. Hallam 1986). It is widely accepted that diagenesis often played an important role in enhancing the sometimes subtle primary variations in carbonate content, but in the absence of primary criteria, rhythmic successions have also been explained as resulting merely from differential diagenesis (e.g. Munnecke & Samtleben 1996). For that purpose, criteria for a primary origin of calcareous rhythmites were presented as a means to assess their suitability for high-resolution stratigraphic applications and orbital dating (Westphal *et al.* 2010). The problem encountered in the Monte dei Corvi section (Westphal *et al.* 2008) is

of special importance as it hosts the Tortonian GSSP and its tuning underlies the GTS for the interval between 8 Ma and 12.5 Ma. The primary character of the cycles at Monte dei Corvi stems from the characteristic cycle patterns, which reflect precession-obliquity interference in addition to the precession-eccentricity hierarchy (Hilgen *et al.* 2003; Hüsing *et al.* 2007). It is further substantiated by the high-resolution proxy (e.g. Ti/Al) records from the slightly older cycles in the La Vedova High Cliff section, which clearly indicate a primary origin (Mourik *et al.* 2010). The lack of indications for a primary origin at Monte dei Corvi may come from problems in recognizing the complex quadruplet structure of the basic precession-dominated cyclicity in this section.

Conclusions

From the available literature and collective experience of the community of scientists involved in cyclostratigraphy, we conclude that:

- Sedimentary successions can be continuous at Milankovitch time scales over millions of years. This is shown for deep marine and lacustrine successions, and probably even some fluvial successions. In Cenozoic, Mesozoic and Palaeozoic examples, this continuity and the presence of Milankovitch cyclicity has been independently confirmed by magnetobiostratigraphic and/or radio-isotopic dating.
- There are many examples of continuous successions at Milankovitch time scales with relatively constant sedimentation rates over multiple temporal orders of magnitude that do not follow the empirical inverse power law between sedimentation rate and time. This needs to be taken into account for the nature of the stratigraphic record to be understood in all its facets.
- The authenticity of Milankovitch cycles in the stratigraphic record is substantiated by climate modelling, in both transient experiments and time-snapshot experiments for astronomical extremes, although much work still needs to be done to explain Milankovitch variability in stratigraphy (e.g. the Mid-Pleistocene Transition, high-magnitude 100-kyr cyclicity, sea level forcing, oceanographic forcing, etc.).
- The use of high significance levels in spectral analysis is not realistic in view of the statistics of the astronomical forcing signal and the nature of the (cyclo-) stratigraphic record with time-depth distortions stemming from bioturbation and non-linear responses in both climate and depositional systems and resulting variations in sediment accumulation rate.

The two referees R. Bailey and G. Weedon are thanked for their thorough review of the original version of the manuscript. D. Smith is thanked as editor for his comments and for his patience when the revision of the manuscript was delayed.

Appendix

Differences in the L–S and multi-taper spectra

There are striking differences between the L–S and MTM spectra and their null models, especially for the RCS carbonate series (compare Fig. 6a–d). In the RCS spectra, the most noticeable difference is in the very low frequencies. Computation of the L–S spectrum requires dividing the input series into overlapping segments (in this case, five 50%-overlapping segments), which means that for the tuned RCS spectrum periodicities lower than 2.623 cycles per 3 myr = 0.874 myr per cycle cannot be measured. MTM spectrum estimation, while requiring interpolation of the tuned RCS series to a uniform sample spacing (here taken as the average sample spacing of 5.569 kyr) does permit estimation of periodicities as low as 2.623 myr (i.e. the Rayleigh frequency resolution is $\Delta f = 1/(2.623\ \text{myr})$). Thus the tuned RCS MTM spectrum (Fig. 6d) registers a low-frequency term at 1/(1425 kyr); in contrast, the tuned RCS L–S spectrum (Fig. 6b) indicates no power at this frequency. For the AR(1) model shown with the L–S spectra, the estimated ρ (lag-1 autocorrelation coefficient) is calculated by regression on the non-uniformly sampled data, plus a modelled bias correction (Mudelsee 2002), which results in $\rho = 0.03$. For the AR(1) model shown with the MTM spectra, ρ is estimated directly from the autocorrelation operation on the original interpolated data set and is sensitive to the interpolated sample spacing, here taken as the average sample spacing. For the RCS interpolated series, ρ is 0.37–0.42, that is, more than one order of magnitude larger than the regression estimate. The difference between the values of ρ arises mainly from methodology. The regression technique (for non-uniformly sampled series) is sensitive to high-power signal components; it is therefore recommended that the series be pre-processed to remove such high frequency components (Usage.pdf in Schulz & Mudelsee 2002). In the RCS spectra, the high-power, high-frequency spectral peaks close to the Nyquist frequency clearly have an influence on regression-based ρ that is not reflected in the interpolation-based ρ. The robust red noise modelling of Mann & Lees (1996), not shown here, addresses the signal contamination problem with robust smoothing of the spectrum to attenuate high-power signal effects and regression on the AR(1) model. However, Meyers (2012) has recently described a low-frequency bias inherent to the Mann & Lees (1996) model, proposing an alternative LOWSPEC procedure to reduce this bias. In summary, defining an appropriate null model for cyclostratigraphic spectra is a 'grand challenge' that has yet to be solved. Further discussion of

problems with the Mann & Lees (1996) method can be found in Vaughan *et al.* (2011).

CLIMBER-2, a coupled model of intermediate complexity

The prescribed ice-sheet areas and heights in CLIMBER-2 were obtained from a five million year simulation using the 3D coupled ice sheet-ice shelf-bedrock model ANICE (De Boer *et al.* 2014). The model reconstructs ice volume of Antarctica, Eurasia, North America (using a grid distance of 40 km for these ice sheets) and Greenland (grid distance of 20 km). Basically, ANICE follows the principles outlined in Huybrechts (1990) and Van de Wal (1999). The ice velocities are determined using a combination of two stress-balance approximations. For the velocities on the ice sheets, the shallow ice approximation (Hutter 1983) is used while the computations of ice-shelf and sliding velocities are based on the shallow shelf approximation (Morland 1987). These two velocities are combined following the approach used by the Parallel Ice Sheet Model (PISM) (Winkelmann *et al.* 2011).

The mass balance model of ANICE is forced by monthly temperature and precipitation rate (De Boer *et al.* 2013). Over Antarctica and Greenland, precipitation is a function of the condensation temperature above the surface inversion layer (Huybrechts 2002) while for the Eurasian and North American ice sheets a precipitation model is used that includes orographic forcing of precipitation and changes in the moisture content (Roe & Lindzen 2001; Roe 2002; De Boer *et al.* 2013). The monthly temperature forcing consists of the continental mean (40–80°N) surface air temperature and is computed by an inverse forward modelling routine (Bintanja *et al.* 2005; Bintanja & Van de Wal 2008; De Boer *et al.* 2010). This routine linearly relates the continental temperature to the difference between the modelled benthic $\delta^{18}O$ and the observed $\delta^{18}O$ 100 years later. The input (i.e. the observed benthic $\delta^{18}O$) is the LR04 benthic stack (Lisiecki & Raymo 2005). The advantage of the forward modelling routine is that a self-consistent record is constructed of surface air temperature, ice volume and benthic $\delta^{18}O$.

The CO_2 concentration as used by CLIMBER-2 was reconstructed using the method as described in Van de Wal *et al.* (2011). They derived an empirical relationship between atmospheric temperatures and CO_2. With this relation the 5 myr CO_2 record is constructed using atmospheric temperatures as simulated by the 3D ice-sheet model (De Boer *et al.* 2014). As a result, the prescribed CO_2 concentration is mutually consistent with the prescribed ice sheets.

References

Abdul Aziz, H., Krijgsman, W., Hilgen, F. J., Wilson, D. S. & Calvo, J. P. 2003. An astronomical polarity timescale for the Late Middle Miocene based on cyclic continental sequences. *Journal of Geophysical Research B: Solid Earth*, **108**, 2159, http://dx.doi.org/10.1029/2002JB001818

Abdul Aziz, H., van Dam, J., Hilgen, F. J. & Krijgsman, W. 2004. Astronomical forcing in Upper Miocene continental sequences: implications for the Geomagnetic Polarity Time Scale. *Earth and Planetary Science Letters*, **222**, 243–258.

Abdul Aziz, H., Hilgen, F. J., van Luijk, G. M., Sluijs, A., Kraus, M. J., Pares, J. M. & Gingerich, P. D. 2008*a*. Astronomical climate control on paleosol stacking patterns in the Upper Paleocene-Lower Eocene Willwood Formation, Bighorn Basin, Wyoming. *Geology*, **36**, 531–534.

Abdul Aziz, H. & Böhme, M. *et al.* 2008*b*. Integrated stratigraphy and $^{40}Ar/^{39}Ar$ chronology of the Early to Middle Miocene Upper Freshwater Molasse in eastern Bavaria (Germany). *International Journal of Earth Sciences*, **97**, 115–134.

Abels, H. A., Abdul Aziz, H., Ventra, D. & Hilgen, F. J. 2009*a*. Orbital climate forcing in mudflat to marginal lacustrine deposits in the Miocene Teruel Basin (North-East Spain). *Journal of Sedimentary Research*, **79**, 831–847.

Abels, H. A., Abdul Aziz, H., Calvo, J. P. & Tuenter, E. 2009*b*. Shallow lacustrine carbonate microfacies document orbitally paced lake-level history in the Miocene Teruel basin (North-East Spain). *Sedimentology*, **56**, 399–419.

Abels, H. A., Clyde, W. C., Gingerich, P. D., Hilgen, F. J., Fricke, H. C., Bowen, G. J. & Lourens, L. J. 2012. Terrestrial carbon isotope excursions and biotic change during Palaeogene hyperthermals. *Nature Geoscience*, **5**, 326–329.

Abels, H. A., Kraus, M. & Gingerich, P. D. 2013. Orbital climate cycles triggering river avulsion in the lower Eocene Willwood Formation, Bighorn Basin, Wyoming (USA). *Sedimentology*, **60**, 1467–1483.

Adhémar, J. A. 1842. *Révolutions de la mer, déluges périodiques*. Private edn. Paris, Carilian-Goeury et V. Dalmont.

Ager, D. V. 1973. *The Nature of the Stratigraphical Record*. Macmillan, London.

Algeo, T. J. & Wilkinson, B. H. 1988. Periodicity of Phanerozoic sedimentary cycles and the role of Milankovitch orbital modulation. *Journal of Geology*, **88**, 313–322.

An, Z. 2000. The history and variability of the East Asian paleomonsoon climate. *Quaternary Science Reviews*, **19**, 171–187.

Anders, M. H., Krueger, S. W. & Sadler, P. M. 1987. A new look at sedimentation rates and the completeness of the stratigraphic record. *The Journal of Geology*, **95**, 1–14.

Anderson, R. Y. 1982. A long geoclimatic record from the Permian. *Journal of Geophysical Research*, **87**, 7285–7294.

Anderson, R. Y. 2011. Enhanced climate variability in the tropics: a 200 000 yr annual record of monsoon variability from Pangea's equator. *Climate of the Past*, **7**, 757–770.

Anderson, R. Y., Dean, W. E., Kirkland, D. W. & Snider, H. I. 1972. Permian Castile varved evaporite

sequence, West Texas and New Mexico. *Geological Society of America Bulletin*, **77**, 241–256.

ASWASEREELERT, W., MEYERS, S. R., CARROLL, A. R., PETERS, S. E., SMITH, M. E. & FEIGL, K. L. 2012. Basin-scale cyclostratigraphy of the Green River Formation, Wyoming. *Geological Society of America Bulletin*, **125**, 216–228.

AUBRY, M.-P. 1991. Sequence stratigraphy: eustasy or tectonic imprint? *Journal of Geophysical Research*, **96**, 6641–6679.

BAILEY, R. J. 1998. Review: stratigraphy, metastratigraphy and chaos. *Terra Nova*, **10**, 222–230.

BAILEY, R. J. 2009. Cyclostratigraphic reasoning and orbital time calibration. *Terra Nova*, **21**, 340–351.

BAILEY, R. J. & SMITH, D. G. 2008. Quantitative tests for stratigraphic cyclicity. *Geological Journal*, **43**, 431–446.

BAKSI, A. K., HSÜ, V., MCWILLIAMS, M. O. & FARRAR, E. 1992. $^{40}Ar/^{39}Ar$ dating of the Brunhes-Matuyama geomagnetic field reversal. *Science*, **256**, 356–357.

BATENBURG, S. J. & SPROVIERI, M. *ET AL.* 2012. Cyclostratigraphy and astronomical tuning of the Late Maastrichtian at Zumaia (Basque country, northern Spain). *Earth and Planetary Science Letters*, **359–360**, 264–278.

BATENBURG, S. J., GALE, A. S., SPROVIERI, M., HILGEN, F. J., THIBAULT, N., BOUSSAHA, M. & ORUE-ETXEBARRIA, X. 2013. An astronomical time scale for the Maastrichtian based on the Zumaia and Sopelana sections (Basque country, northern Spain). *Journal of the Geological Society, London*, **171**, 165–180.

BEERBOWER, J. R. 1964. Cyclothems and cyclic deposition mechanisms in alluvial plain sedimentation. *In*: Merriam, D.F. (ed.) *Symposium on Cyclic Sedimentation*. Kansas Geological Survey Bulletin 169, Lawrence, Kansas, **1**, 31–42.

BERGER, A. 1996. Comment on 'Insolation in terms of Earth's orbital parameters', by D.P. Rubincam – Theor. Appl. Climatol. 48, 195–202, 1994. *Theoretical and Applied Climatology*, **53**, 253–255.

BERGER, A., LOUTRE, M. F. & DEHANT, V. 1989. Astronomical frequencies for pre-Quaternary palaeoclimate studies. *Terra Nova*, **1**, 474–479.

BINTANJA, R. & VAN DE WAL, R. S. W. 2008. North American ice-sheet dynamics and the onset of 100,000-year glacial cycles. *Nature*, **454**, 869–872.

BINTANJA, R., VAN DE WAL, R. S. W. & OERLEMANS, J. 2005. A new method to estimate ice age temperatures. *Climate Dynamics*, **24**, 197–211.

BLACKBURN, T. J. & OLSEN, P. E. *ET AL.* 2013. Zircon U–Pb geochronology links the End-Triassic extinction with the Central Atlantic Magmatic Province. *Science*, **340**, 941–945.

BLUM, M. D. & TÖRNQVIST, T. E. 2000. Fluvial responses to climate and sea-level change: a review and look forward. *Sedimentology*, **47**, 2–48.

BLUM, M. D., TOOMEY, R. S., III & VALASTRO, S., JR. 1994. Fluvial response to Late Quaternary climatic and environmental change, Edwards Plateau, Texas. *Palaeogeography, Palaeoclimatology, Palaeoecology*, **108**, 1–21.

BOSMANS, J. H. C., DRIJFHOUT, S. S., TUENTER, E., LOURENS, L. J., HILGEN, F. J. & WEBER, S. L. 2012. Monsoonal response to mid-Holocene orbital forcing in a high resolution GCM. *Climate of the Past*, **8**, 723–740.

BOULILA, S., GALBRUN, B., HINNOV, L. A. & COLLIN, P.-Y. 2008. High-resolution cyclostratigraphic analysis from magnetic susceptibility in a Lower Kimmeridgian (Upper Jurassic) marl-limestone succession (La Méouge, Vocontian Basin, France). *Sedimentary Geology*, **203**, 54–63.

BOULILA, S., GALBRUN, B., HINNOV, L. A., COLLIN, P.-Y., OGG, J. G., FORTWENGLER, D. & MARCHAND, D. 2010. Milankovitch and sub-Milankovitch forcing of the Oxfordian (Late Jurassic) Terres Noires Formation (SE France) and global implications. *Basin Research*, **22**, 712–732, http://dx.doi.org/10.1111/j.1365-2117.2009.00429.x

BOULILA, S. & GALBRUN, B. *ET AL.* 2014. Astronomical calibration of the Toarcian Stage: implications for sequence stratigraphy and duration of the early Toarcian OAE. *Earth and Planetary Science Letters*, **386**, 98–111.

BOWEN, G. J., KOCH, P. L., GINGERICH, P. D., NORRIS, R. D., BAINS, S. & CORFIELD, R. M. 2001. Refined isotope stratigraphy across the continental Paleocene–Eocene boundary on Polecat Bench in the northern Bighorn Basin. *In*: GINGERICH, P. D. (ed.) *Paleocene–Eocene Stratigraphy and Biotic Change in the Bighorn and Clarks Fork Basins, Wyoming*. University of Michigan Papers on Paleontology, Ann Arbor, MI, USA, **33**, 73–88.

BRACONNOT, P. & OTTO-BLIESNER, B. *ET AL.* 2007. Results of PMIP2 coupled simulations of the Mid-Holocene and Last Glacial Maximum – Part 1: experiments and large-scale features. *Climate of the Past*, **3**, 261–277.

BRADLEY, W. H. 1929. The varves and climate of the Green River epoch. *United States Geological Survey Professional Paper*, **158**, 87–110.

BROWN, R. E., KOEBERL, C., MONTANARI, A. & BICE, D. M. 2009. Evidence for a change in Milankovitch forcing caused by extraterrestrial events at Massignano, Italy, Eocene-Oligocene boundary GSSP. *Geological Society of America Special Papers*, **452**, 119–137.

BRÜGGEMANN, W. 1992. A minimal cost function method for optimizing the age-depth relation of deep-sea sediment cores. *Paleoceanography*, **7**, 467–487.

CASTRADORI, D., RIO, D., HILGEN, F. J. & LOURENS, L. J. 1998. The Global Standard Stratotype section and Point (GSSP) of the Piacenzian Stage (Middle Pliocene). *Episodes*, **21**, 88–93.

CHANNELL, J. E. T., HODELL, D. A., SINGER, B. S. & XUAN, C. 2010. Reconciling astrochronological and $^{40}Ar/^{39}Ar$ ages for the Matuyama-Brunhes boundary and Late Matuyama Chron. *Geochemistry, Geophysics, Geosystems*, **11**, Q0AA12, http://dx.doi.org/10.129/2010GC003203

CHARLES, A. J. & CONDON, D. J. *ET AL.* 2011. Constraints on the numerical age of the Paleocene-Eocene boundary. *Geochemistry, Geophysics, Geosystems*, **12**, Q0AA17, http://dx.doi.org/10.1029/2010GC003426

CLARK, P. U., ALLEY, R. A. & POLLARD, D. 1999. Northern hemisphere ice-sheet influences on global climate change. *Science*, **286**, 1104–1111.

CLAUSSEN, M. 2009. Late Quaternary vegetation-climate feedbacks. *Climate of the Past*, **5**, 203–216.

CLAUSSEN, M., KUBATZKI, C., BROVKIN, V., GANOPOLSKI, A., HOELZMANN, P. & PACHUR, H.-J. 1999. Simulation of an abrupt change in Saharan vegetation in the mid-Holocene. *Geophysical Research Letters*, **26**, 2037–2040.

COUGHENOUR, C. L., ARCHER, A. W. & LACOVARA, K. J. 2012. Tides, tidalites and secular changes in the Earth-Moon system. *Earth-Science Reviews*, **97**, 59–79.

CROLL, J. 1864. On the physical cause of the change of the climate during geological epochs. *Philosophical Magazine*, **28**, 121–137.

CROMBIE, M. K., ARVIDSON, R. E., STURCHIO, N. C., EL ALFY, Z. & ABU ZEID, K. 1997. Age and isotopic constraints on Pleistocene pluvial episodes in the Western Desert, Egypt. *Palaeogeography, Palaeoclimatology, Palaeoecology*, **130**, 337–355.

DAVYDOV, V. I., CROWLEY, J. L., SCHMITZ, M. D. & POLETAEV, V. I. 2010. High-precision U–Pb zircon age calibration of the global Carboniferous time scale and Milankovitch band cyclicity in the Donets Basin, eastern Ukraine. *Geochemistry, Geophysics, Geosystems*, **11**, Q0AA04, http://dx.doi.org/10.1029/2009GC002736

DE BOER, B., VAN DE WAL, R. S. W., BINTANJA, R., LOURENS, L. & TUENTER, E. 2010. Cenozoic global ice-volume and temperature simulations with 1-D ice-sheet models forced by benthic $\delta^{18}O$ records. *Annals of Glaciology*, **51**, 23–33.

DE BOER, B., VAN DE WAL, R. S. W., LOURENS, L. J., BINTANJA, R. & REERINK, T. J. 2013. A continuous simulation of global ice volume over the past 1 million years with 3-D ice-sheet models. *Climate Dynamics*, **41**, 1365–1384, http://dx.doi.org/10.1007/s00382-012-1562-2

DE BOER, B., LOURENS, L. J. & VAN DE WAL, R. S. W. 2014. Persistent 400,000-year variability of Antarctic ice volume and the carbon cycle is revealed throughout the Plio-Pleistocene. *Nature Communications*, **5**, 2999, http://dx.doi.org/10.1038/ncomms3999

DE VLEESCHOUWER, D., DA SILVA, A. C., BOULVAIN, F., CRUCIFIX, M. & CLAEYS, P. 2012*a*. Precessional and half-precessional climate forcing of mid-Devonian monsoon-like dynamics. *Climate of the Past*, **8**, 337–351.

DE VLEESCHOUWER, D., WHALEN, M. T., DAY, J. E. & CLAEYS, P. 2012*b*. Cyclostratigraphic calibration of the Frasnian (late Devonian) time scale (western Alberta, Canada). *Geological Society of America Bulletin*, **124**, 928–942.

DE VLEESCHOUWER, D., RAKOCIŃSKI, M., RACKI, G., BOND, D. P. G., SOBIEŃ, K. & CLAEYS, P. 2013. The astronomical rhythm of late-Devonian climate change (Kowala section, Holy Cross mountains, Poland). *Earth and Planetary Science Letters*, **365**, 25–37.

DINARÈS-TURELL, J., STOYKOVA, K., BACETA, J. I., IVANOV, M. & PUJALTE, V. 2010. High-resolution intra- and interbasinal correlation of the Danian–Selandian transition (Early Paleocene): the Bjala section (Bulgaria) and the Selandian GSSP at Zumaia (Spain). *Palaeogeography, Palaeoclimatology, Palaeoecology*, **297**, 511–533.

DINARÈS-TURELL, J., PUJALTE, V., STOYKOVA, K., BACETA, J. I. & IVANOV, M. 2012. The Palaeocene ''top chron C27n'' transient greenhouse episode: evidence from marine pelagic Atlantic and peri-Tethyan sections. *Terra Nova*, http://dx.doi.org/10.1111/j.1365-3121.2012.01086.x

DINARÈS-TURELL, J., PUJALTE, V., STOYKOVA, K. & ELORZA, J. 2013. Detailed correlation and astronomical forcing within the Upper Maastrichtian succession in the Basque Basin. *Boletín Geológico y Minero*, **124**, 253–282.

DING, Z., YU, Z., RUTTER, N. W. & LIU, T. 1994. Towards an orbital time scale for Chinese loess deposits. *Quaternary Science Reviews*, **13**, 39–70.

EMILIANI, C. 1955. Pleistocene temperatures. *Journal of Geology*, **63**, 538–578.

EPICA COMMUNITY MEMBERS 2004. Eight glacial cycles from an Antarctic ice core. *Nature*, **429**, 623–628.

FISCHER, A. G. 1980. Gilbert-bedding rhythms and geochronology. *In*: YOCHELSON, E. L. (ed.) *The Scientific Ideas of G.K. Gilbert*. Geological Society of America, Special Paper, Boulder, USA, **183**, 93–104.

FISCHER, A. G. & ROBERTS, L. T. 1991. Cyclicity in the Green River Formation (lacustrine Eocene) of Wyoming. *Journal of Sedimentary Research*, **61**, 1146–1154.

FISCHER, A. G., HERBERT, T. D., NAPOLEONE, G., PREMOLI SILVA, I. & RIPEPE, M. 1991. Albian pelagic rhythms (Piobbico core). *Journal of Sedimentary Petrology*, **61**, 1164–1172.

FORTE, A. M. & MITROVICA, J. X. 1997. A resonance in the Earth's obliquity and precession over the past 20 Myr driven by mantle convection. *Nature*, **390**, 676–680.

GALE, A. S. & BOWN, P. *ET AL*. 2011. The uppermost middle and upper Albian succession at the Col de Palluel, Hautes-Alpes, France: an integrated study (ammonites, inoceramid bivalves, planktonic foraminifera, nannofossils, geochemistry, stable oxygen and carbon isotopes, cyclostratigraphy). *Cretaceous Research*, **32**, 59–130.

GALEOTTI, S. & KRISHNAN, S. *ET AL*. 2010. Orbital chronology of Early Eocene hyperthermals from the Contessa Road section, central Italy. *Earth and Planetary Science Letters*, **290**, 192–200.

GILBERT, G. K. 1895. Sedimentary measurement of Cretaceous time. *Journal of Geology*, **3**, 121–127.

GRIPPO, A., FISCHER, A. G., HINNOV, L. A., HERBERT, T. M. & PREMOLI SILVA, I. 2004. Cyclostratigraphy and chronology of the Albian stage (Piobbico core, Italy). *SEPM (Society for Sedimentary Geology) Special Publication*, **81**, 57–81.

HALLAM, A. 1986. Origin of minor limestone–shale cycles: climatically induced or diagenetic? *Geology*, **14**, 609–612.

HAYS, J. D., IMBRIE, J. & SHACKLETON, N. J. 1976. Variations in the Earth's orbit: pacemaker of the ice ages. *Science*, **194**, 1121–1132.

HECKEL, P. H. 1986. Sea-level curve for Pennsylvanian eustatic marine transgressive-regressive depositional cycles along midcontinent outcrop belt, North America. *Geology*, **14**, 330–334.

HECKEL, P. H. 1994. Evaluation of evidence for glacial-eustatic control over marine Pennsylvanian cyclothems

in North America and consideration of possible tectonic effects. *In*: DENNISON, J. M. & ETTENSOHN, F. R. (eds) *Tectonic and Eustatic Controls on Sedimentary Cycles*. SEPM (Society for Sedimentary Geology) Concepts in Sedimentology and Paleontology, Tulsa, USA, **4**, 65–87.

HECKEL, P. H. & ALEKSEEV, A. S. M. *ET AL.* 2007. Cyclothem ['digital'] correlation and biostratigraphy across the global Moscovian-Kasimovian-Gzhelian stage boundary interval (Middle-Upper Pennsylvanian) in North America and eastern Europe. *Geology*, **35**, 607–610.

HERBERT, T. D. 1994. Reading orbital signals distorted by sedimentation: models and examples. *In*: DE BOER, P. L. & SMITH, D. G. (eds) *Orbital Forcing and Cyclic Sequences*. International Association of Sedimentologists, Special Publications, Wiley-Blackwell, Oxford, UK, **19**, 483–507.

HERBERT, T. D., PREMOLI SILVA, I., ERBA, E. & FISCHER, A. G. 1995. Orbital chronology of Cretaceous–Paleogene marine strata. *SEPM (Society for Sedimentary Geology) Special Publication*, **54**, 81–93.

HILGEN, F. & ABDUL AZIZ, H. *ET AL.* 2005. The Global boundary Stratotype Section and Point (GSSP) of the Tortonian Stage (Upper Miocene) at Monte Dei Corvi. *Episodes*, **28**, 6–17.

HILGEN, F., BRINKHUIS, H. & ZACHARIASSE, W. J. 2006. Unit stratotypes for global stages: the Neogene perspective. *Earth-Science Reviews*, **74**, 113–125.

HILGEN, F. J. 1991*a*. Astronomical calibration of Gauss to Matuyama sapropels in the Mediterranean and implication for the Geomagnetic Polarity Time Scale. *Earth and Planetary Science Letters*, **104**, 226–244.

HILGEN, F. J. 1991*b*. Extension of the astronomically calibrated (polarity) time scale to the Miocene-Pliocene boundary. *Earth and Planetary Science Letters*, **107**, 349–368.

HILGEN, F. J. 2010. Astronomical dating in the 19th century. *Earth Science Reviews*, **98**, 65–80.

HILGEN, F. J. & LANGEREIS, C. G. 1989. Periodicities of $CaCO_3$ cycles in the Pliocene of Sicily: discrepancies with the quasi-periods of the Earth's orbital cycles? *Terra Nova*, **1**, 409–415.

HILGEN, F. J., KRIJGSMAN, W., LANGEREIS, C. G., LOURENS, L. J., SANTARELLI, A. & ZACHARIASSE, W. J. 1995. Extending the astronomical (polarity) time scale into the Miocene. *Earth and Planetary Science Letters*, **136**, 495–510.

HILGEN, F. J., KRIJGSMAN, W. & WIJBRANS, J. R. 1997. Direct comparison of astronomical and $^{40}Ar/^{39}Ar$ ages of ash beds: potential implications for the age of mineral dating standards. *Geophysical Research Letters*, **24**, 2043–2046.

HILGEN, F. J., ABDUL AZIZ, H., KRIJGSMAN, W., RAFFI, I. & TURCO, E. 2003. Integrated stratigraphy and astronomical tuning of the Serravallian and lower Tortonian at Monte dei Corvi (Middle-Upper Miocene, northern Italy). *Palaeogeography, Palaeoclimatology, Palaeoecology*, **199**, 229–264.

HILGEN, F. J., KUIPER, K. F. & LOURENS, L. J. 2010. Evaluation of the Astronomical Time Scale for the Paleocene and earliest Eocene. *Earth and Planetary Science Letters*, **300**, 139–151.

HILGEN, F. J., LOURENS, L. J. & VAN DAM, J. A. 2012. The Neogene Period. *In*: GRADSTEIN, F., OGG, J., SCHMITZ, M. & OGG, G. (eds) *The Geological Time Scale 2012*. Elsevier, Amsterdam, 923–978.

HINNOV, L. A. 2000. New perspectives on orbitally forced stratigraphy. *Annual Reviews of Earth and Planetary Sciences*, **28**, 419–475.

HINNOV, L. A. 2013*a*. Prospects for a Paleozoic Astronomical Time Scale. *Proceedings of the 3rd IGCP 591 Annual Meeting*, Lund, Sweden, 19–20.

HINNOV, L. A. 2013*b*. Cyclostratigraphy and its revolutionizing applications in the Earth and Planetary Sciences. *Geological Society of America Bulletin*, 125th Anniversary Volume, **125**, 1703–1734.

HINNOV, L. A. & HILGEN, F. J. 2012. Cyclostratigraphy and astrochronology. *In*: GRADSTEIN, F., OGG, J., SCHMITZ, M. & OGG, G. (eds) *The Geological Time Scale 2012*. Elsevier, Amsterdam, 63–82.

HINNOV, L. A. & PARK, J. 1998. Detection of astronomical cycles in the stratigraphic record by frequency modulation (FM) analysis. *Journal of Sedimentary Research*, **B68**, 524–539.

HOLBOURN, A., KUHNT, W., SCHULZ, M., FLORES, J. A. & ANDERSEN, N. 2007. Orbitally paced climate evolution during the middle Miocene 'Monterey' carbon-isotope excursion. *Earth and Planetary Science Letters*, **261**, 534–550.

HOLBOURN, A., KUHNT, W., FRANK, M. & HALEY, B. A. 2013. Changes in Pacific Ocean circulation following the Miocene onset of permanent Antarctic ice cover. *Earth and Planetary Science Letters*, **365**, 38–50.

HOUSE, M. R. 1985. A new approach to an absolute timescale from measurements of orbital cycles and sedimentary microrhythms. *Nature*, **315**, 721–725.

HOVAN, S. A., REA, D. K., PISIAS, N. G. & SHACKLETON, N. J. 1989. A direct link between the China loess and marine $\delta^{18}O$ records: aeolian flux to the north Pacific. *Nature*, **340**, 296–298.

HUANG, C., HINNOV, L., FISCHER, A. G., GRIPPO, A. & HERBERT, T. 2010*a*. Astronomical tuning of the Aptian Stage from Italian reference sections. *Geology*, **38**, 899–902.

HUANG, C., HESSELBO, S. P. & HINNOV, L. A. 2010*b*. Astrochronology of the Late Jurassic Kimmeridge Clay (Dorset, England) and implications for Earth system processes. *Earth and Planetary Science Letters*, **289**, 242–255.

HÜSING, S. K., HILGEN, F. J., ABDUL AZIZ, H. & KRIJGSMAN, W. 2007. Completing the Neogene geological time scale between 8.5 and 12.5 Ma. *Earth and Planetary Science Letters*, **253**, 340–358.

HÜSING, S. K., KUIPER, K. F., LINK, W., HILGEN, F. J. & KRIJGSMAN, W. 2009. The Upper Tortonian-Lower Messinian at Monte dei Corvi (northern Apennines, Italy): completing a Mediterranean reference section for the Tortonian Stage. *Earth and Planetary Science Letters*, **282**, 140–157.

HÜSING, S. K. & BENIEST, A. *ET AL.* 2014. Astronomically-calibrated magnetostratigraphy of the Lower Jurassic marine successions at St. Audrie's Bay and East Quantoxhead (Hettangian–Sinemurian; Somerset, UK). *Palaeogeography, Palaeoclimatology, Palaeoecology*, **403**, 43–56.

Husson, D. 2013. RedNoise_ConfidenceLevels, http://www.mathworks.com/matlabcentral/fileexchange/45539-rednoise-confidencelevels [accessed 27 April 2014]

Husson, D., Galbrun, B., Laskar, J., Hinnov, L. A., Thibault, N., Gardin, S. & Locklair, R. E. 2011. Astronomical calibration of the Maastrichtian (Late Cretaceous). *Earth and Planetary Science Letters*, **305**, 328–340.

Hutter, L. 1983. *Theoretical Glaciology*. D. Reidel, Dordrecht.

Huybrechts, P. 1990. A 3-D model for the Antarctic ice sheet: a sensitivity study on the glacial-interglacial contrast. *Climate Dynamics*, **5**, 79–92.

Huybrechts, P. 2002. Sea-level changes at the LGM from ice-dynamic reconstructions of the Greenland and Antarctic ice sheets during the glacial cycles. *Quaternary Science Reviews*, **21**, 203–231.

Huybers, P. 2007. Glacial variability over the last 2 Ma: an extended depth-derived age model, continuous obliquity pacing, and the Pleistocene progression. *Quaternary Science Reviews*, **26**, 37–55.

Huybers, P. & Aharonson, O. 2010. Orbital tuning, eccentricity, and the frequency modulation of climatic precession. *Paleoceanography*, **25**, PA4228, http://dx.doi.org/10.1029/2010PA001952

Huybers, P. & Curry, W. 2006. Links between annual, Milankovitch and continuum temperature variability. *Nature*, **441**, 329–332.

Huybers, P. & Wunsch, C. 2003. Rectification and precession signals in the climate system. *Geophysical Research Letters*, **30**, http://dx.doi.org/10.1029/2003GL017875

Huybers, P. & Wunsch, C. 2004. A depth-derived Pleistocene age model: uncertainty estimates, sedimentation variability, and nonlinear climate change. *Paleoceanography*, **19**, PA1028, http://dx.doi.org/10.1029/2002PA000857

Hyland, E. & Murphy, B. *et al.* 2009. Integrated stratigraphic and astrochronologic calibration of the Eocene-Oligocene transition in the Monte Cagnero section (northeastern Apennines, Italy): a potential parastratotype for the Massignano global stratotype section and point (GSSP). *Geological Society of America Special Paper*, **452**, 303–322.

Ikeda, M. & Tada, R. 2013. Long period astronomical cycles from the Triassic to Jurassic bedded chert sequence (Inuyama, Japan); Geologic evidences for the chaotic behavior of solar planets. *Earth, Planets and Space*, **65**, 1–10.

Ikeda, M., Tada, R. & Sakuma, H. 2010. Astronomical cycle origin of bedded chert: a middle Triassic bedded chert sequence, Inuyama, Japan. *Earth and Planetary Science Letters*, **297**, 369–378.

Imbrie, J. & Imbrie, K. P. 1979. *Ice Ages, Solving the Mystery*. Enslow Publishers, Short Hills, New Jersey.

Imbrie, J., Hays, J. D. *et al.* 1984. The orbital theory of Pleistocene climate: support from a revised chronology of the marine $\delta^{18}O$ record. *In*: Berger, A. L. *et al.* (eds) *Milankovitch and Climate*. Part 1, D. Reidel, Dordrecht, 269–305.

Jovane, L., Florindo, F., Sprovieri, M. & Pälike, H. 2006. Astronomic calibration of the late Eocene/early Oligocene Massignano section (central Italy). *Geochemistry, Geophysics, Geosystems*, **7**, Q07012, http://dx.doi.org/10.1029/2005GC001195

Joussaume, S. & Taylor, K. E. *et al.* 1999. Monsoon changes for 6000 years ago: results of 18 simulations from the Paleoclimate Modelling Intercomparison Project (PMIP). *Geophysical Research Letters*, **26**, 859–862.

Keller, G. & Barron, J. A. 1983. Paleoceanographic implications of Miocene deep-sea hiatuses. *Geological Society of America Bulletin*, **94**, 1–30.

Kemp, D. B. 2012. Stochastic and deterministic controls on stratigraphic completeness and fidelity. *International Journal of Earth Sciences*, **101**, 2225–2238.

Kemp, D. B. & Sadler, P. M. 2014. Climatic and eustatic signals in a global compilation of shallow marine carbonate accumulation rates. *Sedimentology*, **61**, 1286–1297.

Kent, D. V. & Olsen, P. E. 1999. Astronomically tuned Geomagnetic Polarity Timescale for the Late Triassic. *Journal of Geophysical Research B: Solid Earth*, **104**, 12 831–12 841.

Kent, D. V. & Olsen, P. E. 2008. Early Jurassic magnetostratigraphy and paleolatitudes from the Hartford continental rift basin (eastern North America): testing for polarity bias and abrupt polar wander in association with the central Atlantic magmatic province. *Journal of Geophysical Research*, **113**, B06105, http://dx.doi.org/10.1029/2007JB005407

Kodama, K. P. & Hinnov, L. A. 2014. Rock Magnetic Cyclostratigraphy. *Wiley-Blackwell Fast-Track Monograph, New Analytical Methods in Earth and Environmental Science Series*, **5**, Wiley-Blackwell, Oxford, UK.

Kruiver, P. P., Dekkers, M. J. & Langereis, C. G. 2000. Secular variation in Permian red beds from Dôme de Barrot, SE France. *Earth and Planetary Science Letters*, **179**, 205–217.

Krijgsman, W., Hilgen, F. J., Langereis, C. G., Santarelli, A. & Zachariasse, W. J. 1995. Late Miocene magnetostratigraphy, biostratigraphy and cyclostratigraphy from the Mediterranean. *Earth and Planetary Science Letters*, **136**, 475–494.

Krijgsman, W., Hilgen, F. J., Raffi, I., Sierro, F. J. & Wilson, D. S. 1999. Chronology, causes and progression of the Messinian salinity crisis. *Nature*, **400**, 652–655.

Krijgsman, W., Gaboardi, S., Hilgen, F. J., Iaccarino, S., de Kaenel, E. & van der Laan, E. 2004. Revised astrochronology for the Ain el Beida section (Atlantic Morocco): no glacio-eustatic control for the onset of the Messinian Salinity Crisis. *Stratigraphy*, **1**, 87–101.

Kuiper, K. F. 2004. Direct intercalibration of radioisotopic and astronomical time in the Mediterranean Neogene. *Geologica ultraiectina*, **235**.

Kuiper, K. F., Deino, A., Hilgen, F. J., Krijgsman, W., Renne, P. R. & Wijbrans, J. R. 2008. Synchronizing rock clocks of Earth history. *Science*, **320**, 500–504.

Kullenberg, B. 1947. The piston core sampler. *Svensk Hydrografisk-Biologiska Komm. Skr. ser. 3, Hydrografi*, **1**, 1–46.

Kutzbach, J. E. & Guetter, P. J. 1986. The influence of changing orbital parameters and surface boundary conditions on climate simulations for the past

18 000 years. *Journal of Atmospheric Science*, **43**, 1726–1759.

KUTZBACH, J. E. & OTTO-BLIESNER, B. 1982. Sensitivity of the African-Asian monsoonal climate to orbital parameter changes for 9000 B.P. in a low-resolution General Circulation Model. *Journal of Atmospheric Sciences*, **39**, 1177–1188.

KUTZBACH, J. E. & STREET-PERROTT, F. A. 1985. Milankovitch forcing of fluctuations in the level of tropical lakes from 18 to 0 kyr BP. *Nature*, **317**, 130–134.

KUTZBACH, J. E., BONAN, G., FOLEY, J. & HARRISON, S. P. 1996. Vegetation and soil feedbacks on the response of the African monsoon to orbital forcing in the early to middle Holocene. *Nature*, **384**, 623–626.

KUTZBACH, J. E., LIU, X., LIU, Z. & CHEN, G. 2008. Simulation of the evolutionary response of global summer monsoons to orbital forcing over the past 280,000 years. *Climate Dynamics*, **30**, 567–579.

KVALE, E. P., JOHNSON, H. W., SONETT, C. P., ARCHER, A. W. & ZAWISTOSKI, A. 1999. Calculating lunar retreat rates using tidal rhythmites. *Journal of Sedimentary Research*, **69**, 1154–1168.

LANGEREIS, C. G. & HILGEN, F. J. 1991. The Rossello composite: a Mediterranean and global reference section for the Early to early Late Pliocene. *Earth and Planetary Science Letters*, **104**, 211–225.

LASKAR, J. 1999. The limits of Earth orbital calculations for geological time-scale use. *Philosophical Transactions of the Royal Society of London, Series A*, **357**, 1735–1759.

LASKAR, J., JOUTEL, F. & BOUDIN, F. 1993. Orbital, precessional, and insolation quantities for the Earth from 320 Myr to +10 Myr. *Astronomy & Astrophysics*, **270**, 522–533.

LASKAR, J., ROBUTEL, P., JOUTEL, F., GASTINEAU, M., CORREIA, A. C. M. & LEVRARD, B. 2004. A long term numerical solution for the insolation quantities of the Earth. *Astronomy & Astrophysics*, **428**, 261–285.

LASKAR, J., FIENGA, A., GASTINEAU, M. & MANCHE, M. 2011*a*. La2010: a new orbital solution for the long term motion of the Earth. *Astronomy & Astrophysics*, **532**, A89, http://dx.doi.org/10.1051/0004-6361/201116836

LASKAR, J., GASTINEAU, M., DELISLE, J.-B., FARRÉS, A. & FIENGA, A. 2011*b*. Strong chaos induced by close encounters with Ceres and Vesta. *Astronomy & Astrophysics*, **532**, L4, http://dx.doi.org/10.1051/0004-6361/201117504

LIEBRAND, D., LOURENS, L. J., HODELL, D. A., DE BOER, B., VAN DE WAL, R. S. W. & PÄLIKE, H. 2011. Antarctic ice sheet and oceanographic response to eccentricity forcing during the early Miocene. *Climate of the Past*, **7**, 869–880.

LISIECKI, L. E. & RAYMO, M. E. 2005. A Pliocene–Pleistocene stack of 57 globally distributed benthic $\delta^{18}O$ records. *Paleoceanography*, **20**, PA1003.

LOCKLAIR, R. E. & SAGEMAN, B. B. 2008. Cyclostratigraphy of the Upper Cretaceous Niobrara Formation, Western Interior, U.S.A.: a Coniacian-Santonian orbital timescale. *Earth and Planetary Science Letters*, **269**, 539–552.

LOULERGUE, L. & SCHILT, A. *ET AL.* 2008. Orbital and millennial-scale features of atmospheric CH_4 over the past 800,000 years. *Nature*, **453**, 383–386.

LOURENS, L. J., HILGEN, F. J., ZACHARIASSE, W. J., VAN HOOF, A. A. M., ANTONARAKOU, A. & VERGNAUD-GRAZZINI, C. 1996. Evaluation of the Pliocene to early Pleistocene astronomical time scale. *Paleoceanography*, **11**, 391–413.

LOURENS, L. J., WEHAUSEN, R. & BRUMSACK, H. J. 2001. Geological constraints on tidal dissipation and dynamical ellipticity of the Earth over the past three million years. *Nature*, **409**, 1029–1033.

LOURENS, L. J., HILGEN, F. J., LASKAR, J., SHACKLETON, N. J. & WILSON, D. 2004. The Neogene Period. *In*: GRADSTEIN, F. M., OGG, J. G. & SMITH, A. G. (eds) *A Geologic Time Scale 2004*. Cambridge University Press, Cambridge, 409–440.

LOURENS, L. J. & SLUIJS, A. *ET AL.* 2005. Astronomical pacing of late Palaeocene to early Eocene global warming events. *Nature*, **435**, 1083–1087.

LOUTRE, M. F., BERGER, A., CRUCIFIX, M., DESPRAT, S. & SÁNCHEZ GOÑI, M. F. 2007. Interglacials as simulated by the LLN 2-D NH and MoBiDic climate models. *Developments in Quaternary Sciences*, **7**, 547–561.

LOWRIE, W., ALVAREZ, W., NAPOLEONE, G., PERCH-NIELSEN, K., PREMOLI SILVA, I. & TOUMARKINE, M. 1982. Paleogene magnetic stratigraphy in Umbrian pelagic carbonate rocks: the Contessa Sections, Gubbio. *Geological Society of America Bulletin*, **93**, 414–432.

LÜTHI, D. & MARTINE, *ET AL.* 2008. High-resolution carbon dioxide concentration record 650,000–800,000 years before present. *Nature*, **453**, 379–382.

MA, C., MEYERS, S. R., SAGEMAN, B. B., SINGER, B. S. & JICHA, B. R. 2014. Testing the astronomical time scale for oceanic anoxic event 2, and its extension into Cenomanian strata of the Western Interior Basin (USA). *Geological Society of America Bulletin*, http://dx.doi.org/10.1130/B30922.1

MACHLUS, M. L., OLSEN, P. E., CHRISTIE-BLICK, N. & HEMMING, S. R. 2008. Spectral analysis of the lower Eocene Wilkins Peak Member, Green River Formation, Wyoming: support for Milankovitch cyclicity. *Earth and Planetary Science Letters*, **268**, 64–75.

MALINVERNO, A., ERBA, E. & HERBERT, T. D. 2010. Orbital tuning as an inverse problem: chronology of the early Aptian oceanic anoxic event 1a (Selli Level) in the Cismon APTICORE. *Paleoceanography*, **25**, PA2203, http://dx.doi.org/10.1029/2009PA001769

MANDELBROT, B. B. 1983. *The Fractal Geometry of Nature*. Freeman, New York.

MANN, M. E. & LEES, J. M. 1996. Robust estimation of background noise and signal detection in climatic time series. *Climate Change*, **33**, 409–445.

MARTIN, L. G., MONTANEZ, I. P. & BISHOP, J. W. 2012. A paleotropical carbonate-dominated archive of Carboniferous icehouse dynamics, Bird Spring Fm., Southern Great Basin, USA. *Palaeogeography, Palaeoclimatology, Palaeoecology*, **329–330**, 64–82.

MARTINSON, D. G., MENKE, W. & STOFFA, P. 1982. An inverse approach to signal correlation. *Journal of Geophysical Research*, **87**, 4807–4818.

MELLES, M. & BRIGHAM-GRETTE, J. *ET AL.* 2012. 2.8 million years of Arctic climate change from Lake El'Gygytgyn, NE Russia. *Science*, **337**, 315–320.

MEYERS, S. R. 2008. Resolving Milankovitchian controversies: the Triassic Latemar Limestone and the

Eocene Green River Formation. *Geology*, **36**, 319–322.

MEYERS, S. R. 2012. Seeing red in cyclic stratigraphy: spectral noise estimation for astrochronology. *Paleoceanography*, **27**, PA3228, http://dx.doi.org/10.1029/2012PA002307

MEYERS, S. R. & SAGEMAN, B. B. 2004. Detection, quantification, and significance of hiatuses in pelagic and hemipelagic strata. *Earth and Planetary Science Letters*, **224**, 55–72.

MEYERS, S. R. & SAGEMAN, B. B. 2007. Quantification of deep-time orbital forcing by average spectral misfit. *American Journal of Science*, **307**, 773–792, http://dx.doi.org/10.2475/05.2007.01

MEYERS, S. R., SAGEMAN, B. B. & HINNOV, L. A. 2001. Integrated quantitative stratigraphy of the Cenomanian-Turonian Bridge Creek Limestone Member using evolutive harmonic analysis and stratigraphic modelling. *Journal of Sedimentary Research*, **71**, 628–644, http://dx.doi.org/10.1306/012401710628

MEYERS, S. R., SAGEMAN, B. B. & PAGANI, M. 2008. Resolving Milankovitch: consideration of signal and noise. *American Journal of Science*, **208**, 770–786.

MEYERS, S. R., SIEWERT, S. E. *ET AL.* 2012. Intercalibration of radioisotopic and astrochronologic time scales for the Cenomanian-Turonian boundary interval, Western Interior Basin, USA. *Geology*, **40**, 7–10.

MIALL, A. D. 1992. Exxon global cycle chart: an event for every occasion? *Geology*, **20**, 787–790.

MIALL, A. D. 2014. Updating uniformitarianism: stratigraphy as just a set of 'frozen accidents'. *In*: SMITH, D. G., BAILEY, R. J., BURGESS, P. M. & FRASER, A. J. (eds) *Strata and Time: Probing the Gaps in Our Understanding*. **404**. First published online April 11, 2014, http://dx.doi.org/10.1144/SP404.9

MIALL, A. D. & MIALL, C. E. 2004. Empiricism and model-building in stratigraphy: around the hermeneutic circle in the pursuit of stratigraphic correlation. *Stratigraphy*, **1**, 27–46.

MILANKOVITCH, M. 1941. Kanon der Erdbestrahlung und seine Anwendung auf das Eiszeitenproblem. *Königlich Serbische Akademie*, Belgrad, Edit. spec. **133**.

MIN, K., MUNDIL, R., RENNE, P. R. & LUDWIG, K. R. 2000. A test for systematic errors in $^{40}Ar/^{39}Ar$ geochronology through comparison with U/Pb analysis of a 1.1-Ga rhyolite. *Geochimica et Cosmochimica Acta*, **64**, 73–98.

MONTANARI, A., ODIN, G. S. & COCCIONI, R. 1997. *Miocene Stratigraphy. An Integrated Approach*. Developments in Palaeontology and Stratigraphy, **15**.

MORLAND, L. W. 1987. Unconfined ice-shelf flow. *In*: DE VEEN, C. J. V. & OERLEMANS, J. (eds) *Dynamics of the West Antarctic Ice Sheet*. D. Reidel, Dordrecht, 99–116.

MOURIK, A. A., BIJKERK, J. F., CASCELLA, A., HÜSING, S. K., HILGEN, F. J., LOURENS, L. J. & TURCO, E. 2010. Astronomical tuning of the La Vedova High Cliff section (Ancona, Italy) - Implications of the Middle Miocene Climate Transition for Mediterranean sapropel formation. *Earth and Planetary Science Letters*, **297**, 249–261.

MUDELSEE, M. 2002. TAUEST: a computer program for estimating persistence in unevenly spaced weather/climate time series. *Computers and Geosciences*, **28**, 69–72.

MUDELSEE, M. 2010. *Climate Time Series Analysis, Classical Statistical and Bootstrap Methods*. Springer Verlag, Dordrecht.

MUNNECKE, A. & SAMTLEBEN, C. 1996. The formation of micritic limestones and the development of limestone–marl alternations in the Silurian of Gotland, Sweden. *Facies*, **34**, 159–176.

NADOR, A., LANTOS, M., TOTH-MAKK, A. & THAMO-BOZSO, E. 2003. Milankovitch-scale multi-proxy records from fluvial sediments of the last 2.6 Ma, Pannonian Basin, Hungary. *Quaternary Science Reviews*, **22**, 2157–2175.

NAISH, T. R. & ABBOTT, S. T. *ET AL.* 1998. Astronomical calibration of a Southern Hemisphere Plio-Pleistocene reference section, Wanganui Basin, New Zealand. *Quaternary Science Reviews*, **17**, 695–710.

OGG, J. G. 2012. Triassic. *In*: GRADSTEIN, F., OGG, J., SCHMITZ, M. & OGG, G. (eds) *The Geological Time Scale 2012*. Elsevier, Amsterdam, 681–730.

OGG, J. & HINNOV, L. A. 2012*a*. The Jurassic Period. *In*: GRADSTEIN, F., OGG, J., SCHMITZ, M. & OGG, G. (eds) *The Geological Time Scale 2012*. Elsevier, Amsterdam, 731–791.

OGG, J. & HINNOV, L. A. 2012*b*. The Cretaceous Period. *In*: GRADSTEIN, F., OGG, J., SCHMITZ, M. & OGG, G. (eds) *The Geological Time Scale 2012*. Elsevier, Amsterdam, 793–853.

OLSEN, P. E. & KENT, D. V. 1996. Milankovitch climate forcing in the tropics of Pangaea during the Late Triassic. *Palaeogeography, Palaeoclimatology, Palaeoecology*, **122**, 1–26.

OLSEN, P. E. & KENT, D. V. 1999. Long-period Milankovitch cycles from the Late Triassic and Early Jurassic of eastern North America and their implications for the calibration of the Early Mesozoic time-scale and the long-term behaviour of the planets. *Philosophical Transactions of the Royal Society A: Mathematical, Physical and Engineering Sciences*, **357**, 1761–1786.

OLSEN, P. E., KENT, D. V., CORNET, B., WITTE, W. K. & SCHLISCHE, R. W. 1996. High-resolution stratigraphy of the Newark rift basin (early Mesozoic, eastern North America). *Geological Society of America Bulletin*, **108**, 40–77.

OLSEN, P. E., KENT, D. V. & WHITESIDE, J. H. 2011. Implications of the Newark Supergroup-based astrochronology and geomagnetic polarity time scale (Newark-APTS) for the tempo and mode of the early diversification of the Dinosauria. *Earth and Environmental Science Transactions of the Royal Society of Edinburgh*, **101**, 201–229.

PÄLIKE, H. & HILGEN, F. 2008. Rock clock synchronization. *Nature Geoscience*, **1**, 282.

PÄLIKE, H. & SHACKLETON, N. J. 2000. Constraints on astronomical parameters from the geological record for the last 25 Myr. *Earth and Planetary Science Letters*, **182**, 1–14.

PÄLIKE, H., LASKAR, J. & SHACKLETON, N. J. 2004. Geologic constraints on the chaotic diffusion of the solar system. *Geology*, **32**, 929–932.

PÄLIKE, H. & NORRIS, R. D. *ET AL.* 2006*a*. The heartbeat of the Oligocene climate system. *Science*, **314**, 1894–1898.

PÄLIKE, H., FRAZIER, J. & ZACHOS, J. 2006*b*. Extended orbitally forced palaeoclimatic records from the equatorial Atlantic Ceara Rise. *Quaternary Science Reviews*, **25**, 3138–3149.

PÄLIKE, H., NISHI, H., LYLE, M., RAFFI, I., KLAUS, A. & GAMAGE, K., and the Expedition 320/321 Scientists 2009. *Pacific Equatorial Transect. IODP Preliminary Report*, **320**, http://dx.doi.org/10.2204/iodp.pr.320.2009

PÄLIKE, H., LYLE, M. W. *ET AL.* 2012. A Cenozoic record of the equatorial Pacific carbonate compensation depth. *Nature*, **488**, 609–614.

PETOUKHOV, V., GANOPOLSKI, A., BROVKIN, V., CLAUSSEN, M., ELISEEV, A., KUBATZKI, C. & RAHMSTORF, S. 2000. CLIMBER-2: a climate system model of intermediate complexity. Part I: Model description and performance for present climate. *Climate Dynamics*, **16**, 1–17.

PETTERSSON, H., JERLOV, N. G. & KULLENBERG, B. 1951. *Reports of the Swedish Deep-Sea Expedition, 1947–1948*. Statens naturvetenskapliga forskningsråd, Sweden.

PHILLIPS, D. & MATCHAN, E. L. 2013. Ultra-high precision $^{40}Ar/^{39}Ar$ ages for Fish Canyon tuff and Alder Creek rhyolite sanidine: new dating standards required? *Geochimica et Cosmochimica Acta*, **121**, 229–239.

PLOTNICK, R. E. 1986. A fractal model for the distribution of stratigraphic hiatuses. *Journal of Geology*, **94**, 885–890.

PRELL, W. L. & KUTZBACH, J. E. 1987. Monsoon variability over the past 150,000 years. *Journal of Geophysical Research*, **92**, 8411–8425.

PRELL, W. L. & KUTZBACH, J. E. 1992. Sensitivity of the Indian monsoon to forcing parameters and implications for its evolution. *Nature*, **360**, 647–652.

PROISTOSESCU, C., HUYBERS, P. & MALOOF, A. C. 2012. To tune or not to tune: detecting orbital variability in Oligo-Miocene climate records. *Earth and Planetary Science Letters*, **325–326**, 100–107.

PROKOPENKO, A. A., HINNOV, L. A., WILLIAMS, D. F. & KUZMIN, M. I. 2006. Orbital forcing of continental climate during the Pleistocene: a complete astronomically tuned climatic record from Lake Baikal, SE Siberia. *Quaternary Science Reviews*, **25**, 3431–3457.

RAYMO, M. E., RUDDIMAN, W. F., BACKMAN, J., CLEMENT, B. M. & MARTINSON, D. G. 1989. Late Pliocene variation in northern Hemisphere ice sheets and North Atlantic deep water circulation. *Paleoceanography*, **4**, 413–446.

READ, J. F. 1995. Overview of carbonate platform sequences, cycle stratigraphy and reservoirs in greenhouse and icehouse worlds. *In*: READ, J. F., KERANS, C., WEBER, L. J., SARG, J. F. & WRIGHT, F. W. (eds) *Milankovitch Sea Level Changes, Cycles and Reservoirs on Carbonate Platforms in Greenhouse and Icehouse Worlds*. SEPM (Society for Sedimentary Geology) Short Course Notes, Tulsa, USA, **35**, 1–102.

REINHARDT, L. & RICKEN, W. 2000. The stratigraphic and geochemical record of playa cycles: monitoring a Pangaean monsoon-like system (Triassic, Middle Keuper, S. *Germany). Palaeogeography, Palaeoclimatology, Palaeoecology*, **161**, 205–227.

RENNE, P., WALTER, R., VEROSUB, K., SWEITZER, M. & ARONSON, J. 1993. New data from Hadar (Ethiopia) support orbitally tuned time scale to 3.3 Ma. *Geophysical Research Letters*, **20**, 1067–1070.

RENNE, P. R. & DEINO, A. L. *ET AL.* 1994. Intercalibration of astronomical and radioisotopic time. *Geology*, **22**, 783–786.

RENNE, P. R., SWISHER, C. C., DEINO, A. L., KARNER, D. B., OWENS, T. L. & DEPAOLO, D. J. 1998. Intercalibration of standards, absolute ages and uncertainties in $^{40}Ar/^{39}Ar$ dating. *Chemical Geology*, **145**, 117–152.

RENNE, P. R., MUNDIL, R., BALCO, G., MIN, K. & LUDWIG, K. R. 2010. Joint determination of ^{40}K decay constants and $^{40}Ar^*/^{40}K$ for the Fish Canyon sanidine standard, and improved accuracy for $^{40}Ar/^{39}Ar$ geochronology. *Geochimica et Cosmochimica Acta*, **74**, 5349–5367.

RENNE, P. R., BALCO, G., LUDWIG, K. R., MUNDIL, R. & MIN, K. 2011. Response to the comment by Schwarz *et al*. on 'Joint determination of ^{40}K decay constants and $^{40}Ar^*/^{40}K$ for the Fish Canyon sanidine standard, and improved accuracy for $^{40}Ar/^{39}Ar$ geochronology' by Renne et al. 2010. *Geochimica et Cosmochimica Acta*, **75**, 5097–5100.

RENNE, P. R. & DEINO, A. L. *ET AL.* 2013. Time scales of critical events around the Cretaceous-Paleogene boundary. *Science*, **339**, 684–687.

RIAL, J. A. 1999. Pacemaking the ice ages by frequency modulation of Earth's orbital eccentricity. *Science*, **285**, 564–568.

RIAL, J. A. & ANACLERIO, C. A. 2000. Understanding nonlinear responses of the climate system to orbital forcing. *Quaternary Science Reviews*, **19**, 1709–1722.

RIPEPE, M. & FISCHER, A. G. 1991. Stratigraphic rhythms synthesized from orbital variations. *In*: FRANSEEN, E. K., WATNEY, W. L. & STC KENDALL, C. G. (eds) *Sedimentary Modelling: Computer Simulations and Methods for Improved Parameter Definition*. Kansas Geological Survey Bulletin, Lawrence, **233**, 335–344.

RIVERA, T. A., STOREY, M., ZEEDEN, C., HILGEN, F. J. & KUIPER, K. 2011. A refined astronomically calibrated $^{40}Ar/^{39}Ar$ age for Fish Canyon sanidine. *Earth and Planetary Science Letters*, **311**, 420–426.

RIVERA, T. A., STOREY, M., SCHMITZ, M. D. & CROWLEY, J. L. 2013. Age intercalibration of $^{40}Ar/^{39}Ar$ sanidine and chemically distinct U/Pb zircon populations from the Alder Creek Rhyolite Quaternary geochronology standard. *Chemical Geology*, **345**, 87–98.

RIVERA, T. A., SCHMITZ, M. D., CROWLEY, J. L. & STOREY, M. 2014. Rapid magma evolution constrained by zircon petrochronology and $^{40}Ar/^{39}Ar$ sanidine ages for the Huckleberry Ridge Tuff, *Geology*, **42**, 643–646.

ROE, G. H. 2002. Modelling precipitation over ice sheets: an assessment using Greenland. *Journal of Glaciology*, **48**, 70–80.

ROE, G. H. & LINDZEN, R. S. 2001. The mutual interaction between continental-scale ice sheets and atmospheric stationary waves. *Journal of Climatology*, **14**, 1450–1465.

ROEHLER, H. W. 1993. *Eocene climates, depositional environments and geography, greater Green River basin, Wyoming, Utah and Colorado*. U.S. Geological Survey Professional Paper, **1506F**.

ROSSIGNOL-STRICK, M. 1985. Mediterranean Quaternary sapropels, an immediate response to African monsoons

to variations of insolation. *Palaeogeography, Palaeoclimatology, Palaeoecology*, **49**, 237–263.

RUBINCAM, D. P. 1994. Insolation in terms of Earth's orbital parameters. *Theoretical and Applied Climatology*, **48**, 195–202.

RUBINCAM, D. P. 1996. Reply to Comment on 'Insolation in terms of Earth's orbital parameters'. *Theoretical and Applied Climatology*, **53**, 257–258.

RUBINCAM, D. P. 2004. Black body temperature, orbital elements, the Milankovitch precession index, and the Seversmith psychroterms. *Theoretical and Applied Climatology*, **79**, 111–131.

RUDDIMAN, W. F. & RAYMO, M. E. 2003. A methane-based time scale for Vostok ice. *Quaternary Science Reviews*, **22**, 141–155.

RUDDIMAN, W. F., CAMERON, D. & CLEMENT, B. M. 1987. Sediment disturbance and correlation of offset holes drilled with the hydraulic piston corer: Leg 94. *Initial Reports of the Deep Sea Drilling Program*, **94**, 615–634.

RUDDIMAN, W. F., RAYMO, M. E., MARTINSON, D. G., CLEMENT, B. M. & BACKMAN, J. 1989. Pleistocene evolution: northern hemisphere ice sheets and North Atlantic Ocean. *Paleoceanography*, **4**, 353–412.

RUHL, M., DEENEN, M. H. L., ABELS, H. A., BONIS, N. R., KRIJGSMAN, W. & KÜRSCHNER, W. M. 2010. Astronomical constraints on the duration of the early Jurassic Hettangian stage and recovery rates following the end-Triassic mass extinction (St Audrie's Bay/East Quantoxhead, UK). *Earth and Planetary Science Letters*, **295**, 262–276, http://dx.doi.org/10.1016/j.epsl.2010.04.008

SADLER, P. M. 1981. Sedimentation rates and the completeness of stratigraphic sections. *Journal of Geology*, **89**, 569–584.

SADLER, P. M. 1999. The influence of hiatuses on sediment accumulation rates. *In*: BRUNS, P. & HASS, H. C. (eds) *On the Determination of Sediment Accumulation Rates*. GeoResearch Forum, Trans Tech Publications, Switzerland, **5**, 15–40.

SADLER, P. M. & STRAUSS, D. J. 1990. Estimation of the completeness of stratigraphical sections using empirical data and theoretical models. *Journal of the Geological Society, London*, **147**, 471–485.

SAGEMAN, B. B. & SINGER, B. S. *ET AL.* 2014. Integrating $^{40}Ar/^{39}Ar$, U–Pb, and astronomical clocks in the Cretaceous Niobrara Formation, Western Interior Basin, USA. *Geological Society of America Bulletin*, **126**, 956–973.

SCHIFFELBEIN, P. & DORMAN, L. 1986. Spectral effects of time-depth nonlinearities in deep sea sediment records; a demodulation technique for realigning time and depth scales. *Journal of Geophysical Research*, **91**, 3821–3835.

SCHLAGER, W. 2010. Ordered hierarchy v. scale invariance in sequence stratigraphy. *International Journal of Earth Sciences*, **99**, 139–151.

SCHMITZ, M. D. 2012. Radiogenic isotope geochronology. *In*: GRADSTEIN, F., OGG, J., SCHMITZ, M. & OGG, G. (eds) *The Geological Time Scale 2012*. Elsevier, Amsterdam, 115–126.

SCHOENE, B., CONDON, D. J. & MORGAN, L. 2013. Precision and accuracy in geochronology. *Elements*, **9**, 19–24.

SCHULZ, M. & MUDELSEE, M. 2002. REDFIT: estimating red-noise spectra directly from unevenly spaced paleoclimatic time series. *Computers and Geosciences*, **28**, 421–426.

SHACKLETON, N. J. & CROWHURST, S. 1997. Sediment fluxes based on an orbitally tuned time scale 5 Ma to 14 Ma, Site 926. *In*: SHACKLETON, N. J., CURRY, W. B., RICHTER, C. & BRALOWER, T. J. (eds) *Proceedings ODP, Scientific Results*. Ocean Drilling Program, College Station, TX, **154**, 69–82.

SHACKLETON, N. J., BERGER, A. & PELTIER, W. R. 1990. An alternative astronomical calibration of the lower Pleistocene timescale based on ODP site 677. *Transactions - Royal Society of Edinburgh: Earth Sciences*, **81**, 251–261.

SHACKLETON, N. J., HAGELBERG, T. K. & CROWHURST, S. J. 1995. Evaluating the success of astronomical tuning: pitfalls of using coherence as a criterion for assessing pre-Pleistocene timescales. *Paleoceanography*, **10**, 693–697.

SHACKLETON, N. J., CROWHURST, S. J., WEEDON, G. P. & LASKAR, J. 1999. Astronomical calibration of Oligocene–Miocene time. *Philosophical Transactions of the Royal Society A: Mathematical, Physical and Engineering Sciences*, **357**, 1907–1929.

SIEGENTHALER, U. & STOCKER, T. F. *ET AL.* 2005. Stable carbon cycle-climate relationship during the Late Pleistocene. *Science*, **310**, 1313–1317.

SINGER, B. S. 2014. A Quaternary geomagnetic instability time scale. *Quaternary Geochronology*, **21**, 29–52.

SMITH, D. G. 1994. Cyclicity or chaos? Orbital forcing versus non-linear dynamics. *In*: DE BOER, P. L. & SMITH, D. G. (eds) *Orbital Forcing and Cyclic Sequences*. IAS Special Publications, Blackwell Scientific Publications, Oxford, **19**, 533–541.

SMITH, M., CHAMBERLAIN, K. R., SINGER, B. S. & CARROLL, A. R. 2010. Eocene clocks agree: coeval $^{40}Ar/^{39}Ar$, U–Pb, and astronomical ages from the Green River Formation. *Geology*, **38**, 527–530.

SPELL, T. L. & MCDOUGALL, I. 1992. Revisions to the age of the Brunhes-Matuyama boundary and the Pleistocene geomagnetic polarity timescale. *Geophysical Research Letters*, **19**, 1181–1184.

SPROVIERI, M., SABATINO, N., PELOSI, N., BATENBURG, S. J., COCCIONI, R., IAVARONE, M. & MAZZOLA, S. 2013. Late Cretaceous orbitally-paced carbon isotope stratigraphy from the Bottaccione Gorge (Italy). *Palaeogeography, Palaeoclimatology, Palaeoecology*, **379–380**, 81–94.

STAP, L., SLUIJS, A., THOMAS, E. & LOURENS, L. 2009. Patterns and magnitude of deep sea carbonate dissolution during Eocene thermal maximum 2 and H2, Walvis Ridge, SE Atlantic Ocean. *Paleoceanography*, **24**, art. no. PA1211.

STEENBRINK, J., VAN VUGT, N., HILGEN, F. J., WIJBRANS, J. R. & MEULENKAMP, J. E. 1999. Sedimentary cycles and volcanic ash beds in the lower Pliocene lacustrine succession of Ptolemais (NW Greece): discrepancy between $^{40}Ar/^{39}Ar$ and astronomical ages. *Palaeogeography, Palaeoclimatology, Palaeoecology*, **152**, 283–303.

SZURLIES, M. 2007. Latest Permian to Middle Triassic cyclo-magnetostratigraphy from the Central European basin, Germany: implications for the geomagnetic

polarity timescale. *Earth and Planetary Science Letters*, **261**, 602–619.

THIBAULT, N., HUSSON, D., HARLOU, R., GARDIN, S., GALBRUN, B., HURET, E. & MINOLETTI, F. 2012. Astronomical calibration of upper Campanian-Maastrichtian carbon isotope events and calcareous plankton biostratigraphy in the Indian Ocean (ODP hole 762C): implication for the age of the Campanian-Maastrichtian boundary. *Palaeogeography, Palaeoclimatology, Palaeoecology*, **337–338**, 52–71.

TÖRNQVIST, T. E. 1998. Longitudinal profile evolution of the Rhine-Meuse system during the last deglaciation: interplay of climate change and glacioeustasy? *Terra Nova*, **10**, 11–15.

TUENTER, E., WEBER, S. L., HILGEN, F. J., LOURENS, L. J. & GANOPOLSKI, A. 2005. Simulation of climate phase lags in response to precession and obliquity forcing and the role of vegetation. *Climate Dynamics*, **24**, 279–295.

TURNER, J. T. 2002. Zooplankton fecal pellets, marine snow and sinking phytoplankton blooms. *Aquatic Microbial Ecology*, **27**, 57–102.

VAKS, A., BAR-MATTHEWS, M., MATTHEWS, A., AYALON, A. & FRUMKIN, A. 2010. Middle-Late Quaternary paleoclimate of northern margins of the Saharan-Arabian Desert: reconstruction from speleothems of Negev Desert, Israel. *Quaternary Science Reviews*, **29**, 2647–2662.

VAN COUVERING, J. A., CASTRADORI, D., CITA, M. B., HILGEN, F. J. & RIO, D. 2000. The base of the Zanclean Stage and of the Pliocene Series. *Episodes*, **23**, 179–187.

VANDENBERGHE, N., HILGEN, F. J. & SPEIJER, R. P. 2012. The Paleogene Period. *In*: GRADSTEIN, F., OGG, J., SCHMITZ, M. & OGG, G. (eds) *The Geological Time Scale 2012*. Elsevier, Amsterdam, 855–921.

VAN DER LAAN, E., GABOARDI, S., HILGEN, F. J. & LOURENS, L. J. 2005. Regional climate and glacial control on high-resolution oxygen isotope records from Ain El Beida (latest Miocene, Northwest Morocco): a cyclostratigraphic analysis in the depth and time domain. *Paleoceanography*, **20**, 1–22.

VAN DER LAAN, E., HILGEN, F. J., LOURENS, L. J., DE KAENEL, E., GABOARDI, S. & IACCARINO, S. 2012. Astronomical forcing of Northwest African climate and glacial history during the late Messinian (6.5–5.5 Ma). *Palaeogeography, Palaeoclimatology, Palaeoecology*, **313–314**, 107–126.

VAN DE WAL, R. S. W. 1999. The importance of thermodynamics for modelling the volume of the Greenland ice sheet. *Journal of Geophysical Research*, **104**, 3887–3898.

VAN DE WAL, R. S. W., DE BOER, B., LOURENS, L. J., KÖHLER, P. & BINTANJA, R. 2011. Reconstruction of a continuous high-resolution CO_2 record over the past 20 million years. *Climate of the Past*, **7**, 1459–1469.

VAN OS, B. J. H., LOURENS, L. J., HILGEN, F. J., DE LANGE, G. J. & BEAUFORTH, L. 1994. The formation of Pliocene sapropels and carbonate cycles in the Mediterranean: diagenesis, dilution and productivity. *Paleoceanography*, **9**, 601–617.

VAN VUGT, N., STEENBRINK, J., LANGEREIS, C. G., HILGEN, F. J. & MEULENKAMP, J. E. 1998. Magnetostratigraphy-based astronomical tuning of the early Pliocene lacustrine sediments of Ptolemais (NW Greece) and bed-to-bed correlation to the marine record. *Earth and Planetary Science Letters*, **164**, 535–551.

VAUGHAN, S., BAILEY, R. J. & SMITH, D. G. 2011. Detecting cycles in stratigraphic data: spectral analysis in the presence of red noise. *Paleoceanography*, **26**, PA4211, http://dx.doi.org/10.1029/2011PA002195

VOLLMER, T., WERNER, R., WEBER, M., TOUGIANNIDIS, N., RÖHLING, H. G. & HAMBACH, U. 2008. Orbital control on Upper Triassic playa cycles of the Steinmergel-Keuper (Norian): a new concept for ancient playa cycles. *Palaeogeography, Palaeoclimatology, Palaeoecology*, **267**, 1–16.

WANG, Y. & CHENG, H. *ET AL.* 2008. Millennial- and orbital-scale changes in the East Asian monsoon over the past 224,000 years. *Nature*, **451**, 1090–1093.

WEBER, S. L. & TUENTER, E. 2011. The impact of varying ice sheets and greenhouse gases on the intensity and timing of boreal summer monsoons. *Quaternary Science Reviews*, **30**, 469–479.

WEEDON, G. P. 2003. *Time-Series Analysis and Cyclostratigraphy: Examining Stratigraphic Records of Environmental Cycles*. Cambridge University Press, Cambridge.

WEEDON, G. P., COE, A. L. & GALLOIS, R. W. 2004. Cyclostratigraphy, orbital tuning and inferred productivity for the type Kimmeridge Clay (Late Jurassic), Southern England. *Journal of the Geological Society, London*, **161**, 655–666.

WESTERHOLD, T., RÖHL, U., LASKAR, J., RAFFI, I., BOWLES, J., LOURENS, L. J. & ZACHOS, J. C. 2007. On the duration of magnetochrons C24r and C25n and the timing of early Eocene global warming events: implications from the Ocean Drilling Program Leg 208 Walvis Ridge depth transect. *Paleoceanography*, **22**, PA2201, http://dx.doi.org/10.1029/2006PA001322

WESTERHOLD, T. & RÖHL, U. *ET AL.* 2008. Astronomical calibration of the Paleocene time. *Palaeogeography, Palaeoclimatology, Palaeoecology*, **257**, 377–403.

WESTERHOLD, T., RÖHL, U. & LASKAR, J. 2012. Time scale controversy: accurate orbital calibration of the Early Paleogene. *Geochemistry, Geophysics, Geosystems*, **13**, http://dx.doi.org/10.1029/2012GC004096

WESTPHAL, H., BÖHM, F. & BORNHOLDT, S. 2004. Orbital frequencies in the carbonate sedimentary record – distorted by diagenesis? *Facies*, **50**, 3–11.

WESTPHAL, H., MUNNECKE, A. & BRANDANO, M. 2008. Effects of diagenesis on the astrochronological approach of defining stratigraphic boundaries in calcareous rhythmites: the Tortonian GSSP. *Lethaia*, **41**, 461–476.

WESTPHAL, H., HILGEN, F. & MUNNECKE, A. 2010. An assessment of the suitability of individual rhythmic carbonate successions for astrochronological application. *Earth-Science Reviews*, **99**, 19–30.

WILLIAMS, G. E. 2000. Geological constraints on the Precambrian history of Earth's rotation and the Moon's orbit. *Reviews of Geophysics*, **38**, 37–59.

WINKELMANN, R., MARTIN, M. A., HASELOFF, M., ALBRECHT, T., BUELER, E., KHROULEV, C. &

LEVERMANN, A. 2011. The Potsdam Parallel Ice Sheet model (PISM-PIK)—part 1: model description. *The Cryosphere*, **5**, 715–726.

WOTZLAW, J. F., BINDEMAN, I. N., SCHALTEGGER, U., BROOKS, C. K. & NASLUND, H. R. 2012. High resolution insights into episodes of crystallization, hydrothermal alteration and remelting in the Skaergaard intrusive complex. *Earth and Planetary Science Letters*, **355–356**, 199–212.

WOTZLAW, J. F., SCHALTEGGER, U., FRICK, D. A., DUNGAN, M. A., GERDES, A. & GÜNTHER, D. 2013. Tracking the evolution of large-volume silicic magma reservoirs from assembly to supereruption. *Geology*, **41**, 867–870.

WOTZLAW, J.-F., HÜSING, S. K., HILGEN, F. J. & SCHALTEGGER, U. 2014. High-precision zircon U-Pb geochronology of astronomically dated volcanic ash beds from the Mediterranean Miocene. *Earth and Planetary Science Letters*, in press.

WU, H. C., ZHANG, S. H., JIANG, G. Q. & HUANG, Q. H. 2009. The floating astronomical time scale for the terrestrial Late Cretaceous Qingshankou Formation from the Songliao Basin of Northeast China and its stratigraphic and paleoclimate implications. *Earth and Planetary Science Letters*, **278**, 308–323.

WU, H., ZHANG, S. *ET AL*. 2013*a*. Astrochronology of the early Turonian-early Campanian terrestrial succession in the Songliao basin, northeastern China and its implication for long-period behavior of the solar system. *Palaeogeography, Palaeoclimatology, Palaeoecology*, **385**, 55–70.

WU, H., ZHANG, S., HINNOV, L. A., JIANG, G., FENG, Q., LI, H. & YANG, T. 2013*b*. Time-calibrated Milankovitch cycles for the late Permian. *Nature Communications*, **4**, 2452, http://dx.doi.org/10.1038,ncomms3452

WUNSCH, C. 2004. Quantitative estimate of the Milankovitch-forced contribution to observed Quaternary climate change. *Quaternary Science Reviews*, **23**, 1001–1012.

YIN, Q. Z. & BERGER, A. 2012. Individual contribution of insolation and CO_2 to the interglacial climates of the past 800 000 years. *Climate Dynamics*, **38**, 709–724, http://dx.doi.org/10.1007/s00382-011-1013-5

ZEEDEN, C., HILGEN, F., WESTERHOLD, T., LOURENS, L., RÖHL, U. & BICKERT, T. 2012. Revised Miocene splice, astronomical tuning and calcareous plankton biochronology of ODP Site 926 between 5 and 14.4 Ma. *Palaeogeography, Palaeoclimatology, Palaeoecology*, **369**, 430–451.

ZEEDEN, C., LOURENS, L. J. & HILGEN, F. J. 2013. Validating orbitally tuned age models. *In*: ZEEDEN, C. (ed.), *Improving the Neogene Tuned Time Scale. PhD thesis*, Utrecht University.

ZEEDEN, C., HILGEN, F. J., HÜSING, S. K. & LOURENS, L. L. 2014. The Miocene astronomical time scale 9–12 Ma: new constraints on tidal dissipation and their implications for paleoclimatic investigations. *Paleoceanography*, **29**, http://dx.doi.org/10.1002/2014PA002615